NTNU – Trondheim
Norwegian University of
Science and Technology

Analysis of a Multi-Infeed HVDC System in the Norwegian Power System

Alexander Håkan George
Holthe

Master of Energy and Environmental Engineering
Submission date: June 2014
Supervisor: Marta Molinas, ELKRAFT

Norwegian University of Science and Technology
Department of Electric Power Engineering

Problem Description

Statnett is planning to build a new High Voltage Direct Current (HVDC) connection between Norway and Germany (NordLink). It will be connected to the AC grid in Norway near by the already existing HVDC connection to the Netherlands (NorNed). NordLink will consist of a subsea cable and a DC overhead line from the landfall of the cable to the converter station on the Norwegian side. The DC overhead line will partially go in parallel with existing AC overhead lines. NordLink will use Modular Multi-Level Converter (MMC) technology, while NorNed consists of Line Commutated Converter (LCC) technology.

The student is going to investigate how the connection of NordLink will affect the grid configuration in southern Norway. Hence the consequences of a multi-infeed HVDC system consisting of NorNed and NordLink will be explored. It is of special interest to identify whether the new MMC topology can mitigate the weaknesses of the LCC when it comes to commutation failure, and to investigate if the coupling between the AC and DC overhead line is likely to cause problems for the power system. The student is expected to:

- Develop a simulation model of a multi-infeed HVDC system consisting of a MMC-link and LCC-link inverting into the same AC grid, and compare it to the present situation in steady state and in transient state with AC faults.
- Establish a method for detecting commutation failure, and to investigate the susceptibility to commutation failure of the multi-infeed HVDC system as compared to the present situation.
- Investigate the consequences of AC and DC overhead lines sharing the same Rights-of-Way, and study how the parameters affect the interactions.

Start date: January 26th 2014
Supervisor: Marta Molinas, ELKRAFT

Preface

Throughout the specialization project and the master thesis I have learned more about power electronics, control systems and power system in general than I could ever imagined. It has been a valuable learning experience.

There are been many people that have helped me throughout this learning process. I would like to thank my supervisors Marta Molinas, Raymundo Torres and Elisabeth Abildgaard who have guided me. A special thanks goes to Raymundo for his countless efforts with technical guidance and encouragements. Especially correcting my numerous errors when building the simulation model, but also for help with the control design and general technical knowledge. His contribution has been important for my progress and motivation. Marta has encouraged me to build a simulation model consisting of a complete MMC-link. Her guidance helped me pursue a more technical model than I originally planned to do. I am glad that I followed her advice. Elisabeth has improved my understanding of the theoretical aspects of the converters and power systems in general. Her explanations have improved this work substantially, and I really appreciate her efforts.

I would also like to thank my fellow students and friends for the days at NTNU campus, especially my office mates Astrid, Ingerid, Johannes, Marte and David for the laughs, encouragements, coffee breaks and football juggling breaks. I would like to thank my girlfriend Idun for making the days with hard work more cheerful. Lastly, I would like to thank my mother Jill and my brother André for moral support through e-mails and phone calls.

Alexander Holthe
Trondheim, June 2014

Sammendrag

Innvirkningen av en ny modulær flernivå-omformer (MMC) på en strømkilde-omformer (LCC) i samme AC-nett er utforsket, og representerer fremtidens system bestående av NordLink og NorNed. Dette multi-inngangssystemet er sammenlignet mot dagens frittstående LCC-system. En metode for å oppdage kommuteringsfeil er foreslått. Kommuteringsfeil-immunitetsindeksen er 36% og 28% for de respektive systemene. Resultatene indikerer at en MMC-link i et multi-inngangssystem mitigerer svakheten til en LCC-link, og gjør LCC-inverteren mindre utsatt for kommuteringsfeil.

En MMC kan kontrollere både aktiv og reaktiv effekt, og gjør spenningsreguleringen i AC-nettet bedre. Eksisterende spenningsregulerende utstyr kan brukes for å få en mer kontinuerlig regulering av spenningen når en ny MMC-link er installert, og for å minimere tap. Enfase- og trefasejordfeil er implementert. Resultatene indikerer at det kan oppstå kommuteringsfeil i en LCC-inverter i svake AC-nett. En MMC-inverter tåler relativt alvorlige AC-feil uten å bli nevneverdig påvirket. Resultatene indikerer at et multi-inngang HVDC-system forbedrer systemets ytelse ved AC-feil, sammenlignet med et frittstående LCC-system. En MMC-link er i stand til å redusere påvirkningen fra AC-feil, dermed hjelper den LCC-linken å hente seg inn raskere.

Koblingseffekten mellom AC- og DC-luftlinjer i samme korridor er undersøkt, og en enpol-jordfeil er implementert. Induserte DC-strømmer inn i AC-linjene er observert. Nøytralstrømmens maksimale rms-verdi i AC-linjene viser seg å være 1000 A for feil nær MMC-inverteren. To mitigeringsmetoder er foreslått. En optimal plassering av det midtre AC-tårnet viser seg å være 45 meter unna DC-tårnet, og fører til en reduksjon på 22.3% (777 A). Revolvering av AC-linjene reduserte koblingseffekten, ettersom det jevner ut ubalansen mellom trefasene.

Abstract

The impact of a new Modular Multi-Level Converter (MMC) on a Line Commutated Converter (LCC) in the same AC-grid, representing the future system of NordLink and NorNed is investigated. This multi-infeed HVDC system is compared against today's LCC stand alone system. A method for detecting commutation failure is proposed. The commutation failure immunity index is 36% and 28% respectively. The result indicate that the MMC-link hence mitigates the weakness of the LCC-link, and makes the LCC inverter less prone to commutation failure.

The multi-infeed HVDC system is analysed in both steady and transient state. The MMC is able to control the active and reactive power, and enhances AC voltage regulation. Existing voltage supporting equipment can thus be utilized for a more continuous voltage regulation when the new MMC-link is connected, and to minimize losses. Single and three phase to ground faults are applied. The results indicate that a LCC inverter in weak AC grids may suffer from commutation failure. The MMC is able to ride through relatively severe AC faults. The results indicates that the multi-infeed system improves the performance when AC faults are applied as compared the existing LCC stand alone system. The MMC-link is able to mitigate the impact of AC faults, thus helping the LCC-link recover faster.

The coupling effect between AC and DC overhead lines sharing the same Rights-of-Way is investigated, and a single pole to ground fault is applied. Induced DC currents into AC lines are detected. The peak rms neutral current in the AC lines is found to be 1000 A for fault location close to MMC inverter. Two mitigation methods are proposed. First, an optimal displacement of the middle AC tower is found to be 45 meters apart from the DC tower, and leads to a reduction of 22.3% (777 A). Second, transposition of the AC-lines efficiently reduced the coupling effect, as it averages the unbalance between the three phases.

Contents

Preface iii

Sammendrag v

Abstract vii

List of Figures xiii

List of Tables xvii

1 Introduction 1
- 1.1 Background . . . 1
- 1.2 Scope of Work . . . 2
- 1.3 Outline . . . 3

2 Converter Technologies for HVDC 5
- 2.1 Line Commutated Converter . . . 5
- 2.2 Voltage Source Converter . . . 6
  - 2.2.1 Pulse Width Modulation . . . 7
- 2.3 Modular Multi-Level Converter . . . 8
- 2.4 Comparison of LCC, VSC and MMC . . . 10
- 2.5 Full-Bridge MMC . . . 12
- 2.6 Hybrid Multi-Level VSC . . . 13
- 2.7 Multi-Infeed HVDC Systems . . . 14
- 2.8 Use of Converters Today and in the Future . . . 16

3 Control Design 17
- 3.1 Control Design of MMC . . . 17
  - 3.1.1 Master Control of the Converter Stations . . . 18
  - 3.1.2 MMC System Structure . . . 19
  - 3.1.3 MMC Currents . . . 22
    - 3.1.3.1 Circulating Current Suppression Control (CCSC) . . . 23
  - 3.1.4 MMC Voltages . . . 24
  - 3.1.5 MMC Active and Reactive Power Control . . . 25
    - 3.1.5.1 System Description . . . 25
    - 3.1.5.2 Current Controller . . . 27

3.1.5.3 Inner Current Controller 28
3.1.5.4 Outer Current Controller 31
3.1.6 Modified Phase-Shifted Sinusoidal PWM Method 32
3.2 Control Design of LCC 34
3.2.1 Control Objective of LCC 34
3.2.2 Master Control 37
3.2.3 Rectifier Control 38
3.2.4 Inverter Control 38
3.2.5 AC Filters 40
3.2.5.1 Low Pass Filter 41
3.2.5.2 High Pass Filter 43
3.2.5.3 Shunt Compensation 44
3.2.6 Converter Transformer Design 45
3.2.6.1 Inverter Transformer Design 45
3.2.6.2 Rectifier Transformer Design 47
3.3 AC and DC Transmission System 48
3.3.1 Short Circuit Ratio 51

4 Analysis of a Multi-Infeed HVDC System in the Norwegian Power System 55
4.1 Steady State Aspects 57
4.1.1 Scenario 1: LCC Stand Alone System 58
4.1.2 Scenario 2: Multi-Infeed MMC and LCC System 59
4.1.3 Power Flow Changes 62
4.2 Transient Aspects 64
4.2.1 Single Phase To Ground Fault: Fault A 65
4.2.2 Single Phase To Ground Fault: Fault B 69
4.2.3 Three Phase To Ground Fault 73
4.2.4 Closing Remarks 77

5 Commutation Failure Immunity Index for a Multi-Infeed HVDC System 79
5.1 Commutation Failure in a LCC 79
5.2 Commuation Failure Detection Method 81
5.3 Commutation Failure Immunity Index for a Multi-Infeed HVDC System 83

6 Coupling Effect Between AC and DC Overhead Lines in Southern Norway 87
6.1 Methodology to Investigate the Coupling Effect 89
6.1.1 Base Case 90
6.1.2 Sensitivity Analysis 94
6.1.2.1 Parallel Overhead Line Length 95
6.1.2.2 Transmission Tower Distance 96
6.1.2.3 Modulation Index 97

6.1.2.4 DC Fault Location 99
6.1.2.5 Fault Resistance 102
6.1.3 Summary and Mitigation Methods 102

7 Accuracy of the Results **109**

Conclusion **112**

Further Work **114**

Bibliography **115**

A PSCAD Model **121**
A.1 MMC Per Unit Values 121

B DQ-Transformation **123**

C Fault Studies Based on Sequence Currents and Voltages **125**
C.1 Symmetrical Components 125
C.2 AC Faults 127

List of Figures

1.1 Overview of the Multi-Infeed Power System in Southern Norway. . . 3

2.1 Line Commutated Converter, 12-Pulse Configuration. 6
2.2 Voltage Source Converter. 7
2.3 Pulse Width Modulator. 8
2.4 Modular Multi-level Converter. 9
2.5 Submodule in a Full-Bridge MMC, H-Bridge. 12
2.6 Hybrid Multi-Level VSC 14
2.7 Multi-Infeed HVDC System Consisting of MMC and LCC. 15

3.1 Control Hierarchy for MMC-HVDC. 19
3.2 Half-Bridge Submodule Configuration 20
3.3 MMC Structure. 21
3.4 Circulating Current Suppression Control. 24
3.5 Overview of a MMC. 26
3.6 MMC Vector Control Principle. 28
3.7 Block Diagram of Inner Current Control. 29
3.8 Inner Current Control. 30
3.9 Outer Current Control. 31
3.10 Step Change q-axis and d-axis 32
3.11 Phase Shifted Carrier Signals. 33
3.12 Block Diagram of the PWM Controller. 33
3.13 Outline of the LCC Model. 35
3.14 Control Principle of LCC. 35
3.15 Control Hierarchy for LCC-HVDC. 36
3.16 Control Objective of a LCC 37
3.17 Rectifier Control. 38
3.18 Rectifier Firing Pulse Generator 39
3.19 Inverter Gamma Control. 39
3.20 Inverter Current Control. 40
3.21 LCC AC Filters. 42
3.22 Harmonic Current Elimination. 45
3.23 Transmission System in Southern Norway. 49
3.24 AC and DC Overhead Towers Used in PSCAD. 49
3.25 NordLink: DC Submarine Cable Used in PSCAD. 50
3.26 NorNed: DC System Connecting LCC Inverter and LCC Rectifier. . 50

3.27 Short Circuit Ratio: Common Busbar (Tonstad). 53
3.28 Short Circuit Ratio: Feda. 53
3.29 Short Circuit Ratio: LCC Rectifier. 54
3.30 Short Circuit Ratio: MMC Rectifier. 54

4.1 System Overview: Scenario 2. 56
4.2 System Overview: Fault Locations. 57
4.3 Scenario 1: Steady State 58
4.4 NordLink Stand Alone: Steady State 60
4.5 Scenario 2: Steady State 62
4.6 Scenario 1: Ramping of DC Current 63
4.7 Scenario 1: Measured DC Current versus AC Voltage 64
4.8 Scenario 2: Measured DC current versus AC Voltage. 64
4.9 Scenario 1: Single Phase to Ground Fault (Fault A) 67
4.10 Scenario 2: Single Phase to Ground (Fault A) 68
4.11 Scenario 1: Single Phase to Ground (Fault B) 71
4.12 Scenario 2: Single Phase to Ground (Fault B) 72
4.13 Scenario 1: Three Phase to Ground 74
4.14 Scenario 2: Three Phase to Ground 75
4.15 Thyristor Valve in the LCC inverter During a Three Phase 76

5.1 Volt-Time Area in an Inverter. 80
5.2 Commutation Failure Detection Method: Error Logic One Valve . . 82
5.3 Commutation Failure Detection Method 84

6.1 Rights-of-Way: Tower Distances. 88
6.2 Base Case: Case 1 91
6.3 Base Case: Case 2 92
6.4 Base Case: Case 3 93
6.5 Base Case: Case 4 94
6.6 Sensitivity Analysis: Overhead Line Length: Four Cases 96
6.7 Sensitivity Analysis: Overhead Line Length: $I_{n,rms}$ 96
6.8 Sensitivity: Transmission Tower Distance: $I_{n,rms}$ 97
6.9 Sensitivity: Modulation Index: $I_{n,rms}$ 99
6.10 Sensitivity: Modulation Index: DC Current Positive Pole 100
6.11 Sensitivity: DC Fault Location 100
6.12 Sensitivity: DC Fault Location: $I_{n,rms}$ 101
6.13 Sensitivity: DC Fault Location: MMC Inverter 103
6.14 Sensitivity: DC Fault Location: DC Current Positive Pole 104
6.15 Sensitivity: Fault Resistance: $I_{n,rms}$ 104
6.16 Mitigation Methods: Changing Tower Distance 106
6.17 Mitigation Methods: Forward Successive Phase Transpositon 108
6.18 Mitigation Methods: Transposition 108

B.1 Park and Clark Transformation 124

C.1 Representation of Symmetrical Components. 126
C.2 AC Faults Types. 128
C.3 AC Faults: AC Sequence Currents 129
C.4 AC Faults: AC Sequence Voltages 130

List of Tables

2.1 Comparison Converter Technologies 11
2.2 List of HVDC Projects 16

3.1 Technical Data for the System 18
3.2 Explanation of Currents in MMC 22
3.3 Grounding Wires of Overhead Lines. 51

4.1 Fault A: Comparison Angles. 69
4.2 Fault A: Comparison Voltages and Powers. 69
4.3 Fault B: Comparison Angles. 70
4.4 Fault B: Comparison Voltages and Powers. 73
4.5 Three Phase to Ground Fault: Comparison Angles. 76
4.6 Three Phase to Ground Fault: Comparison Voltages and Powers. . 77

5.1 Commutation Failure Immunity Index. 85

6.1 Base Case Parameters. 90

Abbreviations

AC	**A**lternating **C**urrent
CCSC	**C**irculating **C**urrent **S**uppression **C**ontrol
DC	**D**irect **C**urrent
FACTS	**F**lexible **AC** **T**ransmission **S**ystem
HVDC	**H**igh **V**oltage **D**irect **C**urrent
IGBT	**I**nsulated **G**ate **B**ipolar **T**ransistor
LCC	**L**ine **C**ommutated **C**onverter
MMC	**M**odular **M**ulti-Level **C**onverter
PI	**P**roportional **I**ntegrator
PLL	**P**hase **L**ocked **L**oop
PS-PWM	**P**hase **S**hifted **P**ulse **W**idth **M**odulation
PWM	**P**ulse **W**idth **M**odulation
RoW	**R**ight-**o**f-**W**ay
RSF	**R**educed **S**witching **F**requency
SCR	**S**hort **C**urcuit **R**atio
SCL	**S**hort **C**urcuit **L**evel
SM	**S**ub**M**odule
THD	**T**otal **H**armonic **D**istortion
VSC	**V**oltage **S**ource **C**onverter

Terms Used in the Text

Symbol	Description
α	Firing angle
β	Equal to $\gamma + \mu$
γ	Extinction angle
Δ	Transformer connection
θ	Angle between d-axis and V_a
μ	Angle duration of volt-time area
τ	Time constant
ϕ	Angle between voltage and current
Ω	Unit for impedance
ω	Angular frequency
$_{120}$	Positive, negative and zero sequence
$_{abc}$	Phases of a three-phase system
$_{B}$	Lower arm
$_{T}$	Upper arm
pu	Per unit
$_{d}$	Real axis Park transformation
$_{q}$	Imaginary axis Park transformation
f	Frequency
n	integer
$_{dif}$	Circulating current
$_{ref}$	Reference value
s	Laplace complex argument

*	Complex conjugate
C	Capacitance
L	Inductance
I	Current
P	Active power
Q	Reactive power
R	Resistance
S	Apparent power
V	Voltage
Z	Impedance

Chapter 1

Introduction

1.1 Background

Being able to safely integrate large amounts of unregulated renewable energy has been one of the main drivers behind new converter technologies. Recent advances in the field of power electronics have spurred developments of fully-controlled semiconductors which in turn have had a significant impact on High Voltage Direct Current (HVDC) transmission. The Modular Multi-Level Converter (MMC) technology aims at reducing the need for filtering, while simultaneously handling fault scenarios in an entirely different way.

New European Union directives require member states to increase their renewable energy production to a total of 20 % by 2020. The challenge is that renewable energy, by nature, is hard to regulate. Many countries in the European Union are now looking for ways to utilize the potential of renewables. The main use of HVDC in Norway has been connections to northern Europe. Norway's highly flexible hydro power can contribute to safely integrate renewable energy in northern Europe by stabilizing the power production from solar and wind. Even though the Norwegian hydro power cannot provide energy to all of Europe, it could still make a remarkable contribution towards making Europe's power production greener and more sustainable [1].

Along with the growing demand for long distance HVDC power transmissions, more converters have been built in close proximity to each other. The interactions between more than one converter feeding into the same AC system have been widely studied in the literature. These multi-infeed systems have traditionally consisted of more than one LCC-link in the same AC system. As new MMC topologies emerges with completely different operational principles as compared to the LCC, it is important to revisit the study of multi-infeed HVDC systems

once again. This report studies the effect of a MMC-link and LCC-link in a multi-infeed HVDC system with respect to AC voltage stability and on whether the new MMC topology can mitigate the weaknesses of the LCC topology when it comes to commutation failure.

Parts of the presented material is based on the work done in the specialization project [2]. This mainly includes sections concerning different HVDC technologies and LCC control design. When necessary to achieve completeness of the master thesis, parts of the study performed in the specialization project is included.

1.2 Scope of Work

Statnett is planning to build a new HVDC interconnector between Norway and Germany (NordLink). It is going to be connected to the AC grid in Norway near by the already existing HVDC interconnector to Netherlands (NorNed). NordLink will consist of a subsea cable and a DC overhead line from the landfall of the cable to the converter station on the Norwegian side. The DC overhead line will partially go in parallel with existing 420 kV AC overhead lines. NordLink will use MMC technology, while NorNed consists of LCC technology. This multi-infeed HVDC system of NorNed and NordLink is shown in Fig. 1.1.

The purpose of this report is to investigate how the new connection of NordLink will affect the grid configuration in southern Norway. Hence the consequences of a multi-infeed HVDC system consisting of NorNed and NordLink will be explored. It is of special interest to identify whether the new MMC topology can mitigate the weaknesses of the LCC topology when it comes to commutation failure, and to investigate if the coupling effects between the AC and DC overhead lines are likely to cause problems for the power system.

The scope of this report is to:

1. Develop a simulation model of a multi-infeed HVDC system consisting of a MMC-link and a LCC-link inverting into the same AC grid. The focus is to identify the control design and operational principles of the two converter technologies. This work also consists of obtaining essential theoretical background of HVDC technologies.

2. Study the steady state and transient state behaviour of a multi-infeed HVDC system, and compare it to the present situation. For steady state the goal is to investigate the start-up behaviour of the two converters, and also to investigate the AC voltage stability. For transient state the motivation is to investigate the effects of different AC faults at various locations in the power system.

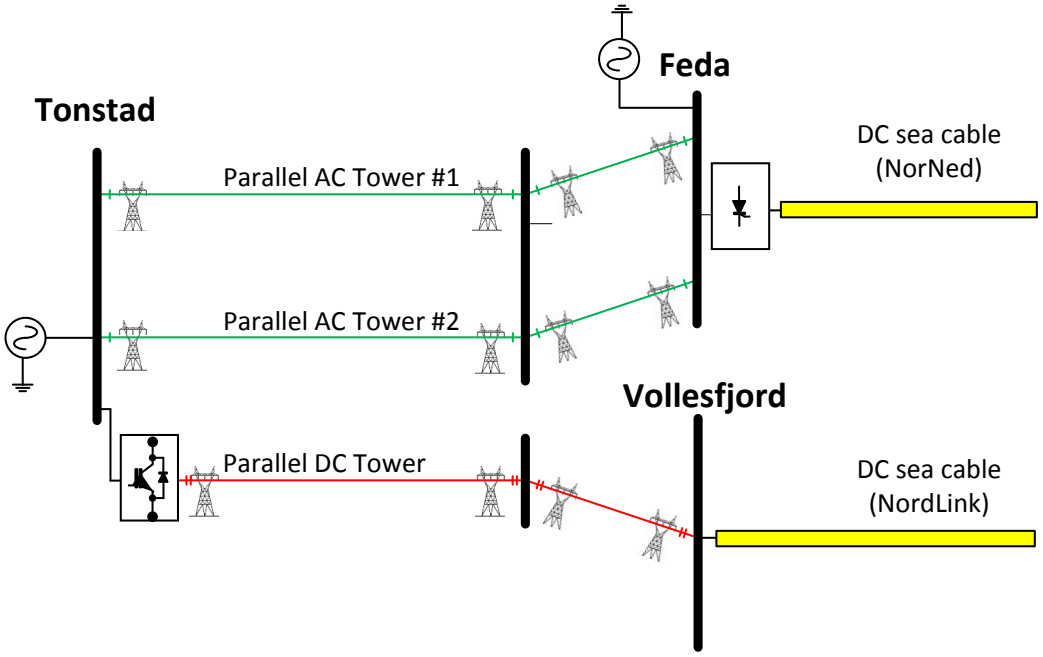

FIGURE 1.1: Overview of the Multi-Infeed Power System in Southern Norway.

3. Establish a method for detecting commutation failure, and to investigate the susceptibility to commutation failure of the multi-infeed HVDC system as compared to the present situation.

4. Investigate the consequences of AC and DC overhead lines in the same Rights-of-Way (RoW). The focus is to identify if there is any coupling effect, and investigate which parameters are critical in transient state when a single pole to ground fault occurs. Based on the analysis mitigation methods should be discussed.

The simulation tool used in this report is PSCAD. As for plotting of graphs both MATLAB and LaTeXhave been used.

1.3 Outline

The work presented in this report can be divided into five main parts. The first part consists of research related to different HVDC technologies focusing on what is commercial available (Chapter 2). It is aimed to compare the technologies and to give a theoretical backbone for the rest of the study.

The second part develops and explains the theory behind the simulation model (Chapter 3). Control objectives for the two converter technologies, namely MMC

and LCC, will be introduced. How these objectives have been implemented in the control design will be emphasized. Explanations of the transmission system will also be made.

The third part studies the performance of a multi-infeed HVDC system in the Norwegian power system (Chapter 4). Two scenarios will be developed, namely (1) a LCC stand alone system and (2) a multi-infeed system consisting of MMC-link and LCC-link, as to emphasize the difference of today's system compared to the future multi-infeed system. This includes a study of (i) start-up of the systems, (ii) load flow fluctuations in steady state and (iii) transient behaviour during various AC faults at different locations. At the end of Chapter 4 a discussion will be made regarding how NordLink affects the present grid configuration.

The fourth part is an investigation of how the multi-infeed HVDC system will affect the likelihood of commutation failures in the LCC-link (Chapter 5). A commutation failure detection method will be proposed as to identify if a commutation failure has occurred, followed by a method for describing the susceptibility to commutation failure of a converter. The immunity of commutation failure will be tested for both the multi-infeed HVDC system and the LCC stand alone system. At the end of Chapter 5 a conclusion will be made whether the new system will be more or less prone to commutation failure.

The fifth part investigates the coupling effect between the AC and DC overhead lines in the system (Chapter 6). As the overhead lines will share the same Rights-of-Way (RoW) it is probable that there will be induced currents from AC to DC and vice versa. The aim of the fifth part is therefore to investigate any coupling effect between the overhead lines, and to develop a parametric sensitivity analysis in order to identify critical parameters. At the end of Chapter 6 there will be proposed mitigation methods for the coupling effect.

The results obtained in Chapter 4, Chapter 5 and Chapter 6 will be concurrently evaluated and discussed. A summary based on the discussion will be made at the end of these chapters. A discussion chapter will therefore be omitted.

Chapter 2

Converter Technologies for HVDC

HVDC technology has a wide range of applications. HVDC makes use of compact and reliable converter technology that aims to provide large power capability, handle fault situations, limit losses and minimize the need for filters as well as leaving a small footprint in urban areas. This chapter presents and compares different converter technologies, focusing on what is commercially available today, namely Line Commutated Converter (LCC), two-level Voltage Source Converter (VSC) and Modular Multi-level Converter (MMC).

2.1 Line Commutated Converter

Line Commutated Converter (LCC) is the most common converter in HVDC applications, and is known as the classical HVDC [3]. The first commercial HVDC transmission line using mercury-arc valve converters was built in 1954 between the island Gotland and the mainland in Sweden, and was in 1967 upgraded with thyristor valves [4].

LCC technology is based on thyristor valves, which are devices that can be triggered into conduction mode by applying a pulse to the gate terminal, provided that the voltage over the thyristor is positive [5]. The gate terminal can only turn the thyristor ON and not OFF. The thyristor will keep conducting until the AC current crosses to zero, where the gate regains its blocking potential. The fact that the thyristor can be turned on makes it more controllable than a diode [6].

In Fig. 2.1 a graphical representation of LCC is shown, a 12-pulse configuration with two six-pulse bridges in series. The DC current in a LCC cannot change direction instantaneously because of the line inductance ($V_L = L\frac{di}{dt}$), and the

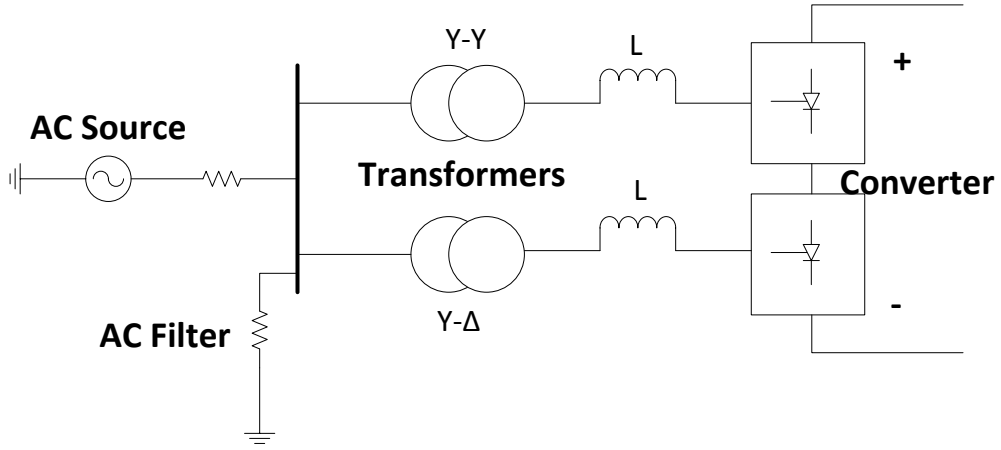

FIGURE 2.1: Line Commutated Converter, 12-Pulse Configuration.

current direction therefore remains the same [7]. The power flow can be reversed by changing the voltage polarity at the converter stations. From AC side the LCC can therefore be seen as a current source converter.

In a LCC system the converter station consumes reactive power. This is due to the fire angle control in the converter. Without the fire angle control the thyristor will start to conduct current at the instant when the voltage over the thyristor becomes positive. However, this would lead to unwanted harmonics. Instead the valves are triggered to conduct after a time delay. The difference in the natural fire instant and the actual fire instant can be measured, and is called the fire angle. Because of this delay, the current will always lag the voltage, thus making the converter consume reactive power [4].

2.2 Voltage Source Converter

A two-level Voltage Source Converter (VSC) is based on switching of insulated gate bipolar transistors (IBGTs). Diodes are connected in anti-parallel to the IGBTs to ensure four quadrant operations in an IV plane. IGBTs have, in addition to the thyristors turn on ability, also a turn off ability. It can be turned on and off in about 1 μs [5]. The first HVDC cable using VSC was introduced in Sweden between Hellsjön and Grängesberg in 1997.

In Fig. 2.2 a graphical representation of a VSC is shown. A VSC is self-commutated since the current can be turned on and off, and it does not need to commutate against a network consisting of rotating machines [8]. The current can therefore

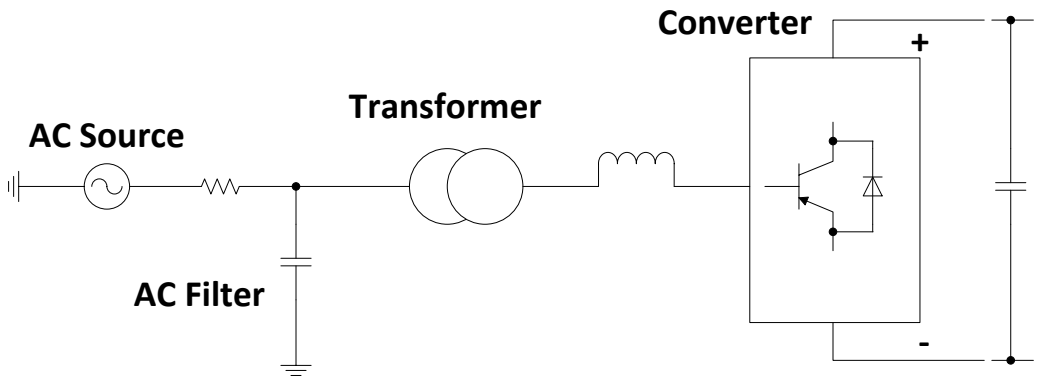

FIGURE 2.2: Voltage Source Converter.

either lag or lead the AC voltage. This means that the converter can either consume or supply reactive power to the grid [9]. The voltage polarity in a VSC is fixed. In order to reverse power flow the current must change direction. The converter can therefore be seen as a voltage source [7].

The AC voltage in a VSC is created by using a Pulse Width Modulator (PWM) that switches very fast between two fixed voltages [8]. Low pass filters must be used to obtain the fundamental frequency in the AC system, and to remove unwanted distortion [10]. In a two- or three level converter a very large number of IGBTs are connected in series, depending on the voltage level. This is because the IGBTs can only block a few kilovolts each, thus requiring as many as a few hundred per converter arm to function properly in high voltage applications. All the series-components have to switch simultaneously to ensure uniform voltage distribution across each arm. This requires accurate and advanced switching technology [11].

2.2.1 Pulse Width Modulation

To generate two different voltage outputs, a PWM is normally used. A time varying control signal (V_c) is compared to a triangular waveform (V_{tri}) with much higher frequency, (f_s). This frequency is the same as the switching frequency of the IGBTs, and can be typically around 1000 Hz. The control signal is normally a sinusoidal signal, hence naming the method sinusoidal PWM, and is illustrated in Fig. 2.3. When $V_c > V_{tri}$ the IGBT is turned ON (PWM signal = 1) and when $V_c < V_{tri}$ the IGBT is turned OFF (PWM signal = -1)

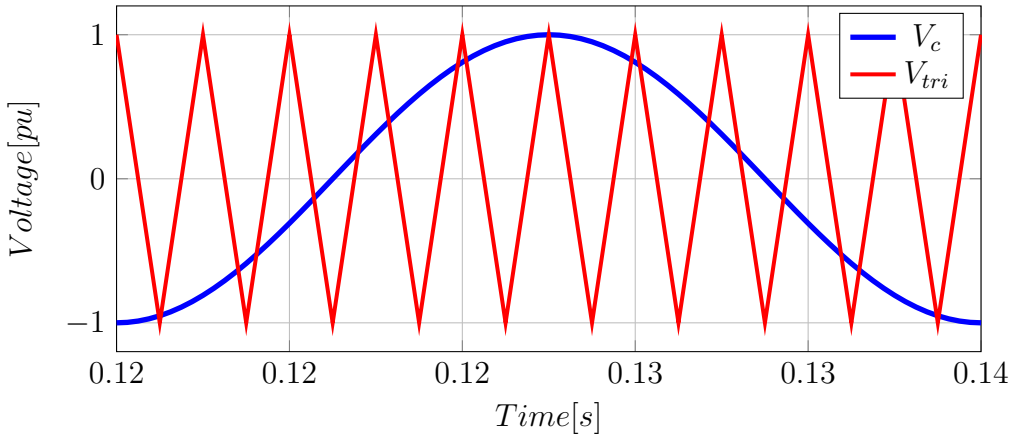

(a) Comparison between V_c and V_{tri}.

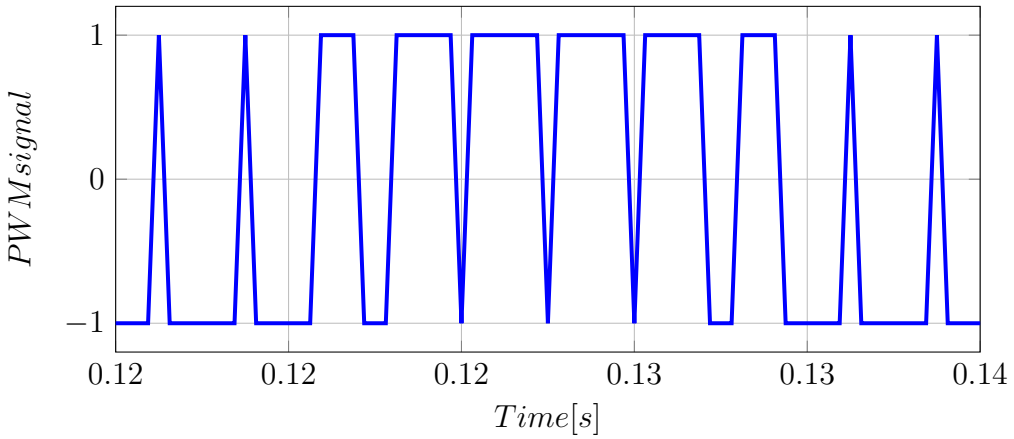

(b) PWM Output Signal.

FIGURE 2.3: Pulse Width Modulator.

2.3 Modular Multi-Level Converter

A new type of VSC called Modular-Multi-level Converter (MMC) was first proposed in 2003 [12]. The world's first connection built with MMC technology was the Trans Bay Cable Project in San Francisco in 2010 [13]. A schematic representation of a MMC is shown in Fig. 2.4. A MMC consists of three phases and six arms, much like the VSC. Each arm consists of a large number of submodules (SM). Every SM has a DC capacitor for energy storage, and a number of IGBTs depending on the MMC variant. By careful switching of the IGBTs, the SM is either switched ON or OFF. Every SM therefore has the ability to generate either 0 or V_c [11]. Instead of switching between two, the MMC is hence able to switch between many different voltage levels, equal to the number of SM in each arm. This significantly decreases the total harmonic distortion (THD) in the converter [11]. The technology is scalable, which means that the desired voltage output can be achieved by adding many SM in series [13].

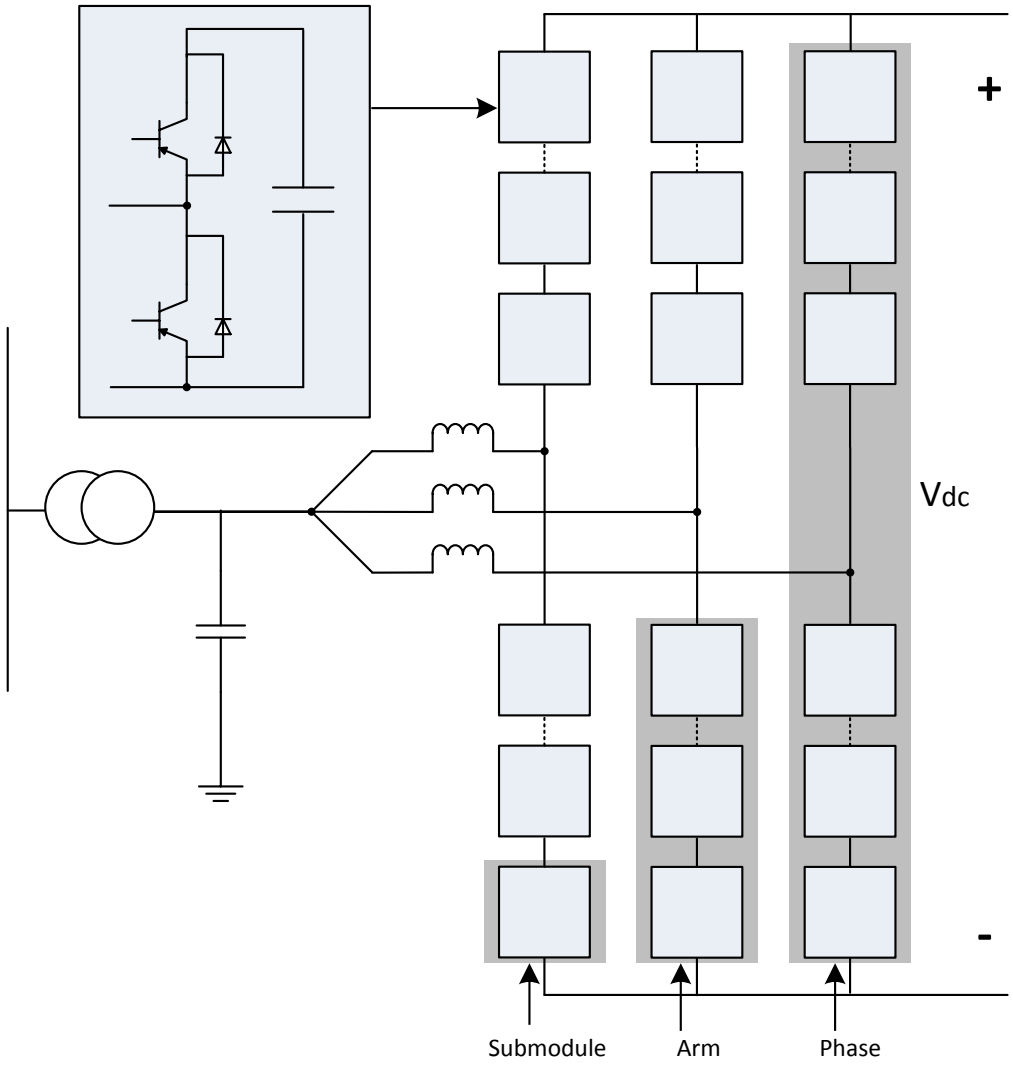

FIGURE 2.4: Modular Multi-level Converter.

In order to continue reliable operation if a fault inside a SM occurs, redundant SMs are added in each converter arm. One way of implementing redundant SMs is to bypass it in normal operation. It is possible to design the converter so that upon a failure in one SM, the faulty SM is bypassed (and the redundant SM connected) without increasing the voltage over the remaining SMs. The faulty SM is now just another module that produces zero voltage. Redundant SMs decrease the circulating second order harmonic current in the converter arm. This current is contributing to higher losses, thus reducing it would lead to lower harmonics and smaller filter size. By adding redundant SMs one simply increases the availability, although increasing complexity, conduction losses and total cost of the converter [14].

2.4 Comparison of LCC, VSC and MMC

A LCC is line commutated and must rely on the AC network to commutate properly. The LCC therefore has some technical restrictions, such as a minimum short-circuit power in the AC grid [11]. With the use of IGBTs, the MMC and VSC are able to switch the current off. Being self-commutated makes them an excellent choice for weak grid connections, as they are able to feed power to passive networks [15]. A VSC switches with one single PWM, while the MMC uses a more sophisticated PWM scheme depending on the topology, built up with small discrete voltage steps. A VSC and MMC can control both active and reactive power flow independently, and is able to either supply or consume reactive power [10]. The fast control mechanism in the VSC and MMC makes it possible to change the voltage amplitude and phase very quickly. The converter can thus be used to energize a grid after a blackout, a so called black start capability [15]. This is very useful for unstable wind farms in remote locations [16]. Both the VSC and MMC reduce the need for filtering substantially compared to the LCC. It is therefore a preferred choice on locations where weight and size are important, such as offshore installations [3].

The MMC is superior to the VSC in many ways. The problem associated with simultaneous switching in a VSC to ensure uniform voltage distribution does not yield for a MMC. The switching frequency of the individual SM is lower, typically three times each cycle [17], and the switching losses are therefore lower than for a classical VSC [18]. Determining converter losses in a LCC is well documented. The standard IEC 61803 describes this method in detail [19]. For calculating power losses in a VSC the same principle is used, but since there are major differences in converter technology a new standard was recently drafted, namely IEC 62751 [20]. In a MMC the switching losses are not the dominant part of the losses, but rather conduction losses in the SMs. In practice this means that a half-bridge has lower losses than a full-bridge. Calculating conduction losses in a SM is quite complicated, and there is not yet any standard available for such calculations. The overall calculation of a half-bridge and full-bridge MMC is according to [21] about 1% and 1,3%, which is still higher than LCC ($\simeq$ 0,75%), but lower than VSC ($\simeq$ 1,7% [15]).

MMC is a scalable technology, and can therefore be used at the highest voltage levels [18]. In the case of a single component failure in a MMC the HVDC transmission system can still operate without interruption. It is therefore possible to wait with the component replacement until the next scheduled shut-down, which is a great advantage [11]. A half-bridge MMC requires twice as many IGBTs as a classical VSC, and a full-bridge four times as many. Each SM also requires a DC capacitor, making the MMC heavier and bulkier than a VSC for the same rating [17].

Table 2.1: Comparison of Commercially Available Converter Technologies

	LCC	**VSC**	**MMC**
Semiconductor	Thyristor	IGBT	IGBT
Losses [%]	0.75	1.7	1.0
Filters	Large	Small	Small
Black Start Capability	No	Yes	Yes
Handle DC faults	Yes	No	No
Multi-terminal	Difficult	Yes	Yes
Reactive Power Control	No	Yes	Yes
XLPE cables	No	Yes	Yes
Highest power rating [MW]	7200	400	700
Highest voltage rating [kV]	±800	150	500
Longest cable system [km]	2100	203	970

The LCC must change voltage polarity in order to change power flow. VSC and MMC allow rapid power reversal without changing the voltage polarity. For this reason XPLE cables can be used for VSC and MMC, but not for LCC since these cables cannot handle the stress from a rapid voltage polarity change. A LCC uses oil-impregnated cables instead [22]. A multi-terminal HVDC system is easier to implement with a VSC or MMC than a LCC since the voltage polarity is the same for both converter sides.

The main advantage of the LCC is the DC fault handling. LCC converters can clear DC faults without opening any mechanical switchgear. In a VSC or MMC, every IGBT is connected to an inverse-parallel diode in order to conduct current in both directions. This means that during fault the diode can still conduct current even though the IGBTs are set to block mode. The converter can therefore not block the current path in an efficient way, which eventually leads to high currents and flashovers. For a point-to-point connection it is sufficient to open AC breakers at the converter stations to clear the DC fault. However this is more problematic in a multi-terminal topology, which makes DC breakers the only viable solution. Many advanced DC breakers have been developed such as ABBs prototype hybrid HVDC breaker for 320 kV [23], which is aimed to help overcome these challenges. New advanced MMC technologies such as full-bridge MMC can also deal with DC faults, but this arrangement requires twice as many IGBTs. A comparison of LCC, VSC and MMC has been made in Tab. 2.1.

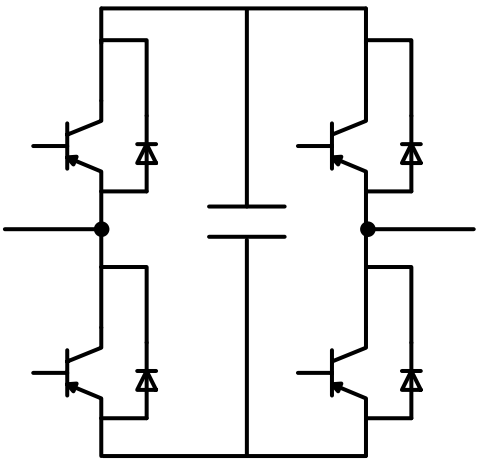

FIGURE 2.5: Submodule in a Full-Bridge MMC, H-Bridge.

2.5 Full-Bridge MMC

Fig. 2.5 illustrates a SM in a full-bridge MMC, consisting of four IGBTs and one capacitor. This arrangement requires twice as many IGBTs as the half-bridge variant. The capacitor can now either be bypassed ($V_{SM} = 0$), connected with positive polarity ($V_{SM} = V_c$) or connected with negative polarity ($V_{SM} = -V_c$) depending on the switching state. Due to its ability to produce a bipolar output, makes a full-bridge able to quickly recover to continous operation after a DC fault [24]. When a DC fault occur the IGBTs are turned so that the cell capacitor produces a signal that opposes the fault current direction, hence blocking current flowing from one side to the other. This is something a classical VSC or half-bridge MMC cannot do.

Each phase consists of two arms, and are both set to produce an offset sine-wave output voltages equal to $\frac{1}{2}V_{dc}$, with AC voltage components shifted 180°. Summing one phase together gives in theory a total of V_{dc}. The voltage over all three phases are identical since they are connected in parallel [17].

In a full-bridge converter all the six arms conduct current at the same time. The current direction in one valve changes every 120°. The negative sequence current that flows in the valve contributes to a circulating current component between the phases. This circulating current helps the DC capacitor to operate in a balanced state, and is important for the converter. To balance the capacitor charge in a SM the active power must equal zero for every cycle. By looking at Eqn. 2.1 one can see that it would be impossible to maintain a balanced state without the negative current component [17].

$$\int_{cycle} V_{valve}(t) I_{valve}(t) dt = 0 \tag{2.1}$$

Despite the full-bridge MMC superior DC fault handling compared to the half-bridge, it remains a question whether this solution is cost effective or not. A full-bridge is more expensive to build, and also generates higher power losses due to the increased conduction losses in the SM. A recent study [25] has compared the cost two alternatives, the half-bridge MMC with a proposed new hybrid HVDC-breaker and a full-bridge MMC, suggesting alternative one to be the best choice.

2.6 Hybrid Multi-Level VSC

A two-level VSC can only produce two different output voltages and need a PWM with very high switching frequency in order to produce the desired signal. A half-bridge MMC solves this problem with SM in series, but this requires twice as many IGBTs. It also not able to handle DC faults. The full-bridge MMC is able to efficiently block DC faults, but doubles the amount of IGBTs once more. Recent research have developed a new technology that combine the advantages of VSC and MMC, in order to reduce the number of IGBTs, and in addition is able to block DC faults.

The new proposed converter is a hybrid multi-level VSC with cascaded H-bridge, illustrated in Fig. 2.6. It is a combination of a two-level VSC, with additional full-bridge SMs connected in series in each phase on the AC side of the converter. The SMs produce a wave-shaping circuit and operate as an active filter to eliminate harmonics in the converter [17]. The VSC operates in the traditional way, but the PWM can now operate at a much lower frequency. Proved by [26], the switching frequency is only 150-Hz hence leading to much lower switching losses.

A hybrid multi-level VSC need one quarter of the SM that a full-bridge MMC need. Similar to the full-bridge MMC this converter also have DC fault reverse-blocking capability. This is achieved in the same way; by switching the cell capacitor to reverse polarity to produce a signal that opposes the fault current. This will suppress the fault current, hence no direct path from AC to DC side. Since there is no current path there will be no active or reactive power transfer between the two sides of the converter. Consequently, the hybrid multi-level VSC can improve the stability of the AC network during DC fault situations. When the fault is cleared, the converter can quickly continue to transfer power, which is a great advantage [17, 26].

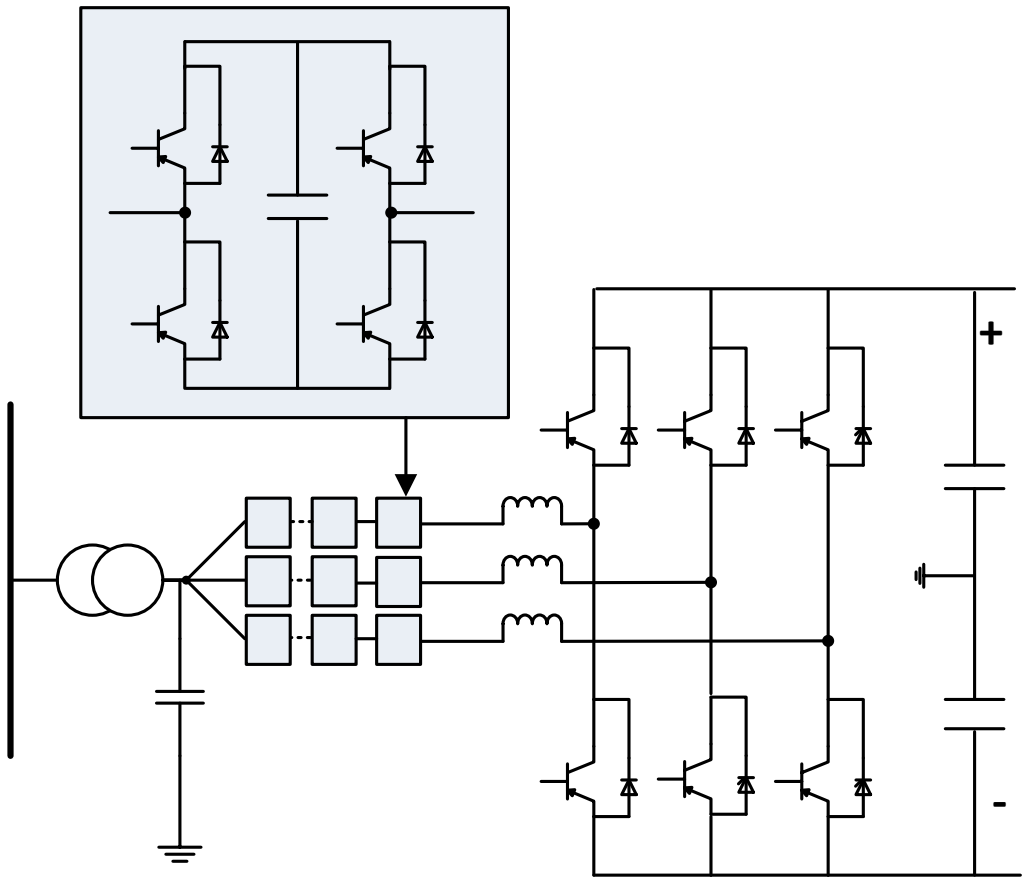

FIGURE 2.6: Hybrid Multi-Level VSC

2.7 Multi-Infeed HVDC Systems

Along with the growing demand for long distance HVDC power transmissions, more converters have been built in close proximity to each other [27]. A system with more than one converter feeding power into the same AC system is defined as a multi-infeed HVDC system. In the extreme case of Brazil, two bipole LCC-HVDC connections feed into the same place in the AC network [28]. A disturbance in the AC grid will affect both these converters equally, and a commutation failure in one of them will also lead to commutation failure in the other. However, most multi-infeed systems are electrically separated from each other, represented by an impedance (shown by Z_{ij} on Fig. 2.7). The two converters will have less interaction, as compared to the previous case with two converters at the same location [28]. Most of the existing multi-infeed HVDC systems today consists of two or more LCC-HVDC feeding into the same AC system. In these multi-infeed HVDC systems there are according to literature a serious concern related to the AC voltage stability, especially in weak AC systems [29].

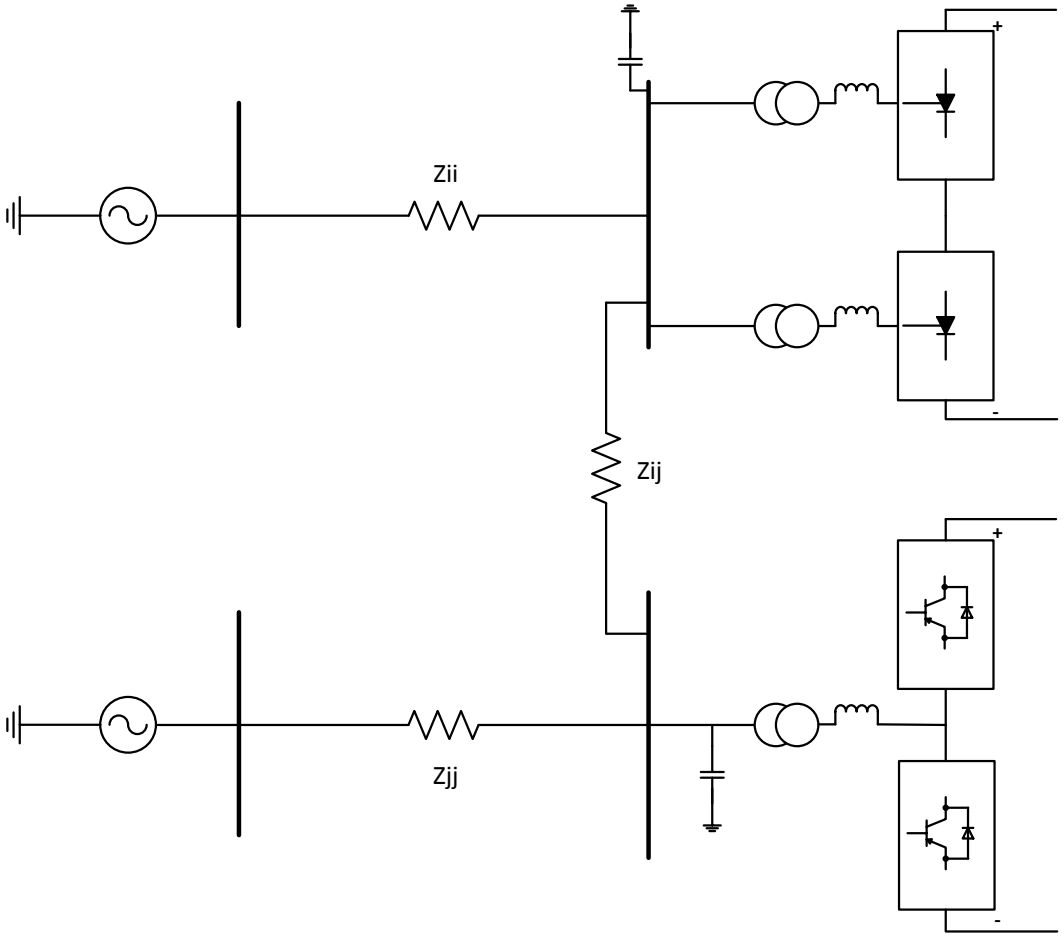

FIGURE 2.7: Multi-Infeed HVDC System Consisting of MMC and LCC.

The development of HVDC technologies have had a significant boost the last decade, with the new MMC topology. As the MMC in many cases appears as the best option for new HVDC connections, a combination of MMC and existing LCC in a multi-infeed system has emerged. Fig. 2.7 shows a graphical representation of a MMC and LCC feeding into the same AC system, separated by an impedance Z_{ij}. The first system with this kind of configuration is the Skagerrak 4 connection between Norway and Denmark [30]. Skagerrak 4 is in the construction phase and will be implemented at the end of 2014. Another project is the NordLink cable between Norway and Germany. The NordLink, consisting of a bipolar MMC-HVDC, will be connected in close proximity to the already existing bipolar LCC-HVDC connection to Netherlands, NorNed. NordLink is in the planning phase and will be implemented by the end of 2018 [31]. These new multi-infeed systems raises the question on how the two completely different converter technologies will interact with each other, especially with respect to voltage stability, and on whether the new MMC-topology can mitigate the weaknesses of the LCC when it comes to commutation failures.

2.8 Use of Converters Today and in the Future

The future trend in Asia, especially countries such as India and China, is still the old LCC technology. This is mainly due to bulk transmission from remote locations using Ultra HVDC, to obtain lower currents and thereby limit losses. The first Ultra HVDC multiterminal HVDC is planned to go from Biswanath Chariali in north-east India to Agra in central India [32]. Low losses and high power ratings makes LCC a suitable choice.

The future trend in Europe is the MMC. Germany is shifting their power production from nuclear energy and fossil fuels to wind and solar power. To facilitate this transition Germany needs to increase their transmission capacity. HVDC seems as the most economical choice compared to HVAC, and it would also provide stability and reliability needed to safely integrate large amounts of wind and solar power [33]. Therefore MMC technology would be a preferred choice. Building LCC in Norway is not economical due to the Norwegian grid code (FIKS) [34], which states that a LCC should be self-supportive with a short circuit capacity of 2.5. In reality a LCC requires 0.7 MVA compensation for 1 MVA. MMC is more cost effective than LCC with this requirement taken into consideration. The Skagerrak 4 is the fourth cable connecting Norway and Denmark and brings the total transfer capacity up to 1640 MW. It will be the first time that LCC and MMC is tied together in a bipolar configuration [35]. NordLink is planned to be two cables similar to Skagerrak 4 in a bipolar connection with a total transfer capacity of 1400 MW. The NordLink interconnector will be connected to the same area as the already existing NorNed interconnector, which is a bipolar LCC. This has never been attempted before.

Table 2.2: List of HVDC Projects [13, 30, 35].

In Operation	Voltage [kV]	Power [MW]	Length [km]	Converter
Jinping-Sunan (2013)	±800	7200	2090	LCC
Rio Madeira (2013)	±600	6300	2375	LCC
Dörpen, Germany(2013)	320	800	165	MMC
San Francisco, USA (2010)	200	400	85	MMC
Planned	Voltage [kV]	Power [MW]	Length [km]	Converter
Norway-Germany (2018)	±500	1400	500	MMC
Agra, India (2015)	±500	6000	1728	LCC
Dörpen, Germany(2015)	±320	900	135	MMC
Norway-Denmark (2014)	500	700	240	MMC

Chapter 3

Control Design

This chapter will introduce the basic principle and control design of the simulation model that has been developed in this report. The system can be seen in Fig. 1.1 on page 3. It consists of two HVDC interconnectors, namely NorNed and NordLink. Both connections are connected to the same AC network in Tonstad, Norway. NorNed is modelled as AC overhead line, LCC inverter, DC sea cable and LCC rectifier. NordLink is modelled as a MMC inverter, DC overhead line, DC sea cable and MMC rectifier. Furthermore, the AC and DC overhead lines of the two interconnectors go in parallel for 38 km before splitting into separate parts. The main technical data for the model can be seen in Tab. 3.1. Section 3.1 will introduce the control design of the MMC, Section 3.2 will introduce the control design of the LCC and Section 3.3 will describe the AC and DC transmission system.

3.1 Control Design of MMC

The control objective of a MMC system is to accurately control both active and reactive power independently. This is done by controlling the reference signals sent to the PWM generator. These reference signals are developed through several steps. There is no need for communication between the sending and receiving end in a MMC-link, and they can therefore be controlled separately. Both sides have the same structure and a similar control system can be adopted on both sides. The only difference is the master controller, explained in Section 3.1.1. In general the MMC control system can be divided into two main parts, namely classical 2-level VSC control and additional MMC control, see Fig. 3.1. The VSC controller is an overall controller for DC voltage, AC voltage, active and reactive power. Its main purpose is to keep these values within acceptable limits to ensure safe operations. In addition the MMC also needs controllers to stabilize internal variables [18].

Table 3.1: Technical Data for the System

NorNed	**Line Commutated Converter**	
Power	700 MW	
DC voltage	450 kV	
Cable Length	580 km	
Overhead AC Line	50 km	
NordLink	**Modular Multilevel Converter**	
Power	1400 MW	
DC voltage	±500 kV	
Cable Length	570 km	
Overhead DC Line	53 km	
Parallel Overhead Line	38 km	
	AC voltage	**Short Circuit Power**	**X/R**
Tonstad	420 kV	6000 MVA	14
Feda	420 kV	6000 MVA	14

Primarily this is a matter of balancing voltage and currents between each arm and phase in the converter.

3.1.1 Master Control of the Converter Stations

Every MMC-link consists of an overall master controller, which mainly focuses on maintaining safe operation in an efficient way. The master controller sits on top of all the other controllers in the system, and decides which control mode each terminal in the MMC-link uses. A MMC converter station is capable of operating on two different modes [36],

(i) DC voltage control mode (DC voltage regulator)

(ii) Current control mode (power dispatcher)

A point-to-point MMC connection is set up so that at least one station uses DC voltage control mode. The system used in this report is set up so that the two stations uses different control modes. The *DC voltage regulator* station is maintaining the DC voltage by alternating the voltage reference $V_{dc,ref}$. This is done by rectifying or inverting AC power from the grid, thus maintaining sufficient DC voltage across the SM capacitors. The DC voltage regulator station is used as DC power slack bus to ensure power balance in the system. The *power dispatcher* station is controlled by alternating the DC power reference P_{ref} in order to keep the

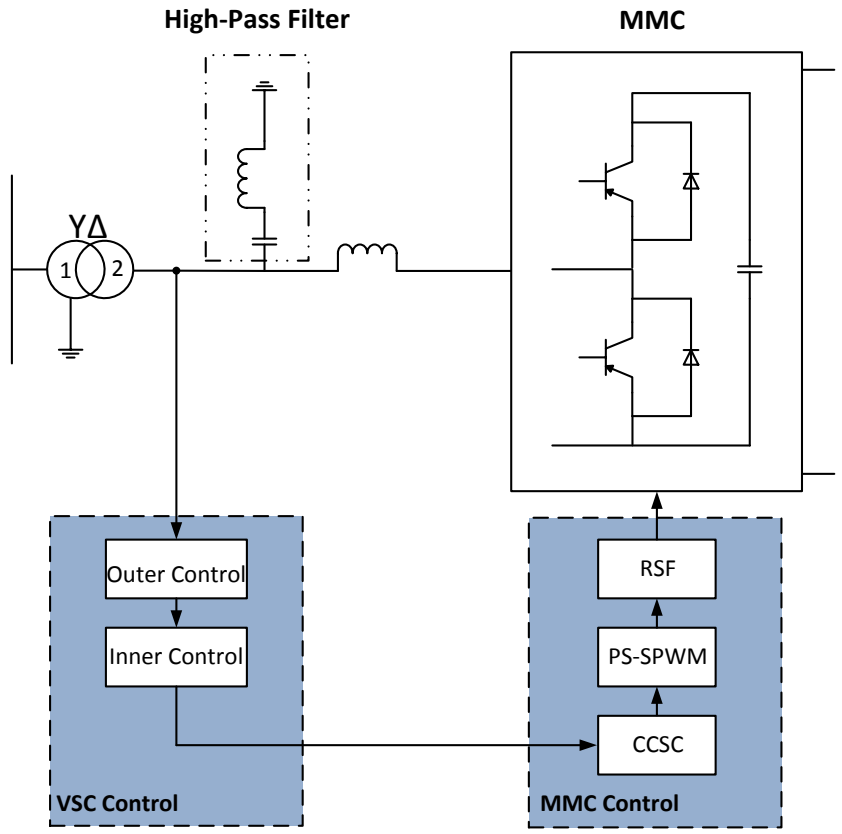

FIGURE 3.1: Control Hierarchy for MMC-HVDC.

DC power in the HVDC-link constant. In addition each converter station is also able to control the AC voltage at its terminal by either supplying or consuming reactive power [36, 37].

3.1.2 MMC System Structure

Shown in Fig. 3.3 a MMC consists of 3 legs, one for each phase where k ∈ {a,b,c}. Each phase consists of two arms, one upper arm (T) and one lower arm (B). Each arm consists of one inductor and n submodules (SMs). The SM is a half-bridge configuration consisting of a capacitor and two valves, see Fig. 3.2. Each valve contains one IGBT and one freewheeling diode in anti-parallel. The half-bridge is constructed so that only one of the two valves are switched ON at the same time.

Upon normal operation the SM capacitor can either be bypassed, charged or discharged [38]. Depending on the current direction and switch positions there are six possible ways to reach these three states, shown in Fig. 3.2 [11]:

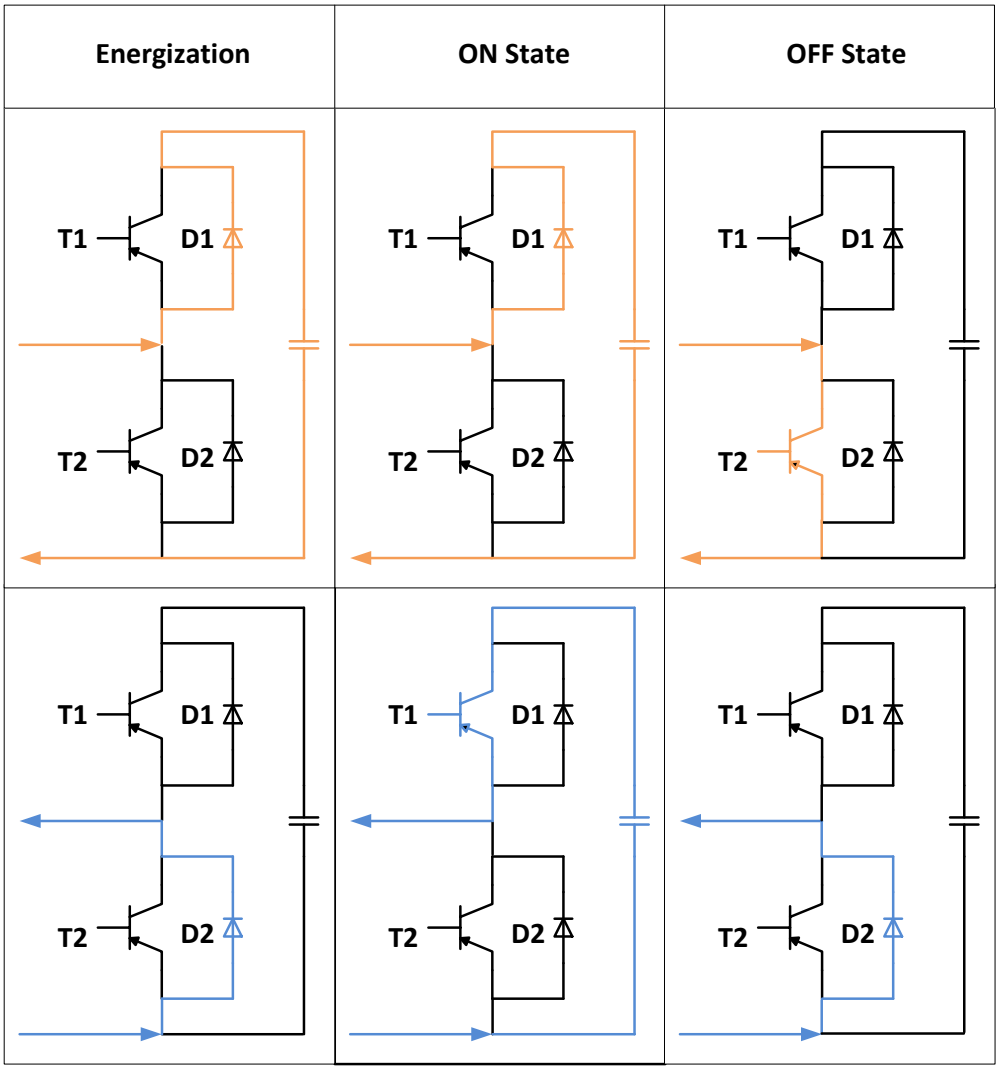

FIGURE 3.2: Half-Bridge Submodule Configuration in MMC: Three Different Switching States.

- Energized: T1 is OFF and T2 is OFF. In this situation the converter is blocked. Depending on current direction the capacitor is either charged or bypassed. This happens typically upon start-up of the converter or during faults, and does not happen under normal conditions. If a serious failure occur all the valves in the converter will be switched to OFF mode.
- ON State: T1 is ON and T2 is OFF. Capacitor is connected ($V_{sm} = V_c$). The capacitor is either charged or discharged depending on current direction.
- OFF State: T1 is OFF and T2 is ON. The capacitor is bypassed and the voltage output of this specific SM is zero ($V_{sm} = 0$). This can be achieved in two ways depending on the current direction.

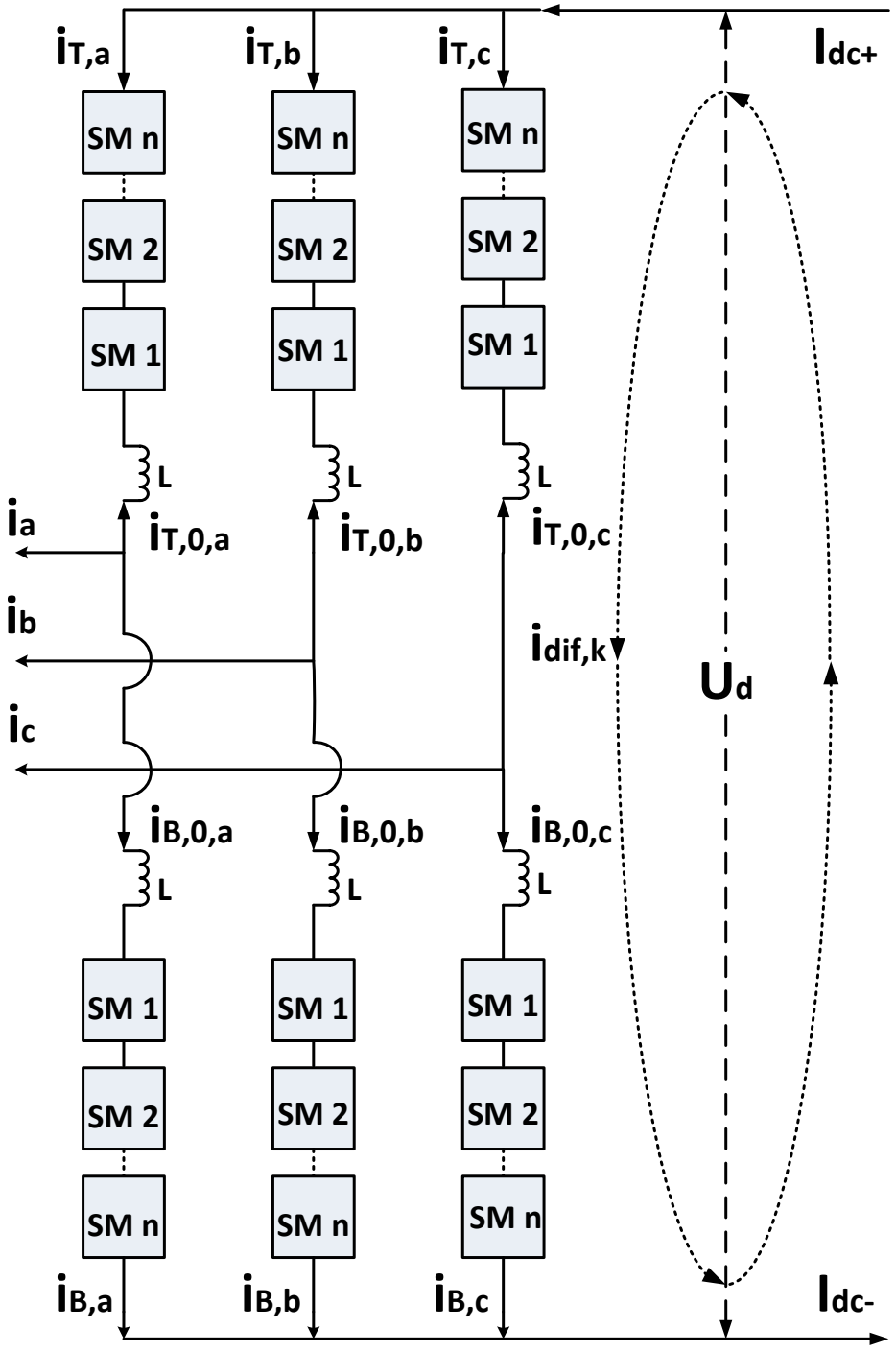

FIGURE 3.3: MMC Structure.

Each arm in the converter builds up a discrete signal with the SMs switched ON or OFF depending on the gating signal sent from the PWM. PWM switching technique is discussed in detail in Section 3.1.6. The resulting signal of the arm can be seen as a sinusoidal signal.

3.1.3 MMC Currents

The terms in Fig. 3.3 is explained in Tab. 3.2. In a MMC the arm currents are continuous, which makes a balancing DC capacitor unnecessary [39]. A circulating current between the phases occurs due to inner voltage differences between each phase [40]. This current can be measured as a negative sequence current with twice the fundamental frequency [41]. It can therefore be seen as a second harmonic current, and contributes to higher power losses in the converter as well as ripple in the SM voltages. This circulating current does not influence the AC voltages or currents and is contained inside the converter, although it is important to control it in order to minimize losses and imbalance between the arm currents. The currents in the three phases can be broken up into different components, see Fig. 3.3. The control systems with respects to the currents are designed to [39]:

Table 3.2: Explanation of Currents in MMC

Term	**Explanation**
k	Phase a,b,c
i_k	Output current phase a,b,c
$i_{T,k}$	Current upper arm phase a,b,c
$i_{B,k}$	Current lower arm phase a,b,c
$i_{dif,k}$	Circulating current phase a,b,c
$i_{T,0,k}$	Zero sequence current upper arm phase a,b,c
$i_{B,0,k}$	Zero sequence current lower arm phase a,b,c
$i_{dc,+}$	DC current positive pole
$i_{dc,-}$	DC current negative pole

- Achieve equal currents in lower and upper arm ($i_{T,k} = i_{B,k}$)
- Achieve equal phase contribution to the DC current ($i_{T,a} = i_{T,b} = i_{T,c} = \frac{I_{dc+}}{3}$)
- Eliminate or minimize zero sequence currents ($i_{0,k} = 0$)
- Minimize circulating currents ($i_{dif,k} \approx 0$)

Assuming that the zero sequence currents are perfectly eliminated, the currents can be written as follows [41],

$$i_{T,k} = i_{dif,k} + \frac{i_k}{2} \tag{3.1}$$

$$i_{B,k} = i_{dif,k} - \frac{i_k}{2} \tag{3.2}$$

$$i_{dif,k} = \frac{i_{T,k} + i_{B,k}}{2} \tag{3.3}$$

3.1.3.1 Circulating Current Suppression Control (CCSC)

The Circulating Current Suppression Control (CCSC) have two main objectives, (i) to eliminate zero sequence currents and (ii) to suppress the circulating current. The zero sequence current is defined in the following way [39],

$$I_0 = (I_a + I_b + I_c) = (I_{dc,+} - I_{dc-}) \tag{3.4}$$

In order to eliminate the zero sequence current one has to keep the positive and negative DC current equal. This is done by alternating the PWM reference signal. For instance if $I_{dc+} > I_{dc-}$ a positive reference signal is added to the upper arm currents equal to half the difference, and a negative reference signal is added to the lower arm currents equal to half the difference. This means that whenever $I_{dc+} \neq I_{dc-}$ the controller will try to minimize the error, leading to a suppression of the zero sequence current [39].

The block diagram for the CCSC can be seen in Fig. 3.4. On Fig. 3.4(a) the circulating current is first calculated (according to Eqn. 3.3) and transferred from abc $\rightarrow$ dq reference frame. Due to the fact that the circulating current is contained in the negative sequence, the coordinates are transformed from abc $\rightarrow$ dq with $\theta = 2\omega t$ (details in Appendix B on page 123). The circulating current is then processed through a PI-controller and transferred to dq $\rightarrow$ abc.

On Fig. 3.4(b) the voltage reference sent from the inner current controller (explained in Section 3.1.5.3 on page 28) is altered with the voltage difference calculated in Fig. 3.4(a). This reference signal is sent to the PWM generator, which controls the firing of the two valves in each SM. The PWM generator is explained in detail in Section 3.1.6 on page 32.

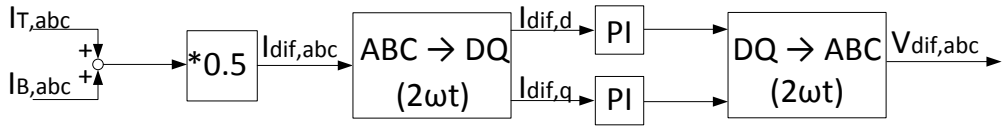

(a)

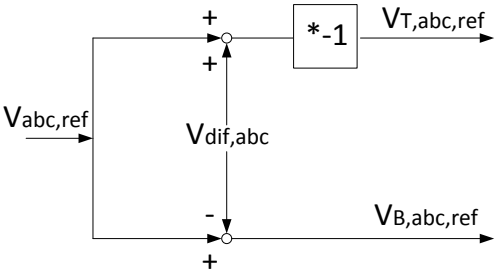

(b)

FIGURE 3.4: Circulating Current Suppression Control.

3.1.4 MMC Voltages

In terms of controlling the voltages in the HVDC-link there are essentially two things that needs to be governed [39],

- Overall DC voltage control (average value = 1 pu)
- SM capacitor voltage balancing

In a traditional two-level VSC the overall DC voltage is controlled by the DC capacitor. However, in a MMC the DC capacitor is omitted, and the DC voltage must be controlled in a different way. In order to keep the DC voltage constant near 1 pu, the total energy stored in the converter must be regulated. This is done by controlling the energy stored in the SM capacitors. The average capacitor voltage ($V_{c,av}$) can be calculated in the following way,

$$V_{c,av} = \sum_{i=1}^{n} V_{c,i} = V_{dc,ref} \tag{3.5}$$

where $V_{c,i}$ is the capacitor voltage of SM i and $V_{dc,ref}$ is the DC voltage reference (=1 pu). $V_{c,av}$ is regulated by alternating the power reference signal in the PQ-controller. For instance if the average capacitor voltage is less than the DC

reference, a negative ΔP_{ref} is added to the P_{ref} in the PQ-controller. This leads to less power injected into the AC grid. The DC power still remains the same, leading to an increase in the stored energy in the capacitors. [39]

The capacitor voltage in each SM are balanced in three different ways,

i) Within each arm

ii) Within each phase

iii) Between the three phases

The control of these are done with the CCSC, outer current controller, inner current controller and the PWM controller.

3.1.5 MMC Active and Reactive Power Control

The active and reactive power controllers of a MMC is controlled in the same way as in a two-level VSC, and is hence called VSC controller in Fig. 3.1. In order to establish a control system for active and reactive power, vector control approach has been used. To be able to do so an axis transformation from a natural reference frame (abc) to a synchronous reference frame (dq) is done. The advantage of the vector control method is that the vectors in the synchronous frame appear as constant vectors. It is therefore possible to remove steady state errors with PI-controllers. The power controller consists of two current controllers, namely inner current controller and outer current controller, and these two will be explained throughout this section.

3.1.5.1 System Description

Fig. 3.5 shows the converter system that will be analysed. Using the Kirchhoff's voltage law the system can be expressed as follows,

$$\begin{bmatrix} V_a \\ V_b \\ V_c \end{bmatrix} = L\frac{d}{dt}\begin{bmatrix} i_a \\ i_b \\ i_c \end{bmatrix} + \begin{bmatrix} V_{a,conv} \\ V_{b,conv} \\ V_{c,conv} \end{bmatrix} \tag{3.6}$$

where V_{abc} are phase to ground voltages on AC side, L are phase line inductances, i_{abc} are phase currents on AC side and $V_{abc,conv}$ are voltage at converter AC side. By transforming from abc to dq reference frame with equation Eqn. B.3 on page 124 in Appendix B.3, the following equation can be obtained [42],

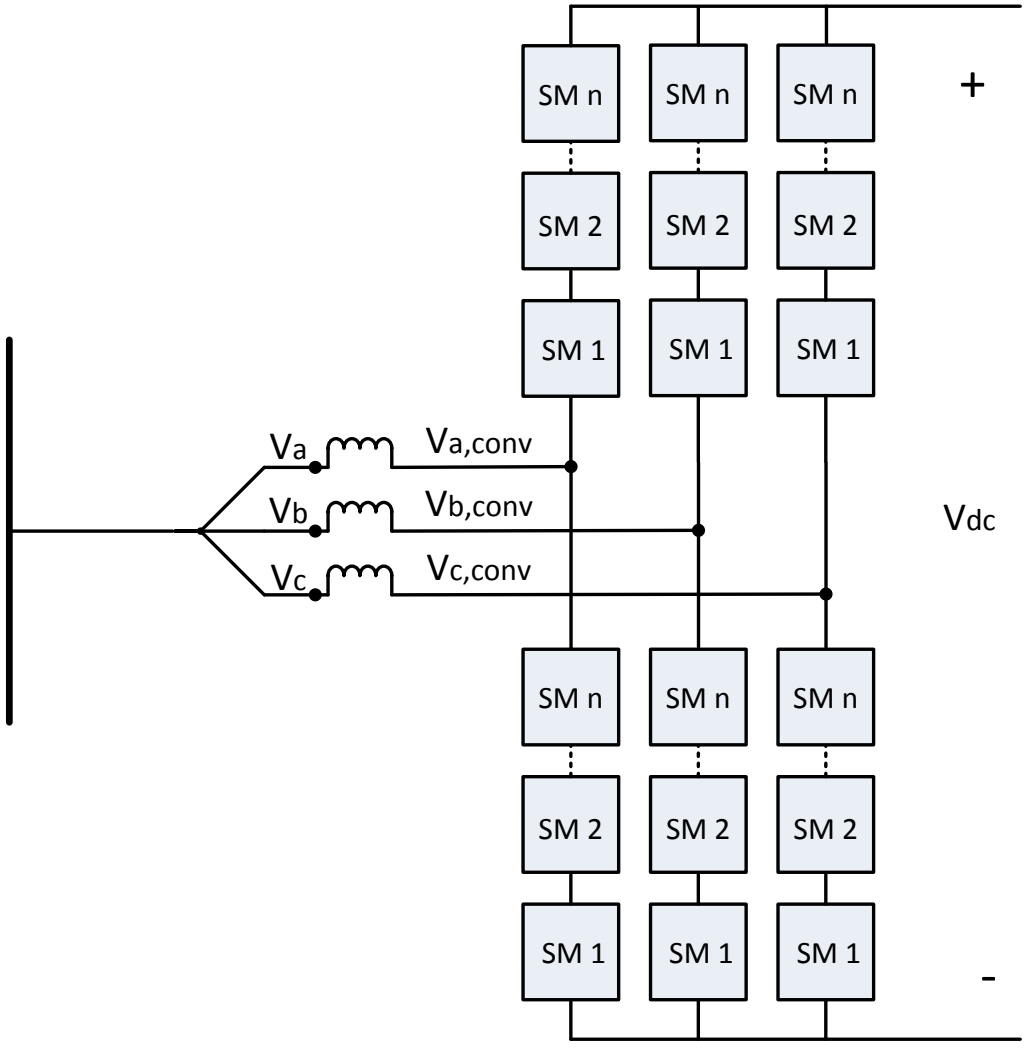

FIGURE 3.5: Overview of a MMC.

$$\begin{bmatrix} V_d \\ V_q \end{bmatrix} = L\frac{d}{dt}\begin{bmatrix} i_d \\ i_q \end{bmatrix} + L\begin{bmatrix} 0 & -\omega \\ \omega & 0 \end{bmatrix}\begin{bmatrix} i_d \\ i_q \end{bmatrix} + \begin{bmatrix} V_{d,conv} \\ V_{q,conv} \end{bmatrix} \tag{3.7}$$

where V_{dq} are AC grid voltages, i_{dq} are AC grid currents and $\omega = 2\pi f$ and V_{dq}. Rearranging the terms with respect to the derivatives give two equations,

$$\begin{aligned} L\frac{di_d}{dt} &= \omega L i_q - V_{d,conv} + V_d \\ L\frac{di_q}{dt} &= -\omega L i_d - V_{q,conv} + V_q \end{aligned} \tag{3.8}$$

The active (P) and reactive power (Q) on AC side of the converter can be expressed with the complex power S as,

$$\begin{aligned} S &= V \cdot I^* \\ S &= \frac{3}{2}(V_d + jV_q)(i_d - ji_q) \\ S &= \frac{3}{2}\Big((V_d i_d + V_q i_q) + j(V_q i_d - V_d i_q)\Big) \\ S &= P + jQ \end{aligned} \tag{3.9}$$

By definition the AC grid voltage vector is aligned in the same direction as the d-axis, and the virtual grid flux vector is aligned in the direction of the q-axis. This gives $V_q = 0$. The active and reactive power on AC side of the converter can therefore be written as,

$$P = \frac{3}{2} V_d i_d \tag{3.10}$$

$$Q = -\frac{3}{2} V_d i_q \tag{3.11}$$

As shown by Eqn. 3.10 and Eqn. 3.11 the two currents i_{dq} are split in two separate equations. This indicates that it is possible to control both active and reactive power independently, by means of controlling the two currents. i_d determines the active power flow from AC to DC side, and similarly, i_q determines the reactive power flow from AC to DC side. This is the fundamental principle behind the current controllers, and will be further elaborated in the next sections.

3.1.5.2 Current Controller

The current controller consists of two major current control systems, namely the inner current controller and outer current controller. Looking at Eqn. 3.10 and Eqn. 3.11 one can see that i_d and i_q control active and reactive power independently. Each controller therefore consist of two separate loops, one for d-axis current (active power, Eqn. 3.10) and one for q-axis current (reactive power, Eqn. 3.11). The outer current controller provides reference signals ($i_{dq,ref}$) for the inner current controller. The inner current controller converters $i_{dq,ref}$ to voltage reference signals for the PWM generator. The PWM generator uses these values to control the IGBTs in the converter. An overview of the vector control principle can be seen on Fig. 3.6. Both current controllers will be explained throughout the following two sections.

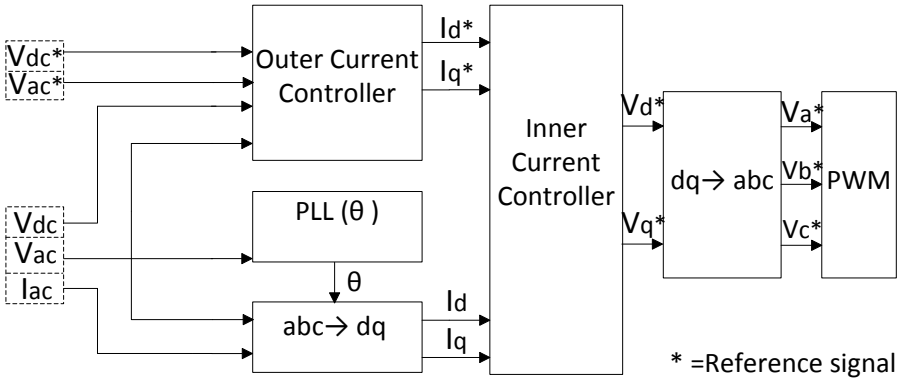

FIGURE 3.6: MMC Vector Control Principle.

3.1.5.3 Inner Current Controller

The inner current controller is based on the block diagram in Fig. 3.7, and this section will explain these blocks respectively. The PI-controller can be represented as a transfer function R(s) as follows [43],

$$R(s) = K_p + \frac{K_i}{s} = K_p \frac{1 + T_i s}{T_i s} \tag{3.12}$$

where K_p is the gain and $T_i = \frac{K_p}{K_i}$ is the integral time constant defined by the user. With basic block diagram summation of Fig. 3.7, the converter voltage error signal, V^*_{conv}, can be written as follows [43],

$$\begin{aligned} V^*_{conv}(s) &= \Big(I_{ref}(s) - I(s)\Big) \cdot R(s) \\ V^*_{conv}(s) &= \Big(I_{ref}(s) - I(s)\Big) \cdot K_p \frac{1 + T_i s}{T_i s} \end{aligned} \tag{3.13}$$

where $I_{ref}(s)$ is reference current and $I(s)$ is the measured AC current. By neglecting switching losses the PWM converter can, from a control point of view, be seen as an ideal power transformer with a time delay from AC to DC side. The PWM converter block in Fig. 3.7 can be represented by the function $Y(s)$ as follows,

$$Y(s) = \frac{1}{1 + T_a s} \tag{3.14}$$

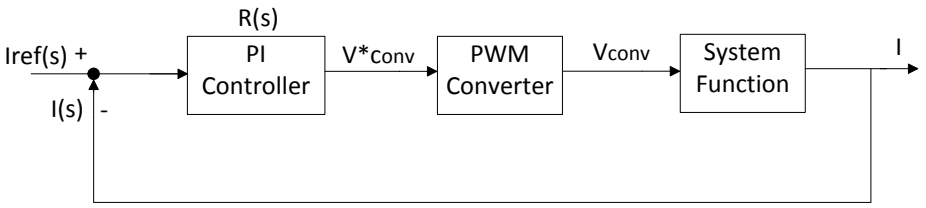

FIGURE 3.7: Block Diagram of Inner Current Control.

where $T_a = T_{switchfreq}/2$ is the time delay it takes for the voltages reference to adjust to the measured value. Again, by using basic block diagram summation, the output converter voltage reference signal $V_{conv}(s)$ can be written as follows,

$$\begin{aligned} V_{conv}(s) &= Y(s) \cdot V^*_{conv}(s) \\ V_{conv}(s) &= \frac{1}{1+sT_a} \cdot V^*_{conv}(s) \\ V_{conv}(s) &= \frac{1}{1+sT_a} \cdot \Big(I_{ref}(s) - I(s)\Big) \cdot K_p \frac{1+T_i s}{T_i s} \end{aligned} \tag{3.15}$$

The inner current controller is based on the system function represented by Eqn. 3.8, which can be rewritten as follows,

$$\begin{aligned} V_{d,conv} &= -L\frac{di_d}{dt} + \omega L i_q + V_d \\ V_{q,conv} &= -L\frac{di_q}{dt} - \omega L i_d + V_q \end{aligned} \tag{3.16}$$

where the last terms in both equations ($\omega L i_{dq}$ and V_{dq}) are the cross-coupling terms between the two voltages. From a control point of view this is seen as a disturbance and must be eliminated. This is done by giving the controller additional reference input, a voltage feed-forward compensation. Splitting Eqn. 3.15 into dq reference frame gives,

$$\begin{aligned} V_{d,conv}(s) &= \frac{1}{1+sT_a} \cdot \Big(I_{d,ref}(s) - I_d(s)\Big) \cdot K_p \frac{1+T_i s}{T_i s} \\ V_{q,conv}(s) &= \frac{1}{1+sT_a} \cdot \Big(I_{q,ref}(s) - I_q(s)\Big) \cdot K_p \frac{1+T_i s}{T_i s} \end{aligned} \tag{3.17}$$

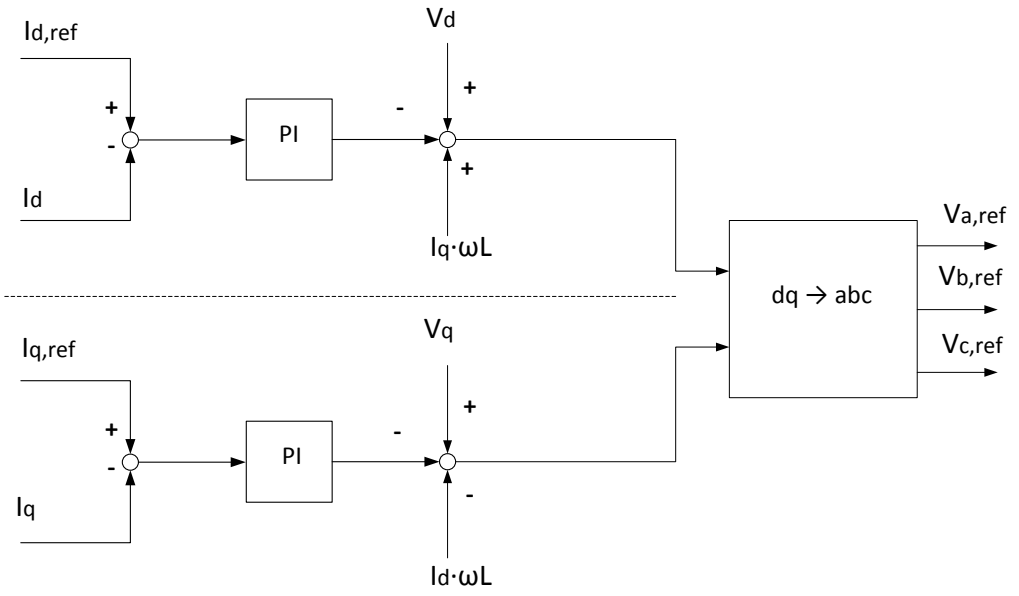

FIGURE 3.8: Inner Current Control.

and by adding the feed-forward loop to the controller,

$$\begin{aligned} V^*_{d,conv} &= -(i_{d,ref} - i_d)\Big(K_p + \frac{K_i}{s}\Big) + \omega L i_q + V_d \\ V^*_{q,conv} &= -(i_{q,ref} - i_d)\Big(K_p + \frac{K_i}{s}\Big) - \omega L i_d + V_q \end{aligned} \tag{3.18}$$

the controller now has an extra input, a feed-forward compensation. By combining Eqn. 3.18, Eqn. 3.17 into the system Eqn. 3.16 it gives the following,

$$\begin{aligned} V_{d,conv} &= L\frac{di_d}{dt} \\ V_{q,conv} &= L\frac{di_q}{dt} \end{aligned} \tag{3.19}$$

The cross coupling term is thus cancelled out and the two loops can operate and be controlled independently. In Fig. 3.8 the inner current controller can be seen [37].

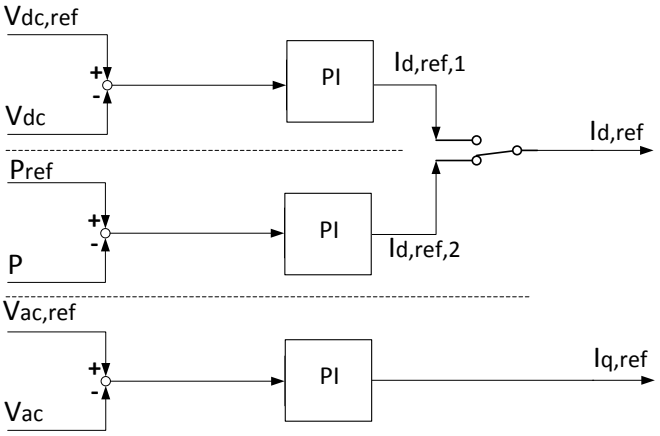

FIGURE 3.9: Outer Current Control.

3.1.5.4 Outer Current Controller

In Fig. 3.9 the outer current controller can be seen. It consists of two loops, one for current d-axis (active power control) and one for current q-axis (reactive power control). The d-axis loop can be controlled by either active power or DC voltage. In a MMC point-to-point connection the two converter stations control the d-axis differently. One station uses AC active power, while the other uses DC voltage. The choice is arbitrary, and depends of the general system layout [44]. The q-axis can be controlled by reactive power control or AC voltage control. According to literature the AC voltage control should be used in weak AC systems where voltage support is needed [45]. AC voltage controller has thus been chosen as controller for the q-axis at both converter stations. The principle of the outer controller is simple: the measured variable is compared to a reference value and sent through a PI-controller. The PI-controller is used to minimize the error signal between the reference and the measured value. The output of the outer current controller is then transferred to the inner current controller [18, 37].

A step change was made to the dq reference currents to illustrate how the measured currents in the system follows the reference currents. In Fig. 3.10 one can see the two decoupled currents and their respective reference currents. The step change was executed when the currents had reached equilibrium. In both the graphs a positive step change of 0.1 pu was implemented, and after 0.1 seconds a negative step change of 0.1 pu was implemented. Fig. 3.10 shows that the currents quickly follows the reference signal. Looking at the reference signal, one can see that it tries to go back to its original value right after the step change has been implemented. This is because the currents tries to reach equilibrium, and thereby moves towards its reference. This indicates that the controller works as intended.

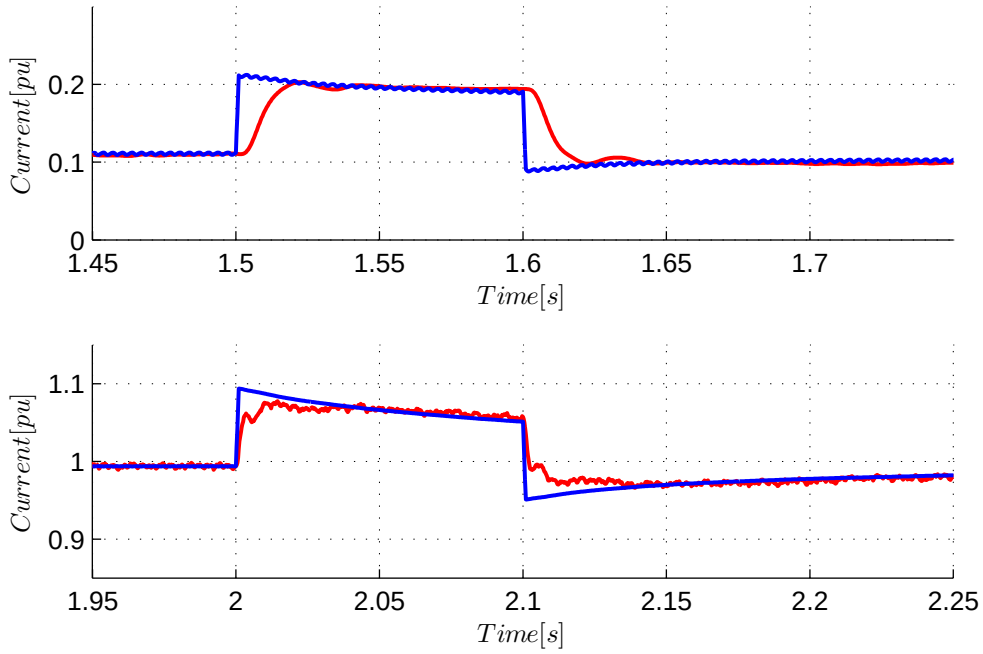

FIGURE 3.10: Step Change. a) I_q (—) and $I_{q,ref}$ (—), b) I_d (—) and $I_{d,ref}$ (—)

3.1.6 Modified Phase-Shifted Sinusoidal PWM Method

There are many different PWM strategies such as,

- Phase disposition PWM
- Alternative phase opposition disposition PWM
- Phase-shifted sinusoidal PWM

The Phase-Shifted Sinusoidal PWM (PS-SPWM) will be used in this report due to its ability to automatically suppress all low-order harmonics. The *Modified* PS-SPWM Method also greatly reduces the effective switching frequency of each SM, since the switching states of the valves does not necessarily change every cycle [41].

In a PS-SPWM there are essentially two control frequencies, namely the carrier frequency f_{cr} and the sampling frequency f_s [41], illustrated in Fig. 3.11. The number of carrier signals depend on how many SMs there are in each arm. If there are N SMs, each carrier is phase shifted $\frac{360^\circ}{N}$ from the next carrier. At every sampling instant the carrier signals are compared with a reference signal.

In Fig. 3.12 the overall block diagram for the PS-SPWM is shown. This block diagram is included in each arm in the converter (six arms), and Fig. 3.12 shows

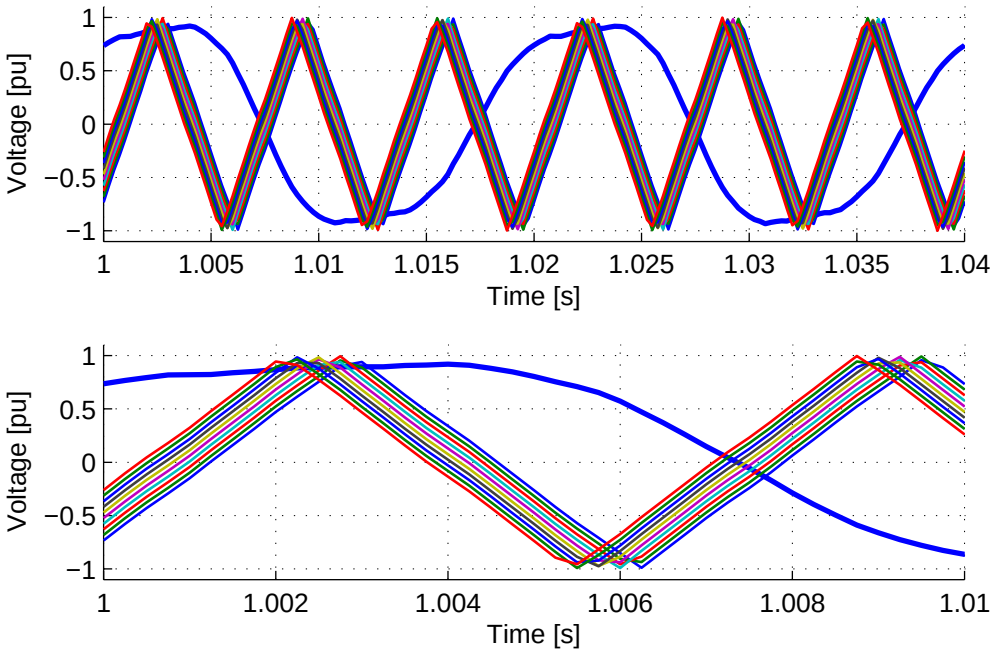

FIGURE 3.11: Phase Shifted Carrier Signals.

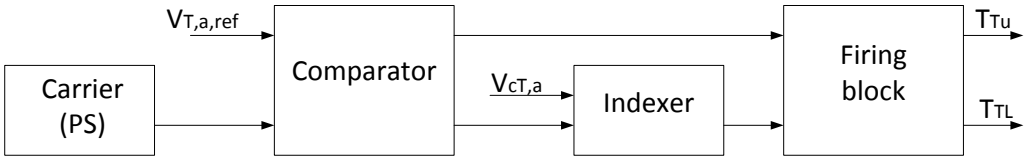

FIGURE 3.12: Block Diagram of the PWM Controller.

upper (T) arm in phase a. The reference signal sent from the CCSC is compared with the carrier signals. At each sampling instant the comparator block decides how many SMs that needs to stay on (N_{on}) in every arm. N_{on} is calculated and the output is sent to the next blocks. The comparator does not determine which SM that gets turned on. [46]

The Modified PS-SPWM Method was first proposed by [41]. The Modified PS-SPWM Method is using a Reduced Switching Frequency (RSF) voltage-balancing algorithm to decide which SM that gets turned on. The idea is to keep all the capacitor voltages as uniform as possible, with as few switches as possible. Each arm is equipped with an indexer. Its job is to determine every capacitor voltage level in the arm. The indexer then sorts all the capacitor voltages from lowest to highest value. There are two different ways to switch the SMs on depending on the current direction in the arm:

- If the arm current is positive it charges the capacitors that are switched ON. The SMs with the highest value are switched OFF, and the ones with the lowest value is switched ON.
- If the arm current is negative it discharges the capacitors that are switched ON. The SMs with highest value is switched ON, and the ones with the lowest value is switched OFF.

This happens at every sampling frequency f_s, and can potentially result in high switching frequency of the SMs. To overcome this a RSF is proposed in addition to the above algorithm [41]. Defining ΔN_{on} as the extra SMs that needs to be turned on during f_s, the RSF is as follows,

- If ΔN_{on} is positive, the SMs currently ON will not be included in the above switching algorithm.
- If ΔN_{on} is negative, the SMs currently OFF will not be included in the above switching algorithm.

The RSF method in combination with the traditional switching method greatly reduces the amount of switches, thus leading to a reduction in power loss in the converter [41].

3.2 Control Design of LCC

The model being used for representing NorNed is a 12-pulse monopolar LCC HVDC system, and is a Cigre Benchmark Model, shown in Fig. 3.13. The upper part of Fig. 3.13 is an overview of the LCC point-point system, the lower part is a close up of the LCC rectifier and LCC inverter stations [47]. Both converter stations are equipped with two six-pulse bridges in series connection seen from DC side, each bridge is connected to a transformer. At the AC busbar there are AC filters installed. The Cigre Benchmark Model is modified to fit the parameters for the NorNed interconnector given in Tab. 3.1 on page 18. The development of this model, and the control objectives of the LCC will be explained throughout this section.

3.2.1 Control Objective of LCC

The control objective of a LCC is to control the power flowing from one side of the DC system to the other. This is done by controlling both DC voltage and

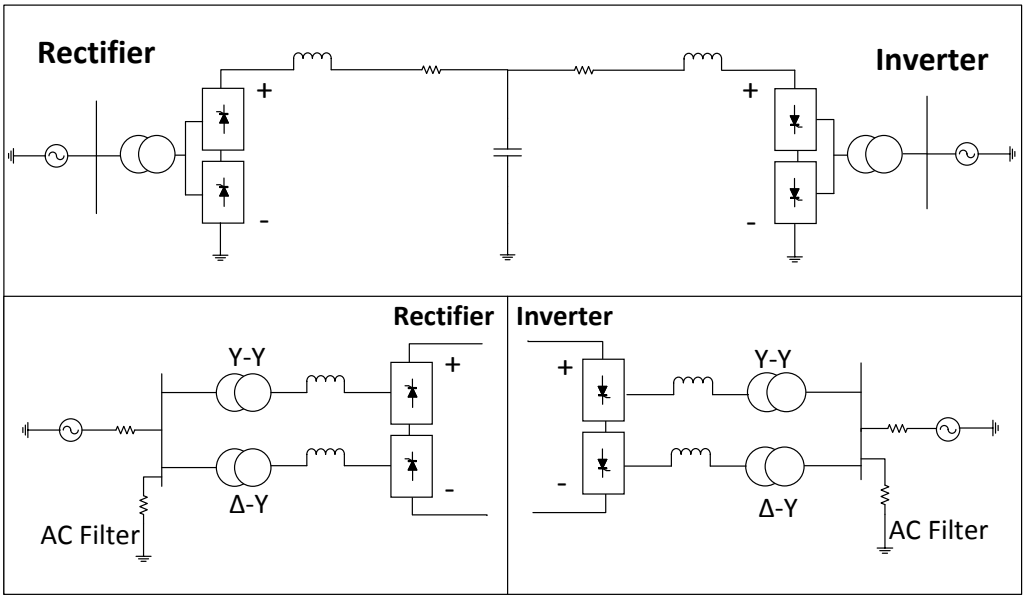

FIGURE 3.13: Outline of the LCC Model.

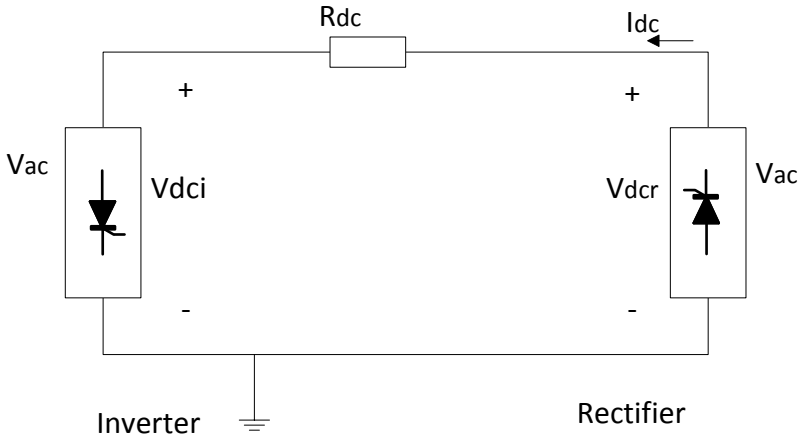

FIGURE 3.14: Control Principle of LCC.

current ($P_{dc} = V_{dc}I_{dc}$). It is possible to design the system so the two stations have different fixed voltage potential, thus leading to a current flowing from the highest potential to the lowest, see Eqn. 3.20 and Fig. 3.14.

$$I_{dc} = \frac{V_{dcr} - V_{dci}}{R_{dc}} \tag{3.20}$$

The main purposes of the control system are to [48],

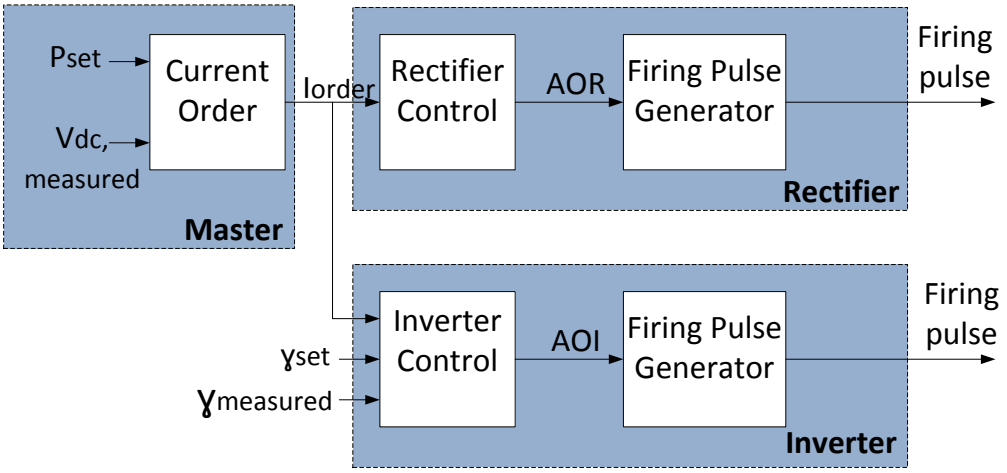

FIGURE 3.15: Control Hierarchy for LCC-HVDC.

- Limit the DC current (avoid equipment damage)
- Maintain a minimum extinction angle (avoid commutation failure)
- Maintain a minimum firing angle (reduce reactive power consumption)

The control objectives in a LCC are fulfilled with three main control parts:

1. Master Control (Section 3.2.2)
2. Rectifier Control (Section 3.2.3)
3. Inverter Control (Section 3.2.4)

The control hierarchy for the LCC system is shown in Fig. 3.15. The control objective of the inverter is to maintain a constant minimum extinction angle γ, by adjusting the firing angle (α_i). It is therefore natural to choose the inverter for DC voltage control. The rectifiers control objective is to control I_{dc} by adjusting the firing angle (α_r) in order to keep it close to $I_{dc,ref}$. The control system in the rectifier and inverter is dependent of each other with a constant power control mode. To illustrate this, let us assume that the AC voltage increase on rectifier side. This would lead to an increase in the DC current, I_{dc}. The rectifier sees this as an increase in error (error=$I_{dc} - I_{dc,ref}$) and the firing angle α is increased accordingly. Taking a look at Fig. 3.16 one can see that an increase in DC current would lead to a decrease in V_{dc}, in order to keep the $\gamma = \gamma_{min}$ constant. In case of a decrease in AC voltage at rectifier side the α will decrease. It can however not go any lower than a minimum value (=5°) in order to keep the rectifier stable.

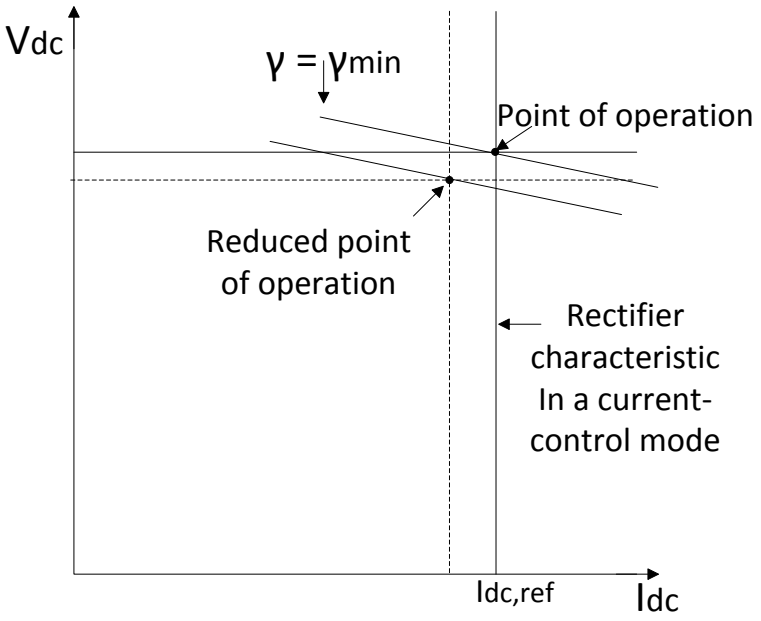

FIGURE 3.16: Control Objective of a LCC

The inverter can under fault situations help stabilize the rectifier by reducing its operating point by increasing γ, and thereby temporarily reduce the transfer capacity of the transmission line, illustrated with dashed lines on Fig. 3.16 [48].

3.2.2 Master Control

The control objective of the master control is to calculate the current order (I_{order}). This is done with a voltage dependent current order limiter, which is included in the inverter current control, upper part of Fig. 3.20 on page 40. By measuring voltage at negative and positive poles and setting a desired power rating of the converter, I_{order} can be calculated with Eqn. 3.21,

$$I_{order} = \frac{P_{set}}{|V_{dc+}| + |V_{dc-}|} \tag{3.21}$$

where P_{set} is rated power for the system, set by the user and $|V_{dc\pm}|$ is absolute value of the DC voltage at both poles. This output is sent to the rectifier as reference value for the current. In case of a reduction in voltage level this controller limits the current to protect the valves from high currents.

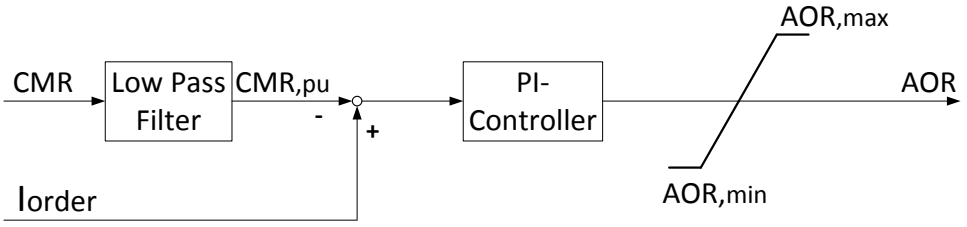

FIGURE 3.17: Rectifier Control.

3.2.3 Rectifier Control

As shown in Fig. 3.15 there are two important controllers in the rectifier, the rectifier controller and the firing pulse generator. First, the rectifier controller is shown in Fig. 3.17. The DC current is measured at rectifier side (CMR) and filtered through a low pass filter. The low pass filter also converts the CMR to pu value through a gain (CMR_{pu}). The measured DC current is then compared to a current order (I_{order}), which is the reference DC current sent from the master controller. The PI-controller eliminates the steady state error. The output of the rectifier controller is an angle order for the rectifier firing angle (AOR). To ensure safe operations and that the rectifier operates within its limits, the AOR is limited between 5° and 90°. The AOR is sent to the firing pulse generator [48].

The next controller is called the firing pulse generator. In a 12-pulse configuration there are two six-pulse firing generators at each converter station. These four firing pulse generators are identical, and one is shown in Fig. 3.18. Within each firing pule generator there is an internal phase locked loop (PLL), here drawn outside for illustration purposes. The PLL ensures that the firing pulse generator is synchronous with the grid voltage. It is doing so by measuring the grid phase voltages (V_{abc}) and calculating the θ by applying the Park Transformation (explained in detail in Appendix B). Being synchronous with the grid voltage is important for accurate switching of the thyristors. Other input parameters are KB (block and deblock control signal), MAR (Measured Alpha angle Rectifier side), MGR (Measured Gamma angle Rectifier side) and AOR (Alpha Angle order Rectifier side).

3.2.4 Inverter Control

In order to avoid commutation failure at inverter side it is necessary to keep the extinction angle (γ) above a certain predefined limit. However the higher extinction angle the more reactive consumption in the valves [49]. As such, there

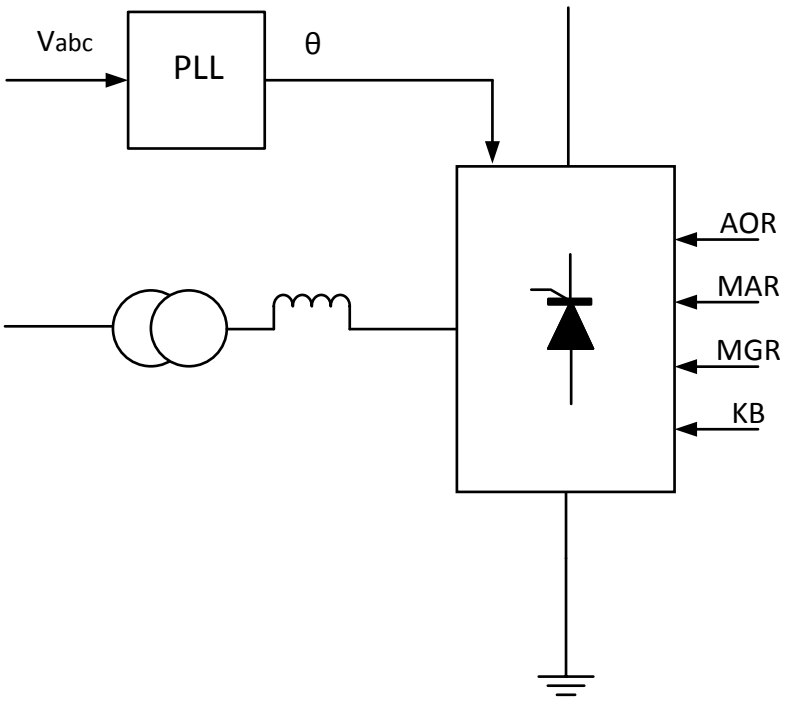

FIGURE 3.18: Rectifier Firing Pulse Generator, Consisting of an Internal PLL and its Input Parameters.

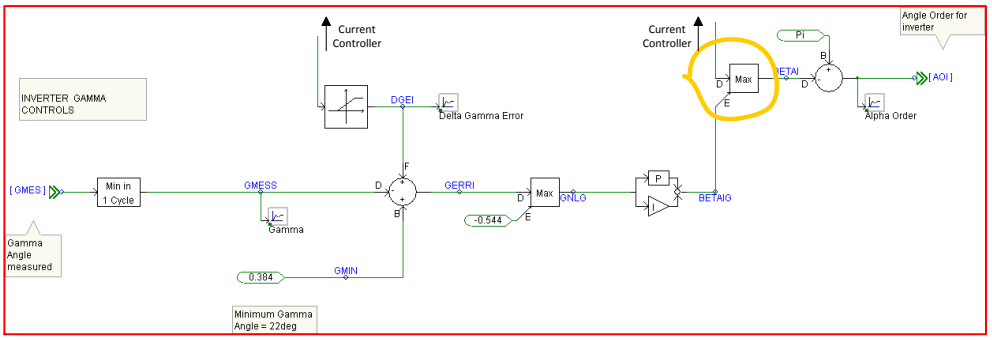

FIGURE 3.19: Inverter Gamma Control.

is a trade-off between safe operation mode and reactive consumption. The control objective of the inverter is thus to maintain a minimum extinction angle in order to avoid commutation failure and to transfer power as efficient as possible. The inverter controller consist of three major control parts namely gamma controller, inverter current controller and firing pulse generator, the latter being similar to the rectifier firing pule generator (Section 3.2.3).

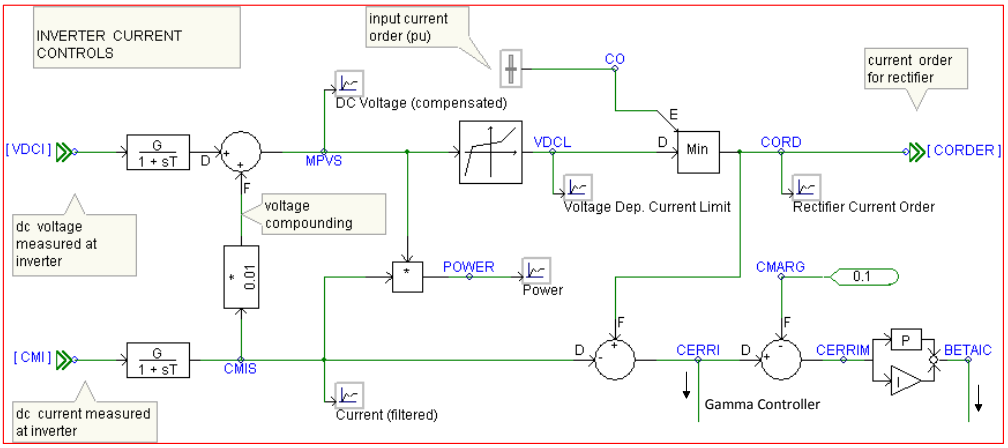

FIGURE 3.20: Inverter Current Control.

The gamma controller can be seen in Fig. 3.19. The purpose of the gamma controller is to keep the DC voltage constant, which is equal to keeping the extinction angle γ as close to its predefined value, set by the user according to system requirements. The γ is measured and compared to this value. The controller then outputs a firing angle to adjust for the deviations in γ. The firing angle must be kept between 90° and 138° (choosing $\gamma = 22°$ according to [49], and assuming $\mu = 20°$ according to [50]) in order to operate at a safe limit, and to ensure the converter is working in inverter mode. It is desirable to keep the γ as close to its predefined value as possible to reduce the reactive consumption in the converter, hence keeping the firing angle close to 138° is optimal.

The second control system in the inverter is called inverter current controller and can be seen in Fig. 3.20. The output of this controller is a current order for the rectifier. However this output is not used under normal operation, only during faults. If the DC current is larger than a predefined value the inverter current controller is used. The purpose is to give additional inputs to the gamma controller during fault situations. The value created by this controller is continuously compared to the gamma controller output. The highest of these two values are chosen for the fire angle in the gamma controller (see yellow circle on Fig. 3.19).

3.2.5 AC Filters

Each converter station is equipped with AC filter banks. The purpose of these AC filters are to eliminate or suppress harmonic components produced during the commutation process in the converter, as to prevent them from entering the AC grid. In a 12-pulse LCC harmonic voltages and currents occur in the order of 12n±1, where n is an integer (harmonics: 11th, 13th, 23rd, 25th etc.). The frequency of any harmonic is given by its number multiplied with the grid frequency. The

higher the harmonic number the higher frequency, and also lower amplitude [5,48]. As the harmonic content in the converter is known, the filters are thus tuned so that to eliminate certain harmonic frequencies. The filters are of passive types, i.e. stationary filters without switch gears. Each AC filter bank consists of three different filter types,

1. Low pass filter
2. High pass filter
3. Shunt compensation

A graphical representation of the filter types is shown in Fig. 3.21. Each filter type has been tuned to match the AC voltage rating at each converter side. The tuning is done according to [48], and the following section will explain the calculations done to obtain these values.

3.2.5.1 Low Pass Filter

The purpose of the low pass filter is to let low frequencies pass through and to suppress higher frequencies, thus removing high order harmonics. The filter is tuned so that the cut-off frequency is around the 11th order harmonic ($11f$ = 550Hz). The low pass filter is designed as a R-L-C circuit (shown in Fig. 3.21), and the following section will account for its values. The AC phase voltage (V_{ph}) in a three phase system is defined as the line-line voltage (V_{LL}) divided by the square root of three,

$$V_{ph} = \frac{V_{LL}}{\sqrt{3}} = \frac{420 \text{ kV}}{\sqrt{3}} = 242.49 \text{ kV} \tag{3.22}$$

Quality factor (Q) is an index of sharpness of tuning and is different for the three filters [48],

$$Q = \frac{\omega_r L}{R} = 200 \tag{3.23}$$

where $\omega_r = \frac{1}{\sqrt{LC}}$ is the cut-off frequency, R is resistance, L is inductance and C is capacitance of the filter. With a total quality factor requirement for the low pass filter of 125 Mvar [48], the requirement per phase would be,

$$Q_{LP} = 125/3 = 41.67 \text{ Mvar} \tag{3.24}$$

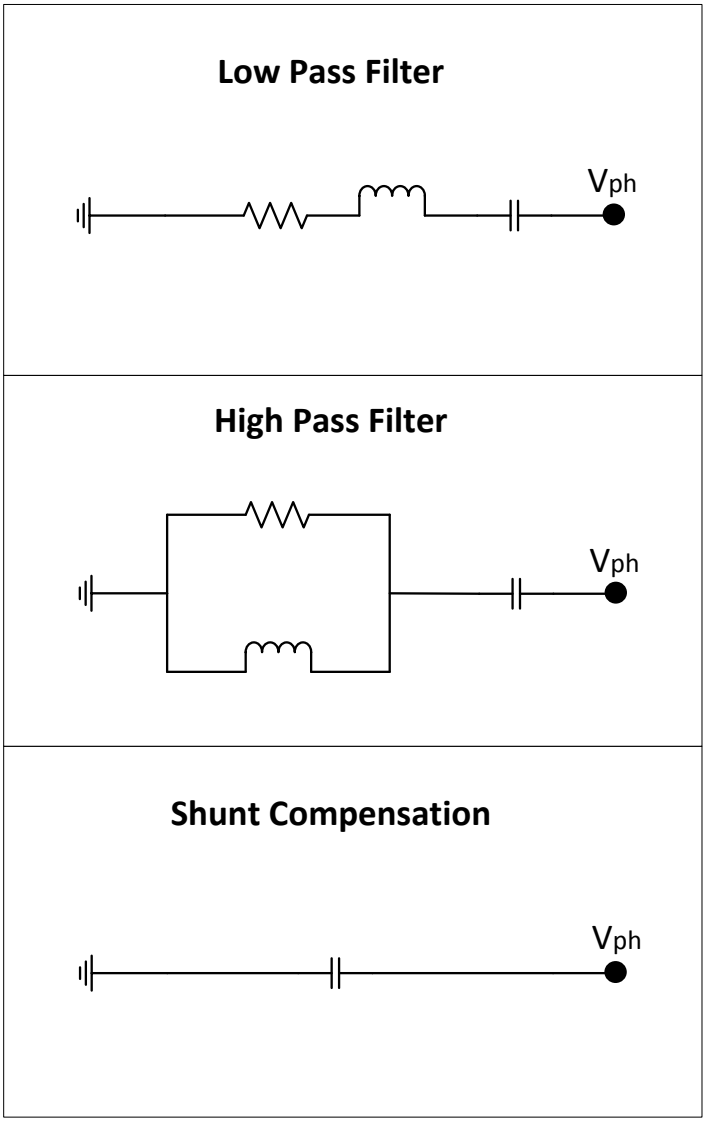

FIGURE 3.21: LCC AC Filters.

Impedance of the filter R-L-C branch is,

$$\begin{aligned} Z &= \sqrt{R^2 + \left(\omega L - \frac{1}{\omega C}\right)^2} \\ Z^2 &= R^2 + \left(\omega L - \frac{1}{\omega C}\right) \\ Z^2 &= \frac{(\omega_r L)^2}{Q^2} + \left(\frac{\omega LC - 1}{\omega C}\right)^2 \\ Z^2 &= \frac{\omega^2/\omega_r^2 + Q(\omega^2/\omega_r^2 - 1)^2}{Q^2\omega^2 C^2} \end{aligned} \tag{3.25}$$

Now for a $Q_{LP} = 125/3$ for each phase,

$$Q_{ph} = \frac{V_{ph}}{Z^2 \omega C} \tag{3.26}$$

and defining $M = \frac{\omega}{\omega_r}$, where M is the number of harmonic filter ($M = \frac{1}{11} = 0.09090909$) and $\omega_r = 550$ Hz,

$$\begin{aligned} C &= \frac{Q_{LP}}{V_{ph}^2} \cdot \Big(\frac{M^4 + Q^2 \cdot (M^2 - 1)^2}{Q^2 \omega} \Big) \\ L &= \frac{1}{\omega_r^2 \cdot C} \\ R &= \frac{\omega L}{Q} \end{aligned} \tag{3.27}$$

By solving Eqn. 3.27 one get $C = 2.065 \cdot 10^{-5}$ F, $L = 0.16$ H and $R = 0.04\Omega$.

3.2.5.2 High Pass Filter

The high pass filter will now be determined. Shown by Fig. 3.21 the filter is a capacitor bank in series with a R-L parallel branch. Quality factor (Q) for high pass filter varies between 0.5-2. The reactive power requirement is $Q_{HP} = 250/3$ Mvar per phase.

The impedance of the filter is,

$$Z = \frac{1}{j\omega C} + \Big(\frac{1}{R} + \frac{1}{j\omega L} \Big)^{-1} \tag{3.28}$$

In this filter the impedance of the capacitor is much larger than the impedance of the parallel branch. Therefore the parallel branch can be neglected for the calculation of C, and then use C to find L and R in similar to the low pass filter. Defining $\omega_r = \frac{1}{\sqrt{LC}}$,

$$\begin{aligned} Q_{HP} &= V_{ph}^2 \omega C \\ C &= \frac{Q_{HP}}{V_{ph}^2 \omega} \\ L &= \frac{1}{\omega_r^2 C} \\ R &= Q\sqrt{\frac{L}{C}} \end{aligned} \tag{3.29}$$

With a quality factor Q=1.85 and cut-off frequency of $\omega_r = 24 \cdot 50 = 1200Hz$, Eqn. 3.29 can be solved,

$$\begin{aligned} C &= 2.27 \cdot 10^{-5} \text{ F} \\ L &= 0.031 \text{ H} \\ R &= 67.9\Omega \end{aligned} \tag{3.30}$$

3.2.5.3 Shunt Compensation

Explained in Section 2.1, the current always lags the voltage due to the delayed firing angle mechanism in the thyristor valves. Because of this delay the converter consumes reactive power. To compensate for this reactive power a shunt compensator is required. How much reactive power is consumed depends on the control strategy implemented, and can be up to 50 % of the active power flow in the converter [9]. For this specific case, the total reactive power requirement for the shunt compensation is 125 Mvar. Per phase compensation is therefore 41.67 Mvar,

$$\begin{aligned} Q_{SH} &= V_{ph}^2 \omega C_{sh} \\ C_{sh} &= \frac{Q_{SH}}{V_{ph}^2 \omega} = 1.4173^{-5} \text{ F} \end{aligned} \tag{3.31}$$

The effect of the three filters has been shown in Fig. 3.22. The harmonic currents of 11th, 13th, 23rd and 25th order respectively have been plotted, with the filters installed and removed from the converter AC side. Fig. 3.22 clearly illustrates the elimination of 23rd and 25th harmonic, while suppressing 11th and 13th to a much lower amplitude.

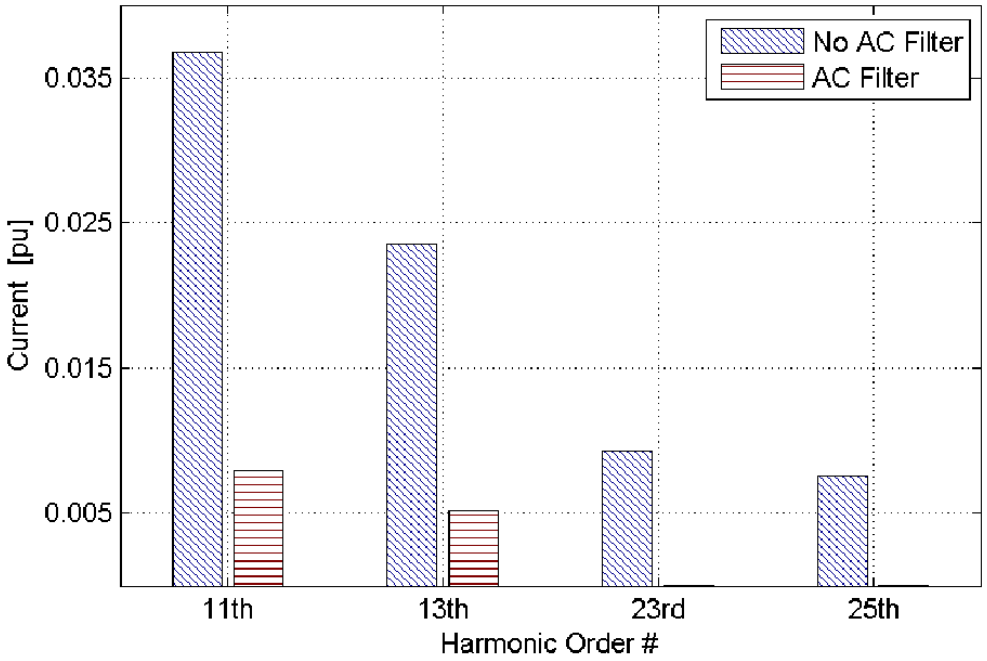

FIGURE 3.22: Harmonic Current Elimination.

3.2.6 Converter Transformer Design

In a 12-pulse configuration there are two six-pulse generators connected in series on DC side with a phase shift of 30°. This phase shift increase elimination of harmonic components in the AC current and DC voltage, and is therefore widely used [5]. The phase shift is implemented by connecting AC side to DC side with two different transformers. Each of the six-pulse bridge is connected to the converter transformers secondary side. Transformer one is Y-Y connected, while the other is Y-Δ. The converter transformers are adjusted to the system requirements, and the technical data for the system is shown in Tab. 3.1 on page 18. The tuning is done according to [49], and the following section will explain how the ratings of the converter transformers on inverter and rectifier side are obtained.

3.2.6.1 Inverter Transformer Design

The rated DC current on inverter side (I_{dci}) is defined as,

$$I_{dci} = \frac{P_{dci}}{V_{dci}} = \frac{700}{450} = 1.56 \text{ kA} \tag{3.32}$$

where P_{dci}, V_{dci} are the DC power and voltage on inverter side respectively. The rms line-line current on the secondary side of the transformers (I_{LLi}) can thus be found,

$$I_{LLi} = \frac{\sqrt{2}}{\sqrt{3}} I_{dci} = 1.27 \text{ kA} \tag{3.33}$$

The rated MVA (S_{ti}) of each transformer can be found as [49],

$$S_{ti} = \sqrt{3} V_{LLi} I_{LLi} \tag{3.34}$$

where V_{LLi} is the line-line voltage at inverter secondary side. To find the rated MVA for the inverter transformer, the line-line voltage at inverter secondary side must be found. First, the base impedance (Z_b) is defined as,

$$Z_b = \frac{V_{LLi}^2}{S_{ti}} \tag{3.35}$$

and the transformer leakage reactance (X_{Li}) [49],

$$\begin{aligned} X_{Li} &= 0.18 \text{ pu} \\ X_{Li} &= 0.18 \cdot Z_b \\ X_{Li} &= 0.18 \cdot \frac{V_{LLi}^2}{S_{ti}} = 0.18 \frac{V_{LLi}}{\sqrt{3} I_{LLi}} = 0.08182 V_{LLi} \end{aligned} \tag{3.36}$$

Equation for inverter voltage using Fig. 3.14 on page 35,

$$\frac{V_{dci}}{2} = 1.35 V_{LLi} cos\gamma - \frac{3 I_{dci} X_{Li}}{\pi} \tag{3.37}$$

where γ is the extinction angle. By assuming minimum extinction angle $\gamma = 22°$ for the NorNed interconnector according to [49], Eqn. 3.37 can be solved,

$$\begin{aligned} 225 &= V_{LLi}(1.2517 - 0.12154) \\ V_{LLi} &= \underline{199.087 \text{ kV}} \end{aligned} \tag{3.38}$$

And finally we can use Eqn. 3.34 to find the rating for inverter transformer,

$$S_{ti} = \underline{437.97 \text{ MVA}} \tag{3.39}$$

The turn ratio for inverter Y-/Δ and Y-Y transformer can thus be calculated [49],

$$n = \frac{V_{LLi}(\text{primary side})}{V_{LLi}(\text{secondary side})} = \frac{420 \text{ kV}}{199.087 \text{ kV}} = \underline{2.11} \tag{3.40}$$

3.2.6.2 Rectifier Transformer Design

A similar approach as for the inverter transformer can be implemented on rectifier side. However, the DC power and voltage must be modified. The voltage drop (V_{drop}) over the cable is defined as the cable impedance (R_{dc}) times the current through the cable. As the DC current is equal on both sides, the DC current from inverter side can be used,

$$\begin{aligned} R_{dc} &= 5\Omega \\ V_{drop} &= I_{dci} R_{dc} = 7.8 \text{ kV} \end{aligned} \tag{3.41}$$

The cable losses (P_{loss}) can thus be found,

$$P_{loss} = V_{drop} I_{dci} = 12.17 \text{ MW} \tag{3.42}$$

which gives the following DC power (P_{dcr}), voltage (V_{dcr}) and current (I_{dcr}) on rectifier side,

$$\begin{aligned} P_{dcr} &= P_{dci} + P_{loss} = 712.17 \text{ MW} \\ V_{dcr} &= V_{dci} + V_{drop} = 457.8 \text{ kV} \\ I_{dcr} &= \frac{P_{dcr}}{V_{dcr}} = 1.56 \text{ kA} \end{aligned} \tag{3.43}$$

the rms line-line current on secondary side of the transformer (I_{LLr}),

$$I_{LLr} = \frac{\sqrt{2}}{\sqrt{3}} I_{dci} = 1.27 \text{ kA} \tag{3.44}$$

The rated MVA (S_{tr}) of each transformer is found in the same way as before [49],

$$S_{tr} = \sqrt{3} V_{LLr} I_{LLr} \tag{3.45}$$

Similar to the inverter side, the line-line voltage on the secondary side of transformer (V_{LLr}) must be found. Assuming fire angle $\alpha = 15°$ and rectifier transformer

leakage reactance $X_{Lr} = 0.18$ pu [49]. By Eqn. 3.36 and Eqn. 3.37 with rectifier as reference,

$$\begin{aligned} \frac{V_{dcr}}{2} &= 1.35 V_{LLr} cos\alpha - \frac{3 I_{dcr} X_{Lr}}{\pi} \\ 228.9 &= V_{LLr}(1.304 - 0.0.09924) \\ V_{LLr} &= \underline{188.92 \text{ kV}} \end{aligned} \tag{3.46}$$

The V_{LLr} was found. It is now possible to obtain the rating of the rectifier transformers with Eqn. 3.45,

$$S_{tr} = \sqrt{3} V_{LLr} I_{LLr} = \underline{415.57 \text{ MVA}} \tag{3.47}$$

The turn ration of the rectifier Y-/Δ and Y-Y transformer can finally be calculated [49],

$$n = \frac{V_{LLr}(\text{primary side})}{V_{LLr}(\text{secondary side})} = \frac{230 \text{ kV}}{193.63 \text{ kV}} = \underline{1.217} \tag{3.48}$$

3.3 AC and DC Transmission System

The transmission system consists of one interconnector to Germany (NordLink) and one interconnector to Netherlands (NorNed). The two interconnectors are electrically connected at Tonstad, displayed in Fig. 3.23. The MMC inverter station for NordLink is located at Tonstad. From Tonstad there will be built a DC overhead lines to Vollesfjord. At Vollesfjord the interconnector will go as a DC submarine cable to Germany.

Tonstad is also electrically connected to Feda with AC overhead lines. The DC overhead lines will share the same Rights-of-Way (RoW) as the AC overhead lines, for 38 km, before splitting into separate parts. At Feda there is a LCC inverter, and another connection to the Norwegian power system. From the LCC inverter NorNed will go as a DC submarine cable to Netherlands. The transmission path distances, and other key parameters are listed in Tab. 3.1 on page 18.

The AC overhead lines consists of two AC towers, each tower with three conductors, which gives a total number of six AC conductors. The DC overhead lines are modelled as two conductors. The parallel overhead lines are mutually coupled in PSCAD. The tower dimensions used in PSCAD can be seen on Fig. 3.24, where the red indicates AC towers and green indicates DC tower.

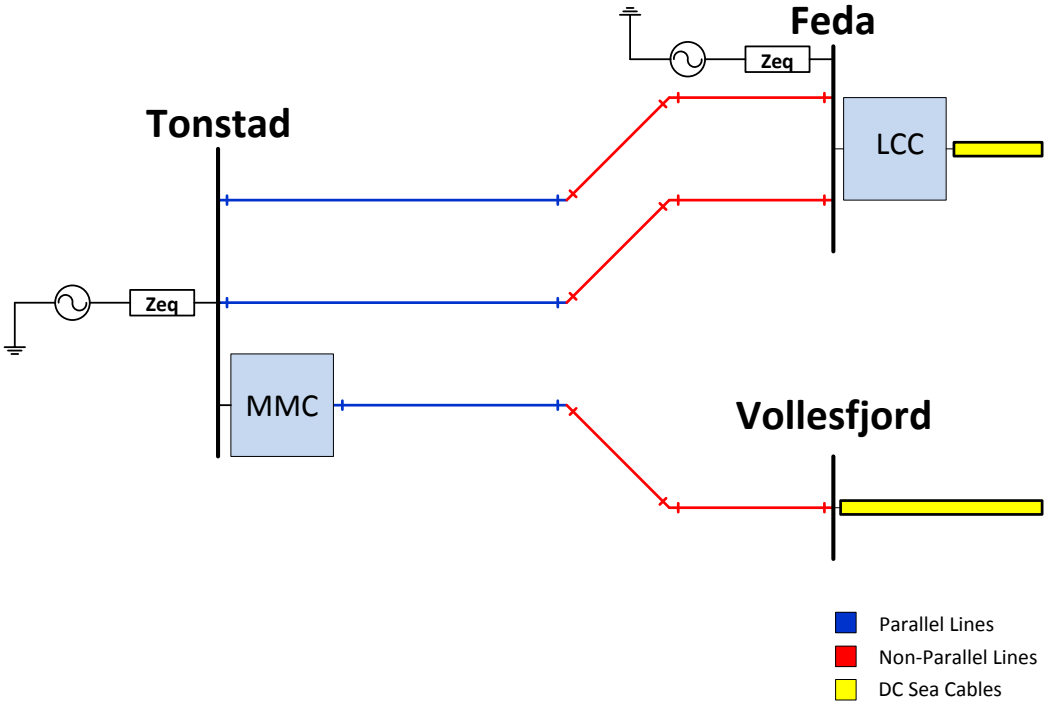

FIGURE 3.23: Transmission System in Southern Norway.

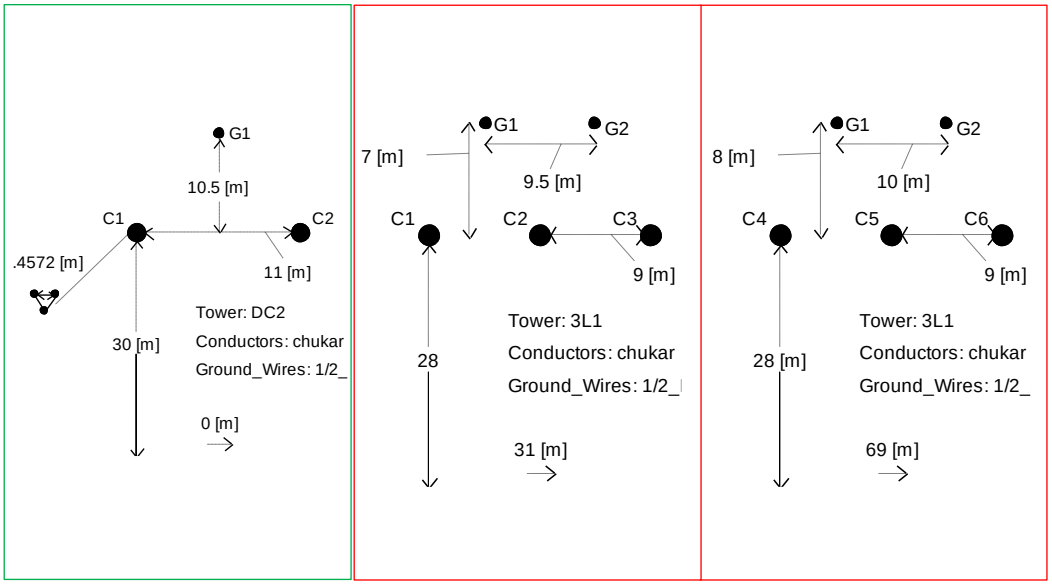

FIGURE 3.24: AC and DC Overhead Towers Used in PSCAD.

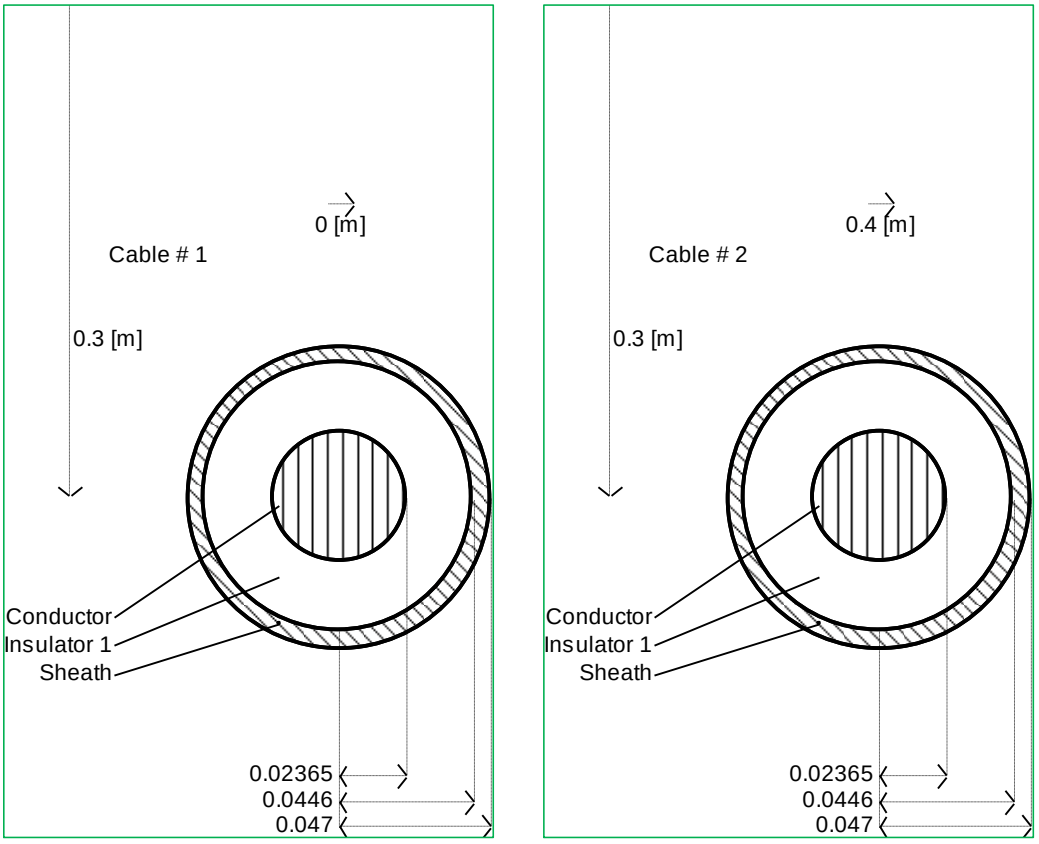

FIGURE 3.25: NordLink: DC Submarine Cable Used in PSCAD.

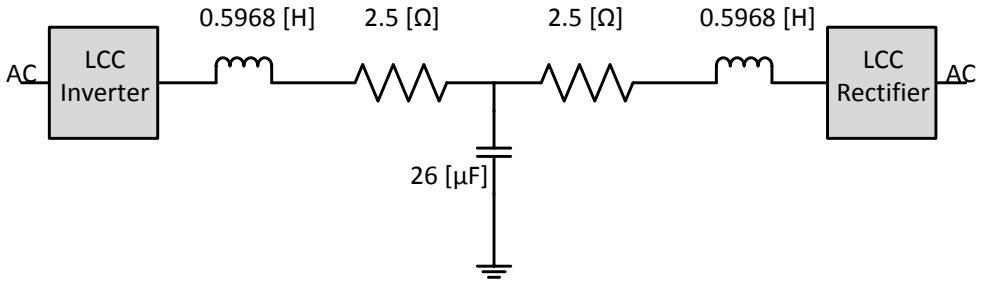

FIGURE 3.26: NorNed: DC System Connecting LCC Inverter and LCC Rectifier.

The DC submarine cable dimension used for NordLink can be seen on Fig. 3.25. The DC submarine cable for NorNed connects the rectifier and the inverter, see Fig. 3.26. It consists of an equivalent DC cable, capacitor and smoothing reactors. The smoothing reactors are used to limit the change in the DC current, and thereby aim to make the commutation more robust. The smoothing reactor and capacitor also make a DC filter to filter out higher harmonics [48].

The grounding wires of the overhead lines can be seen in Tab. 3.3

Table 3.3: Grounding Wires of Overhead Lines.

Parameter	**AC Overhead Line**	**DC Overhead Line**
Number of ground wires	2	1
Outer radius	0.0055245 m	0.0082 m
DC resistance	2.8645 Ω/km	0.2943 Ω/km
Relative permeability	1	1
Sag	10 m	2 m

3.3.1 Short Circuit Ratio

In order to represent the AC systems a short circuit ratio (SCR) has been applied. The SCR is an index for describing the strength of the AC system. It is determined by the Thevenin impedance of the AC system. If the Thevenin impedance is low, the system stability is better. Very strong grids can often be idealized by a stiff grid. A stiff grid is represented by only an AC power source. However if the Thevenin impedance is higher, the system is weaker. Should an AC fault occur, the AC voltage would drop substantially. The SCR is defined as the short circuit level (SCL) at the AC busbar divided by the rated DC power P_d given by Eqn. 3.49 [51],

$$SCR = \frac{SCL}{P_d} \tag{3.49}$$

Using the definition according to [51] a system can be categorized as,

- *Strong system*, SCR > 3.
- *Weak system*, $2 <$ SCR > 3.
- *Very weak system*, SCR < 2.

The rest of the section will develop equivalent impedance circuits to represent the strength of the system, i.e. the SCR. The AC impedance absolute value $|Z_{ac}|$ and its angle ϕ is calculated with [51],

$$SCL = \frac{V_{ac}^2}{|Z_{ac}|} \tag{3.50}$$

$$\phi = tan^{-1}\Big(\frac{X}{R}\Big) \tag{3.51}$$

Inserting values from Tab. 3.1 on page 18 gives the following values for Tonstad,

$$\begin{aligned} SCR &= \frac{SCL}{P_d} = \frac{6000}{2100} = 2.857 \\ |Z_{ac}| &= \frac{V_{ac}^2}{SCL} = \frac{420^2}{6000} = 29.4 \\ \phi &= tan^{-1}\Big(\frac{X}{R}\Big) = tan^{-1}(14) = 85.91^\circ \end{aligned} \tag{3.52}$$

Now in order to complete the equivalent circuit, the real and imaginary part of $|Z_{ac}|$ must be determined,

$$\begin{aligned} Z_{ac} &= R + jX = |Z_{ac}|cos(\phi) + j|Z_{ac}|sin(\phi) \\ Z_{ac} &= 29.4cos(85.91) + j29.4sin(85.91) = 2.1 + j29.32 \end{aligned} \tag{3.53}$$

where R is resistance, $X = \omega L$ is reactance which gives $L = \frac{X}{\omega} = \frac{29.4}{100\pi} = 0.0933$ H. The circuit for the common AC busbar (Tonstad) was constructed according to [51] as a parallel R-L branch in series with a resistor. The circuit can be seen in Fig. 3.27. As for the SCR at Feda, the data from Tab. 3.1 shows that the short circuit level and X/R are the same for both Tonstad and Feda. Therefore, the circuit at Feda is identical to Tonstad, shown in Fig. 3.28.

The LCC rectifier side (Netherlands) is modelled in the same way as the Cigre Benchmark Model, see Fig. 3.29 [47]. The MMC rectifier side (Germany) is modelled with a SCL = 3650 MVA, X/R = 13.27 Ω. The resulting impedance was then found in the same way as before,

$$\begin{aligned} SCR &= \frac{SCL}{P_d} = \frac{3650}{1400} = 2.61 \\ |Z_{ac}| &= \frac{V_{ac}^2}{SCL} = \frac{230^2}{3650} = 14.49 \\ \phi &= tan^{-1}\Big(\frac{X}{R}\Big) = tan^{-1}(13.27) = 85.7^\circ \end{aligned} \tag{3.54}$$

$$Z_{ac} = 14.49cos(85.7) + j14.49sin(85.7) = 1.086 + j14.449 \tag{3.55}$$

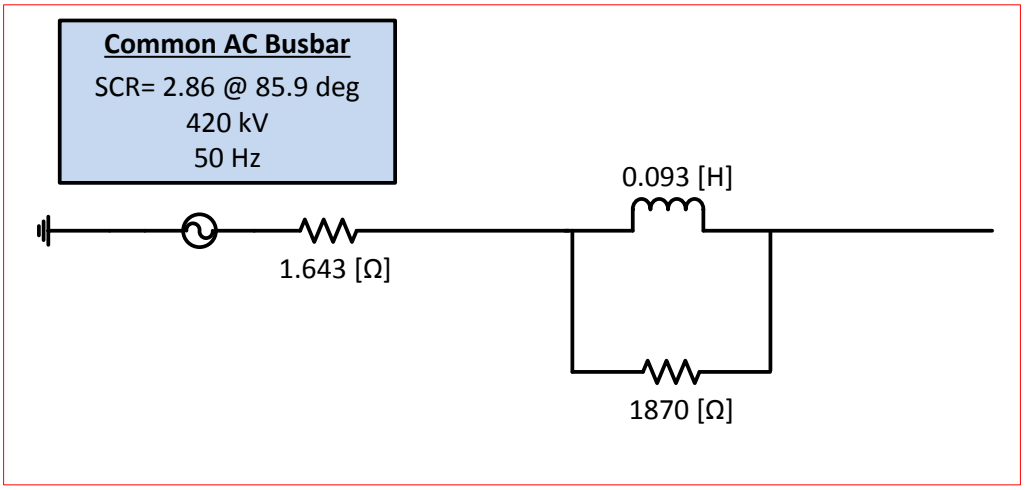

FIGURE 3.27: Short Circuit Ratio: Common Busbar (Tonstad).

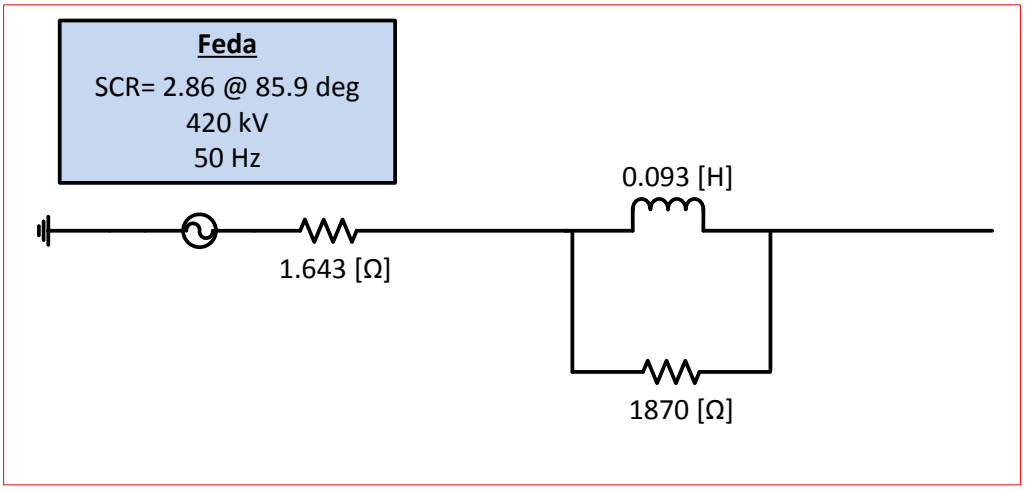

FIGURE 3.28: Short Circuit Ratio: Feda.

The circuit was made as a parallel R-L branch in series with a resistor [51]. The circuit representation of the German AC system is displayed in Fig. 3.30. By using the definition for SCR, one can see that Tonstad (SCR=2.86), Feda (SCR=2.86), Netherlands (SCR=2.5) and Germany (SCR=2.6) can all be categorized as *weak* AC networks.

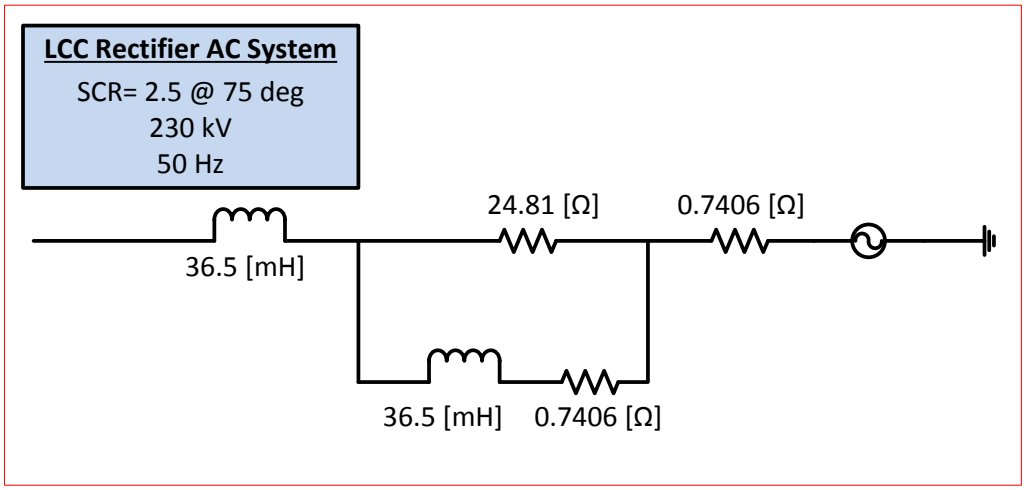

FIGURE 3.29: Short Circuit Ratio: LCC Rectifier.

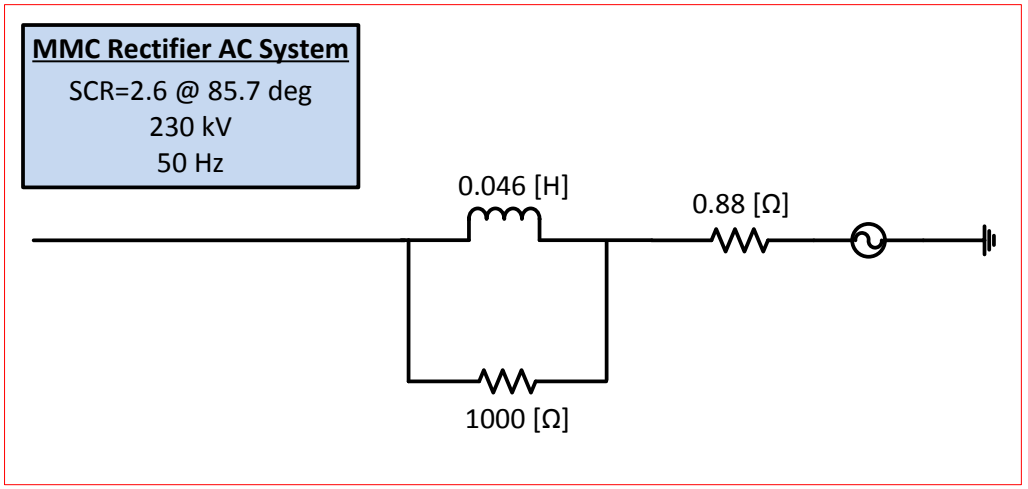

FIGURE 3.30: Short Circuit Ratio: MMC Rectifier.

Chapter 4

Analysis of a Multi-Infeed HVDC System in the Norwegian Power System

The objective of this chapter is to study how the new MMC-link of NordLink will impact the existing configuration in southern Norway. Two scenarios have been considered as study cases:

- Scenario 1: LCC stand alone HVDC system
- Scenario 2: Multi-infeed HVDC system consisting of a MMC-link and LCC-link

The main purpose is to analyse and compare the performance of the LCC stand alone HVDC system and the multi-infeed HVDC system. In this study the multi-infeed HVDC system is defined as MMC inverter station and LCC inverter station connected to a common AC busbar, where both transmission systems convey power into the same receiving end. The study will be performed in steady state and transient conditions, with different AC faults.

A schematic representation of scenario 2 is shown in Fig. 4.1. Scenario 1 illustrates the current system, which is known as NorNed interconnector to the Netherlands, while scenario 2 illustrates the new system with an additional interconnector between Norway and Germany, known as NordLink. The two interconnectors will go in parallel, see Fig. 4.2. Interactions between the AC and DC overhead lines sharing the same Rights-of-Way (RoW) can be expected. This will be studied in Chapter 6.

This chapter is organized as follows: Firstly, the scenarios are tested in steady state (Section 4.1). Start-up of different converters will be discussed, to display that

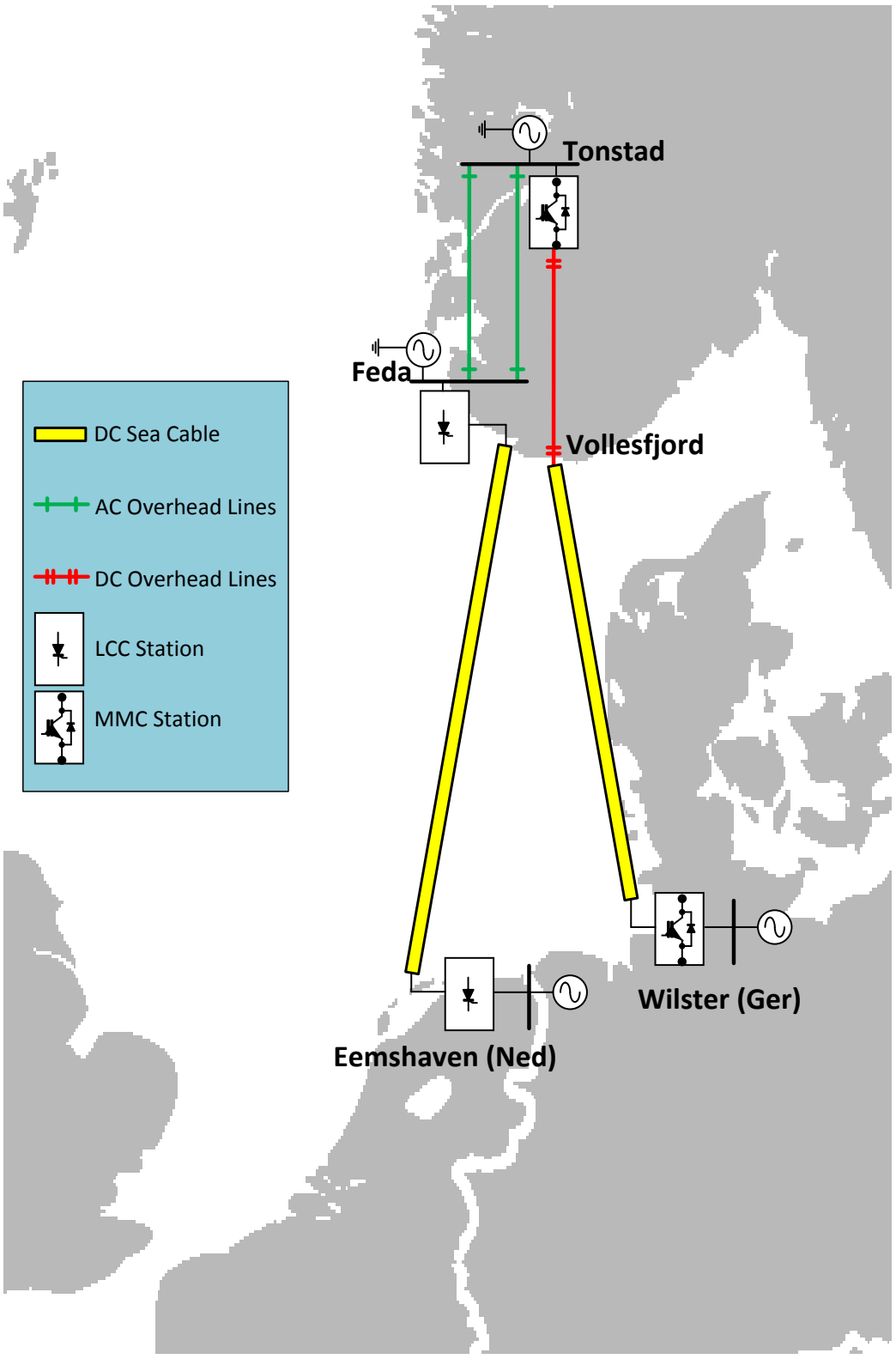

FIGURE 4.1: System Overview: Scenario 2.

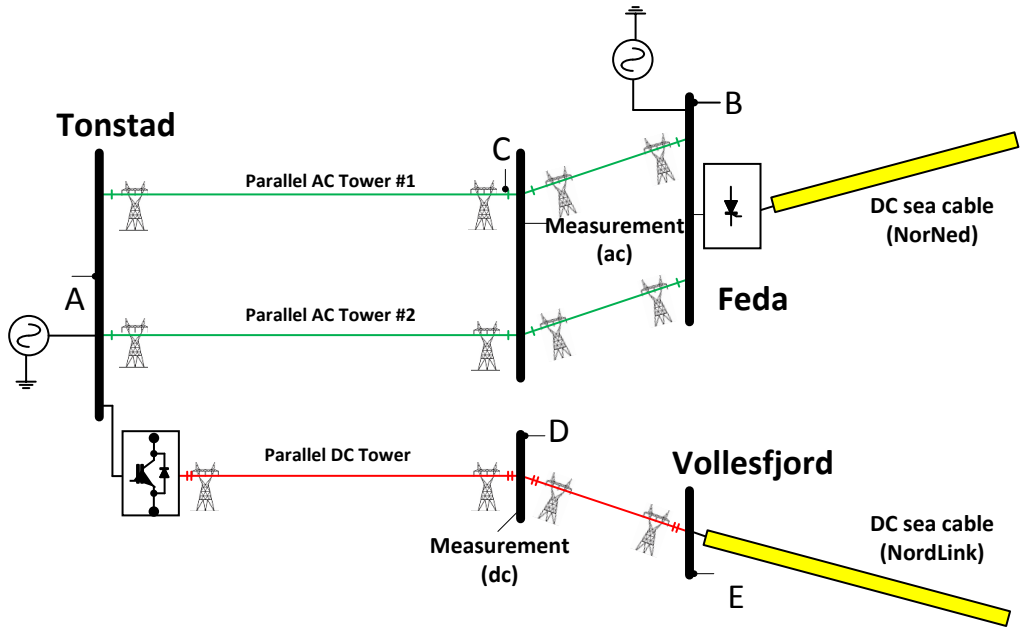

FIGURE 4.2: System Overview: Fault Locations.

the converters operate according to the implemented control design (explained in Chapter 3). The steady state tests also include load flow changes in both converters. Secondly, the scenarios are tested during transient conditions by implementing various AC faults (Section 4.2). A single phase to ground fault will be implemented at two locations (location A: Section 4.2.1, location B: Section 4.2.2). Lastly a three-phase to ground fault will be implemented (Section 4.2.3). As the importance of fault location has been emphasised in the previous section, this fault will only be applied at location A. Different fault locations have been defined in Fig. 4.2. The important locations as for this chapter are *location A*: the common busbar of the two interconnectors at Tonstad, and *location B*: the busbar connecting the two AC networks at Feda. By comparing the two scenarios it will be possible to conclude whether this new connection can enhance system performance or not.

4.1 Steady State Aspects

The steady state aspects of the scenario 1 and 2 will be analysed respectively. The start-up of the converters will be emphasised, and will be related to the control design of the converters to display the operating principles of the converters. The steady state performance of a MMC stand alone system will briefly be discussed,

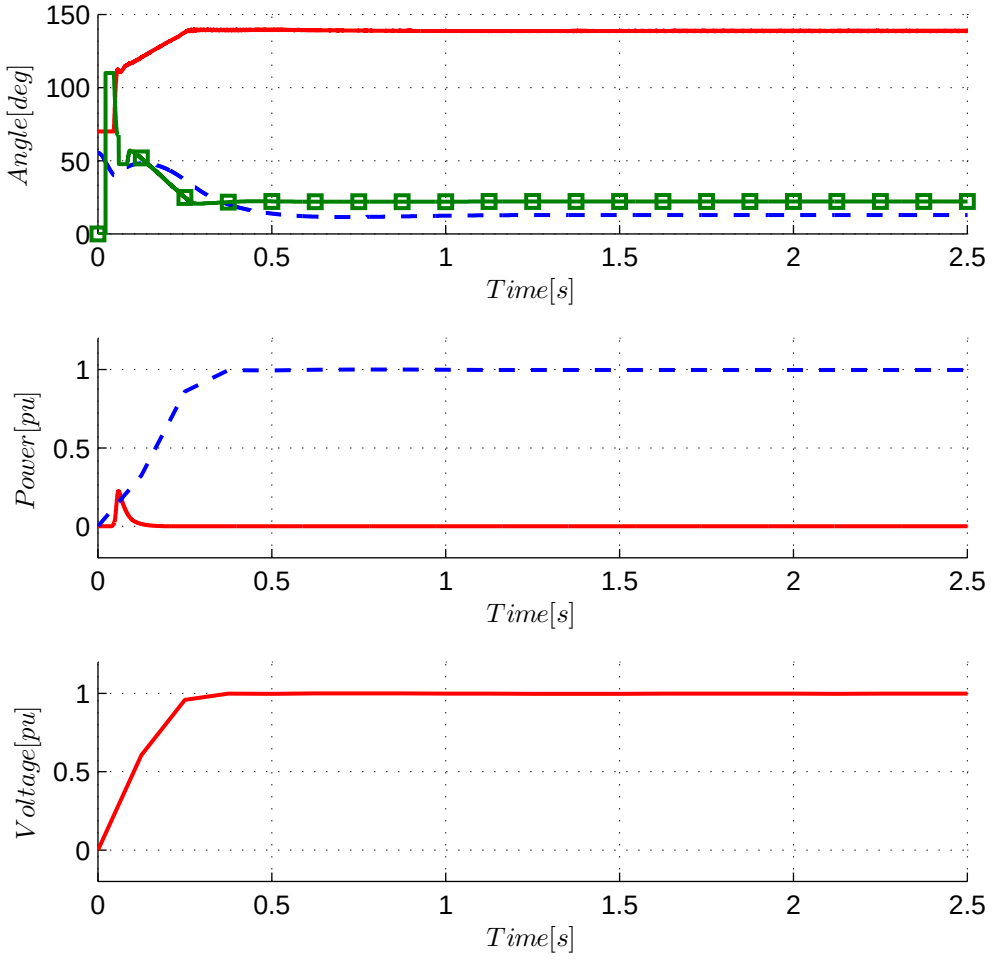

FIGURE 4.3: Scenario 1: Steady State. a) α_i (—), α_r (- - -) and γ (—□—). b) Q (—) and P (- - -). c) V_{dc} inverter side (—)

to display that the multi-infeed scenario operates with the same principle as two stand alone systems.

4.1.1 Scenario 1: LCC Stand Alone System

In Fig. 4.3 the LCC stand alone system's angles (a), powers (b) and DC voltage (c) are displayed during steady state operations. During start-up the converter needs a holding current to be able to commutate properly [52]. Before this current is obtained the converter is blocked to avoid commutation failure [48]. During this period the extinction angle, γ, increases rapidly to about 110°. When the holding current is obtained (about 0.05 seconds) the converter is deblocked, and the LCC controller is initialized. The angles $(\gamma, \alpha_r, \alpha_i)$ starts to move to their corresponding steady state values. The transient behaviour of the γ leads to a

temporary increase in reactive consumption (b). There are no power or voltage limiters installed, and the LCC system reaches its reference values rather quickly after about 0.5 seconds. There are no over-currents or voltages during steady state conditions.

The control objective of the LCC system is to control the power flow from one side of the DC system to the other. In this case the power flow is from the Netherlands to Norway. The power is controlled by keeping the DC voltage at 1 pu on inverter side, and DC current at 1 pu on rectifier side. The inverter is controlling the DC link by regulating V_{dc} to its reference value $V_{dc,ref}$. Similarly the rectifier is controlling I_{dc} to its reference value $I_{dc,ref}$. Shown by Fig. 4.3 the DC voltage (c) and DC power (b) are kept at 1 pu. Controlling the DC current is equivalent to controlling the DC power as $P = V_{dc} \cdot I_{dc}$. Also the γ is kept at its predefined value (22° [49]), and the system does not consume any reactive power. The system therefore behaves as expected and according to the implemented control design.

4.1.2 Scenario 2: Multi-Infeed MMC and LCC System

To be able to evaluate the combined model of NorNed and NordLink, a study of NordLink alone is first done. Fig. 4.4 shows steady state aspects of NordLink stand alone system, where $V_{d,q}$ (a), $I_{d,q}$ (b), powers (c) and V_{dc} (d) are displayed. First the MMC needs a start-up scheme to work properly. This is typically done with a capacitor pre-charging scheme. The scheme can be divided into two stages, *uncontrolled* and *controlled* converter [37]. Under normal operation each converter station is able to work in both DC current or DC voltage control mode. However, during the uncontrolled stage of the start-up scheme, every MMC converter is set to DC voltage control mode. The capacitor SMs are now charged with power from the AC system. This is achieved by setting all the valves in the converter to OFF (Fig. 3.2 on page 20). This state is called energization and the converter is now blocked. The AC current flows into the converter and divides equally into all the three phases. Since the converter is blocked the DC current is zero (hence also the DC power =0), which means that the upper and lower arm current is equal with opposite directions. The AC current charges the capacitors if the arm current is positive, or bypasses the capacitors if the arm current is negative. In order to avoid over-currents in this uncontrolled stage a limiting resistance is connected. The size of this resistance should be chosen to ensure safe operations. The charging speed depends mostly on this resistance, a large resistance would lead to less currents in each phase and eventually slower charging of the capacitors [37]. The capacitors are pre-charged according to the scheme described in [53], where all the capacitor voltages in each arm are charged equally at the same time. This synchronous charging technique can accelerate the black start of a converter. It also avoids the imbalance in capacitor voltages that may happen when charging the capacitors

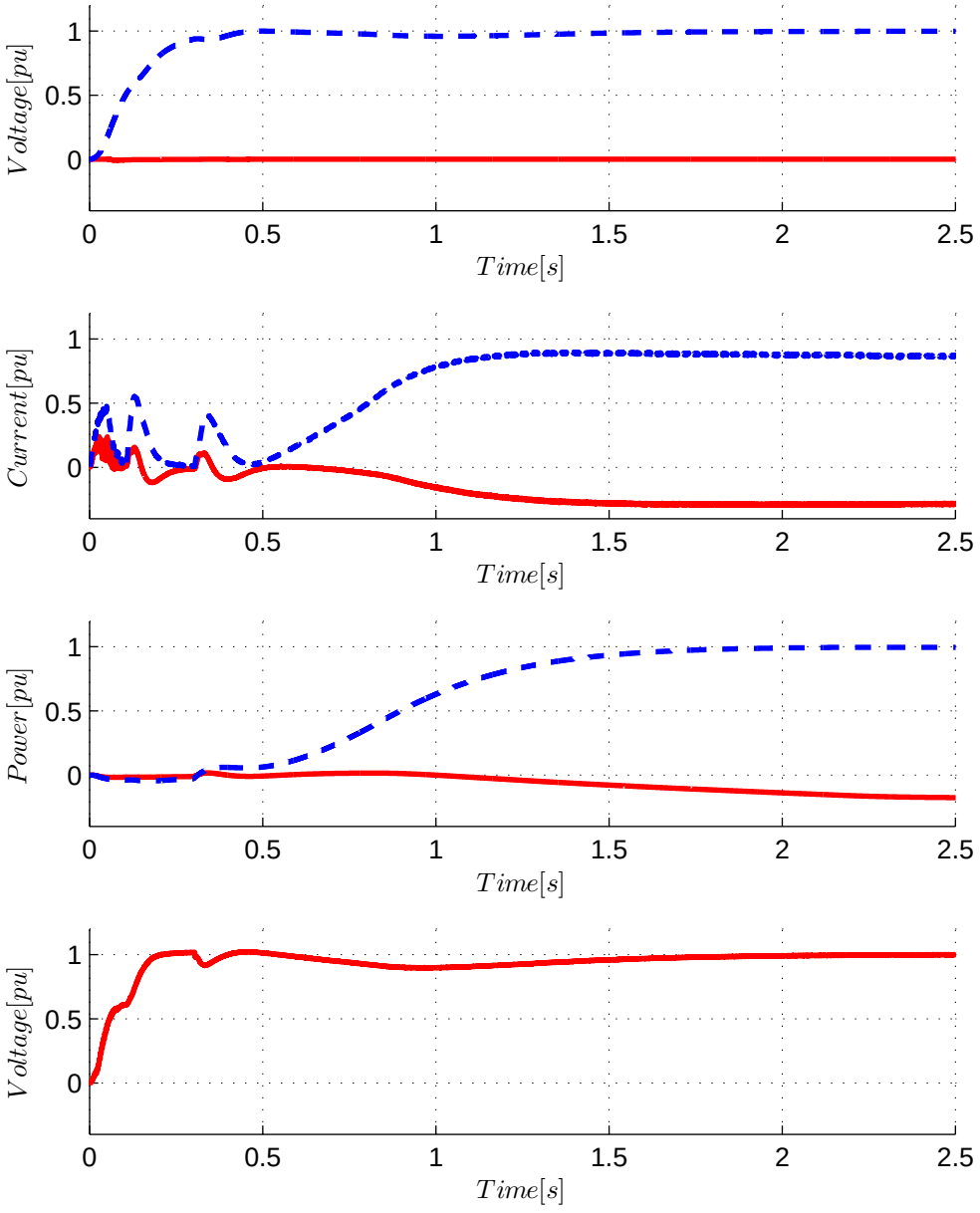

FIGURE 4.4: NordLink Stand Alone: Steady State. a) V_d (- - -) and V_q (——). b) I_d (- - -) and I_q (——). c) P (- - -) and Q (——). d) V_{dc} (——).

one by one. The control system ramps the SM capacitor voltages, and thereby also the DC voltage. This is done gradually in order to avoid damage to the DC cable.

When the DC voltage has reached its reference value, the capacitors are fully charged. The limiting resistor is short-circuited and the converter will begin to operate in a controlled converter mode (at 0.3 seconds in Fig. 4.4). In the controlled stage the converter station returns to its original control mode chosen by the master controller. At this stage the converter is deblocked and the active and reactive controllers start to work. The DC power is now being ramped up to its predefined value. This is done gradually in order to avoid damage and overheating in the equipment. The DC current direction of the MMC system is from Germany to Norway.

The control objectives of the MMC is to control DC voltage, AC voltage, active and reactive power independently. First, the DC voltage is kept close to its reference $V_{dc,ref}$. This is done by the MMC inverter station (Norway) by inverting AC power to the grid. Shown by Fig. 4.4(d) the DC voltage is close to 1 pu, and the MMC inverter thus maintains sufficient DC voltage across the SM capacitors. Second, Fig. 4.4(a) shows that V_d is held close to 1 pu, and since V_d is aligned with the AC grid voltage, controlling V_d is equivalent to controlling AC voltage. Lastly, the currents $I_{d,q}$ in Fig. 4.4(b) controls active and reactive power respectively. The active power is kept to 1 pu in Fig. 4.4(c). The AC voltage is held at 1 pu by controlling the reactive power consumption. This is done with I_q in Fig. 4.4(b). The control objectives are fulfilled and the MMC works as expected, according to the implemented control design. The MMC reaches its reference values after about 1.5 seconds, and there are no over-currents or voltages during steady state conditions.

Scenario 2, the combined system of NorNed and NordLink connected to a common busbar, is tested during steady state. Fig. 4.5 presents scenario 2 where the angles (a), powers (b) and DC voltages (c) are plotted. Fig. 4.5 indicates that the combined system of scenario 2 behaves similar to the two stand alone systems. The angles (a) are changing in the same manner as for scenario 1, and the powers (b) and DC voltages (c) reach their steady state values in the exact same way. The combined model of scenario 2 therefore behaves as expected. Comparing LCC and MMC it has been shown that the LCC start-up is much faster, 0.5 seconds to 1.5 seconds for the MMC. The MMC controller design consists of a power limiter. The limiter is set to 2500 [MW/s] ($\simeq$1.8 [pu/s]). This is to protect the system from any transients that may happen during start-up, and to avoid overheating. Every transient behaviour throughout this report will thus be implemented after 2 seconds, to ensure that both converters have reached equilibrium.

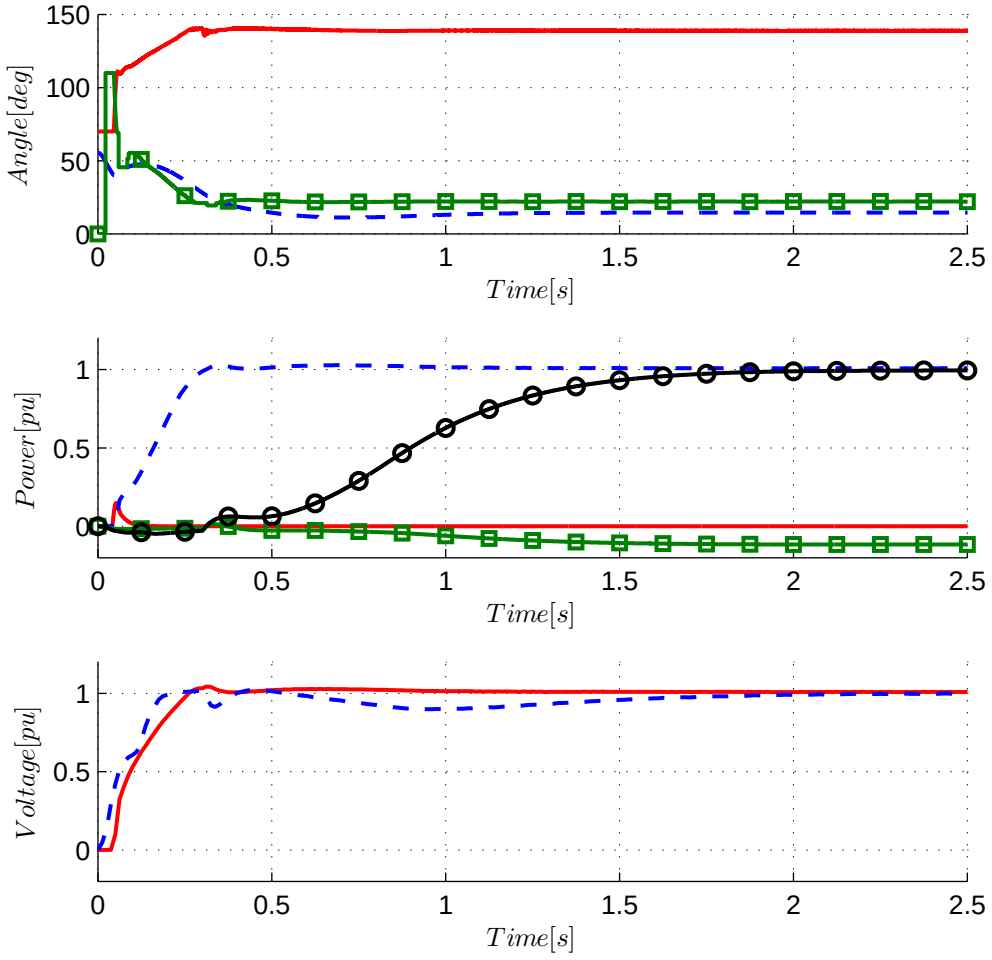

FIGURE 4.5: Scenario 2: Steady State. a) α_i (—),α_r (- - -) and γ (—□—). b) Q_{LCC} (—), P_{LCC} (- - -), Q_{MMC} (—□—) and P_{MMC} (—○—). c) $V_{dc,LCC}$ (—) and $V_{dc,MMC}$ (- - -)

4.1.3 Power Flow Changes

Simulations have been carried out to display the AC voltage effects due to power flow changes for the two scenarios. The power flow direction is the same as before, both MMC inverter and LCC inverter thus feed power into the AC system in Norway. The magnitude of the power flow will be altered between 0 and 1 pu for the converters in each scenario. The DC voltage (V_{dc}) at both converter stations will be kept at 1 pu for all the simulations. As the V_{dc} is kept at 1 pu, increasing the DC current is equal to increasing the DC power in the converters.

First, for scenario 1 the reference DC current order (I_{order}) at rectifier side was ramped from 0 to 1 pu. Ramping the I_{order} results in a ramp of the measured DC current (CMR) in the LCC-link. Fig. 4.6 shows the ramp of the I_{order} and CMR

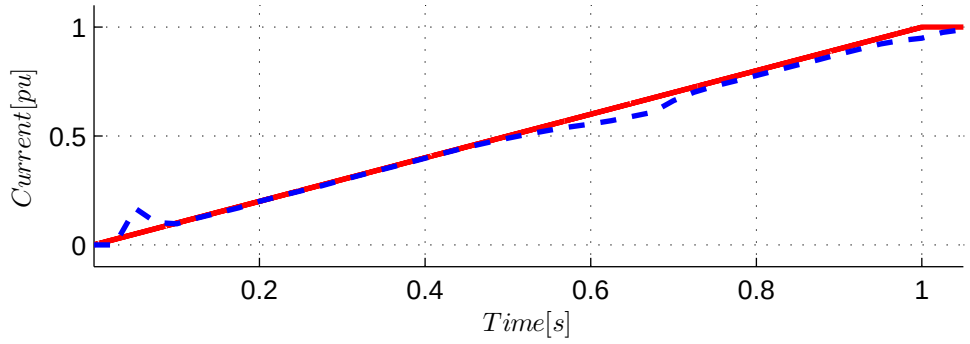

FIGURE 4.6: Scenario 1: Ramping of DC Current, I_{order} (——) and CMR (- - -).

for scenario 1. It is worth mentioning that a LCC in practice needs a minimum holding DC current in order to work properly. This limit is around 0.3 pu [52].

The change in measured DC current (CMR) in the LCC-link was then plotted against the change in AC voltage at the common busbar. Fig. 4.7 shows the result for scenario 1. As the CMR increased, the AC voltage dropped. The AC voltage drop was linear when I_{dc} increase from 0-1 pu, and only a fraction of the plot is presented.

The same test was implemented for scenario 2. As the multi-infeed system consists of two interconnections, two tests were performed. In the first test the DC current reference in MMC inverter ($I_{d,ref}$) was kept constant at 1 pu, while I_{order} in LCC was ramped from 0 to 1 pu, identical to the ramp seen in Fig. 4.6. The AC voltage at the common busbar was plotted against the CMR in the LCC-link, shown in Fig. 4.8 (Test 1). The result shows that the AC voltage is kept at 1 pu for the entire interval. In other words, the AC voltage is unaffected by the change in DC current CMR. A second test for scenario 2 was performed. Now the I_{order} in LCC was kept at 1 pu, while the $I_{d,ref}$ in MMC inverter was ramped from 0 to 1 pu. The AC voltage at the common busbar was plotted against the measured DC current in the MMC (I_d), shown in Fig. 4.8 (Test 2). The result shows that the AC voltage is once again kept at 1 pu, and is unaffected by the change in DC current I_d.

The results indicate that scenario 2 is able to stabilise the AC voltage when the power flow in any of the converters change. This was not the case for scenario 1, where the AC voltage dropped as the power flow increased. Fig. 4.7 is not representative for the real NordLink configuration, as deviations in AC voltage when the power flow changes is highly unwanted in a power system. For scenario 1 it is therefore necessary to install additional voltage supporting equipment, such as flexible AC transmission systems (FACTS) or capacitor banks in order to keep the AC voltage at 1 pu. However, the results reflects the importance of AC voltage stability, and how this can be achieved with the use of MMC AC voltage controllers. It highlights one of the great advantages of the MMC topology as

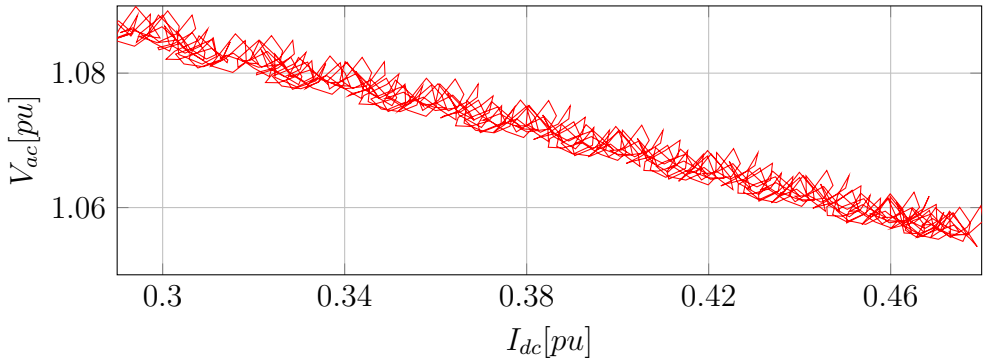

FIGURE 4.7: Scenario 1: Measured DC Current (CMR) versus AC Voltage at the Common Busbar.

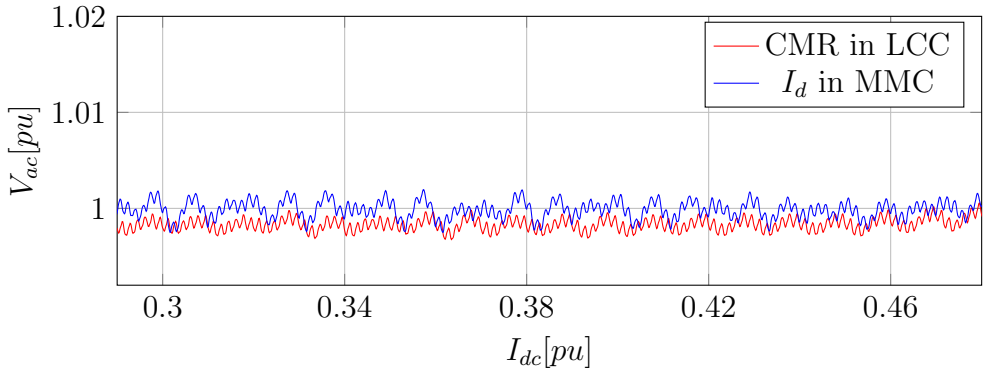

FIGURE 4.8: Scenario 2: Measured DC current versus AC Voltage at the Common Busbar. Test 1 (—) and Test 2 (—).

compared to the LCC topology. The results indicate that the MMC inverter is able to control the AC voltage for any power conditions in steady state. It is doing so by controlling the reactive power consumed by or supplied to the grid. The MMC-link thus enhances the AC voltage regulation. Existing voltage supporting equipment that are already installed in the system can thus be utilized for a more continuous voltage regulation when the new MMC-link is connected, and to minimize losses.

4.2 Transient Aspects

AC faults can be divided between balanced and unbalanced faults. Balanced faults are faults where all the phases connect to ground simultaneously, i.e. a three phase to ground fault. It is called balanced fault because all the three phases are affected equally, and the system therefore remains balanced. These types of faults are relatively rare, and according to literature 5% of all transmission faults are balanced faults [54]. Nevertheless they are the easiest to analyse, because they can be solved by reducing the system to per unit and by replacing the grid with a simple Thevenin equivalent, explained in [54]. Balanced faults are also the most

severe fault type. Circuit-breaker's rated MVA are therefore selected based on a three phase to ground fault [55].

Unbalanced faults are faults involving one or two phases. These faults are more difficult to analyse since the system is no longer balanced. The most common type of unbalanced faults are single phase to ground fault followed by line to line fault and double phase to ground fault. These faults account for 95 % of all faults on a transmission line [54].

Unbalanced faults are solved using symmetrical components, decomposed into three different sequences. Appendix C on page 125 briefly discuss different AC faults with respect to their sequence currents and voltages. This is aimed to give the reader more theoretical understanding of the following fault study.

The system was tested during various AC fault situations, to see how the system operates during abnormal operation. The following section will first investigate a single phase to ground fault on location A (Tonstad, Fig. 4.1). Second, the same fault will be applied on location B (Feda, Fig. 4.1). Third, a three phase to ground fault will be implemented on location A. These three tests will be done for scenario 1 and 2, and a comparison of the two will be made. Lastly, the section will sum up the important remarks of the section.

Tonstad is in the model located at the common busbar of the two interconnectors in close vicinity to the MMC inverter. Feda is located close to the LCC inverter. The distance between Feda and Tonstad is 50 km. All the faults in this section have a duration of 5 cycles (=100 ms) and occurs after 2 seconds, with a fault resistance of 0.01 Ω. The recovery time of the parameters (angles, powers and voltages) will be analysed, in order to determine how the system recovers when a fault occur. The recovery time is defined as the time it takes for the power and voltage to reach 90% of its prefault value, after the fault has been cleared. For the angles the recovery time is defined as the time taken for the angle to reach back to two degrees of its prefault value, after the fault has been cleared. The amplitude changes of the parameters (angles, powers and voltages) will also be analysed, as to see how much they change during the transient behaviour. The amplitude change is measured as the difference between the maximum peak and the prefault value for the given parameter.

4.2.1 Single Phase To Ground Fault: Fault A

A single phase to ground fault was implemented at location A (Fig. 4.2), with a fault duration of 0.1 seconds. The fault is located close to the MMC inverter. Two cases have been performed, one for the LCC stand alone system (scenario 1)

and for the multi-infeed system consisting of a MMC-link and LCC-link (scenario 2). A comparison of these two cases will be made throughout this section.

Fig. 4.9 presents the angles (a), powers (b), DC voltage (c) and three phase currents (d) of scenario 1. Similarly, Fig. 4.10 presents the angles (a), powers (b), DC voltages (c) and three phase currents (d) for scenario 2. Starting with the angles, Fig. 4.9(a) and Fig. 4.10(a) shows that the rectifier firing angle, α_r, increases when the fault occurs. This is because the DC current raises rapidly during the fault period. The rectifier controller, whose main objective is to keep the DC current controlled (explained in Section 3.2.3), tries to limit the change in DC voltage by increasing the α_r. An increase in the α_r means less time for commutation, hence lower DC current. The lower DC current can be seen from the decrease in power (b) in both scenarios. In scenario 1 the α_r increases substantially, and reaches its maximum value 150°.

On the LCC inverter side the extinction angle, γ, drops to zero for 0.08 seconds and 0.07 seconds for scenario 1 and 2 respectively. The γ is defined as the time between the end of the commutation interval to the positive zero crossing of the AC voltage in the grid. In a thyristor-based converter, such as LCC, the thyristor needs to remove the stored energy before the valve can regain its blocking capability. The time it takes for the thyristor to remove its stored energy is denoted by μ. The current must remain zero during this interval. If γ is zero it means that the commutation margin is zero. It indicates that the thyristor is not able to remove all its stored energy before the next commutation sequence begins (this is elaborated in Section 5.1). It is therefore important to keep γ above zero to be make sure that the thyristor has regained its blocking capability, which stops the valve from starting to conduct prematurely, and thereby avoid commutation failure in the converter [48]. The zero value in Fig. 4.9(a) and Fig. 4.10(b) hence indicates that a commutation failure has occurred.

The LCC inverter therefore tries to increase β ($\beta = \pi - \alpha_i = \mu + \gamma$ Fig. 5.1 on page 80) in order to increase $\mu + \gamma$. This can be seen by the decrease in α_i, and it drops from its prefault value 137° to its minimum value 90°, seen in (a) for both scenarios. For scenario 1 it can be seen that α_i is at its minimum value for almost the entire fault period. Eventually the LCC inverter is able to stabilize again in both scenarios after the fault has occurred. The recovery times for the angles have been summarized and can be seen in Tab. 4.1.

By taking a closer look at the DC voltage (c), active and reactive power (b) it is evident that scenario 2 has the lowest recovery times as well as lower amplitude change. The DC power in the LCC drops to negative value because the DC voltage drops to negative value. The negative DC voltage is due to the α_r increasing above 90°. The DC voltage is zero for most of the fault duration in both scenarios. This indicates a short circuit of the 12-pulse bridge in the LCC because the converter

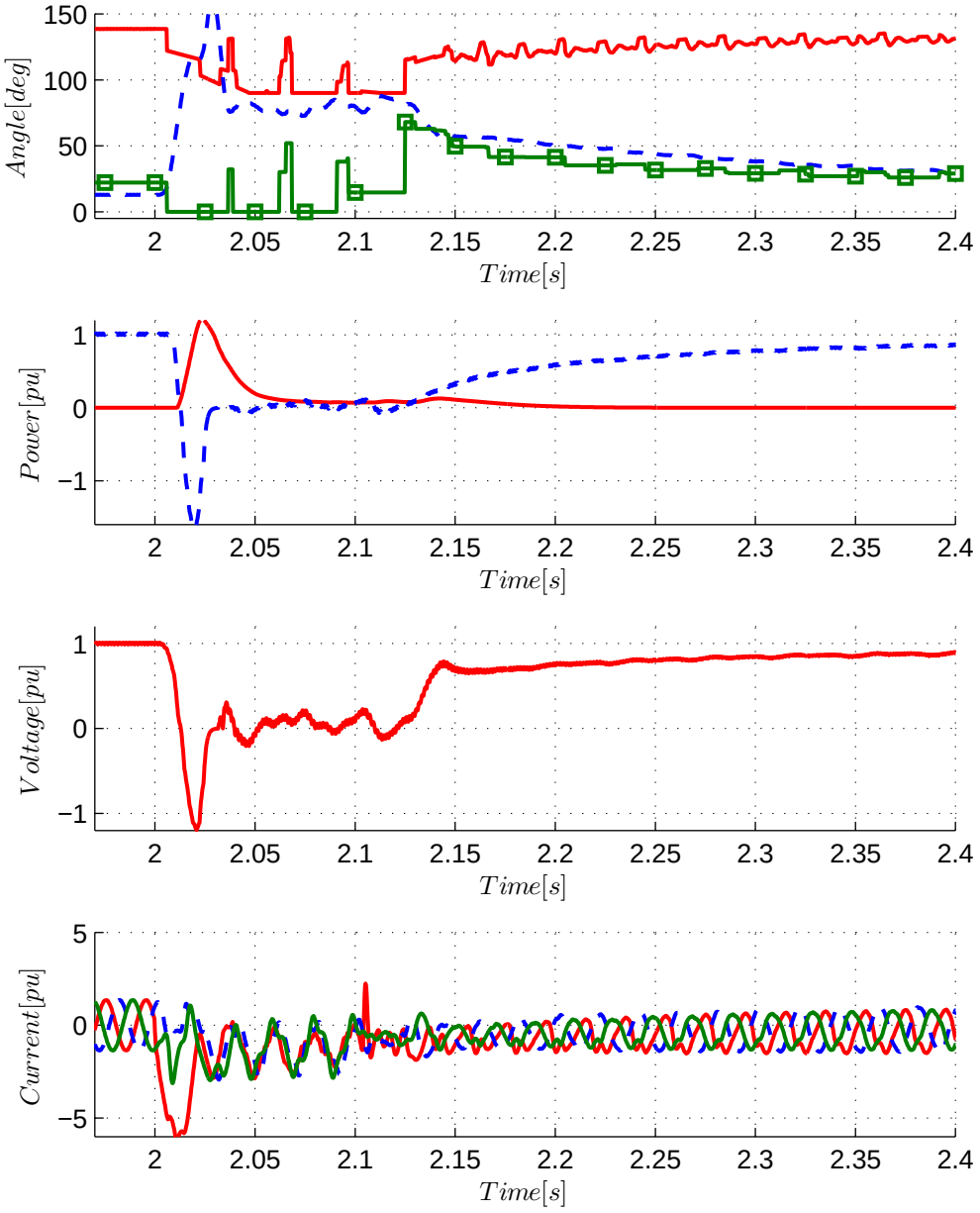

FIGURE 4.9: Scenario 1: Single Phase to Ground (Fault A): a) α_i (—), α_r (- - -) and γ (—□—). b) Q (—) and P (- - -). c) V_{dc} (—). d) Currents in phase a (—), phase b (- - -) and phase c (—).

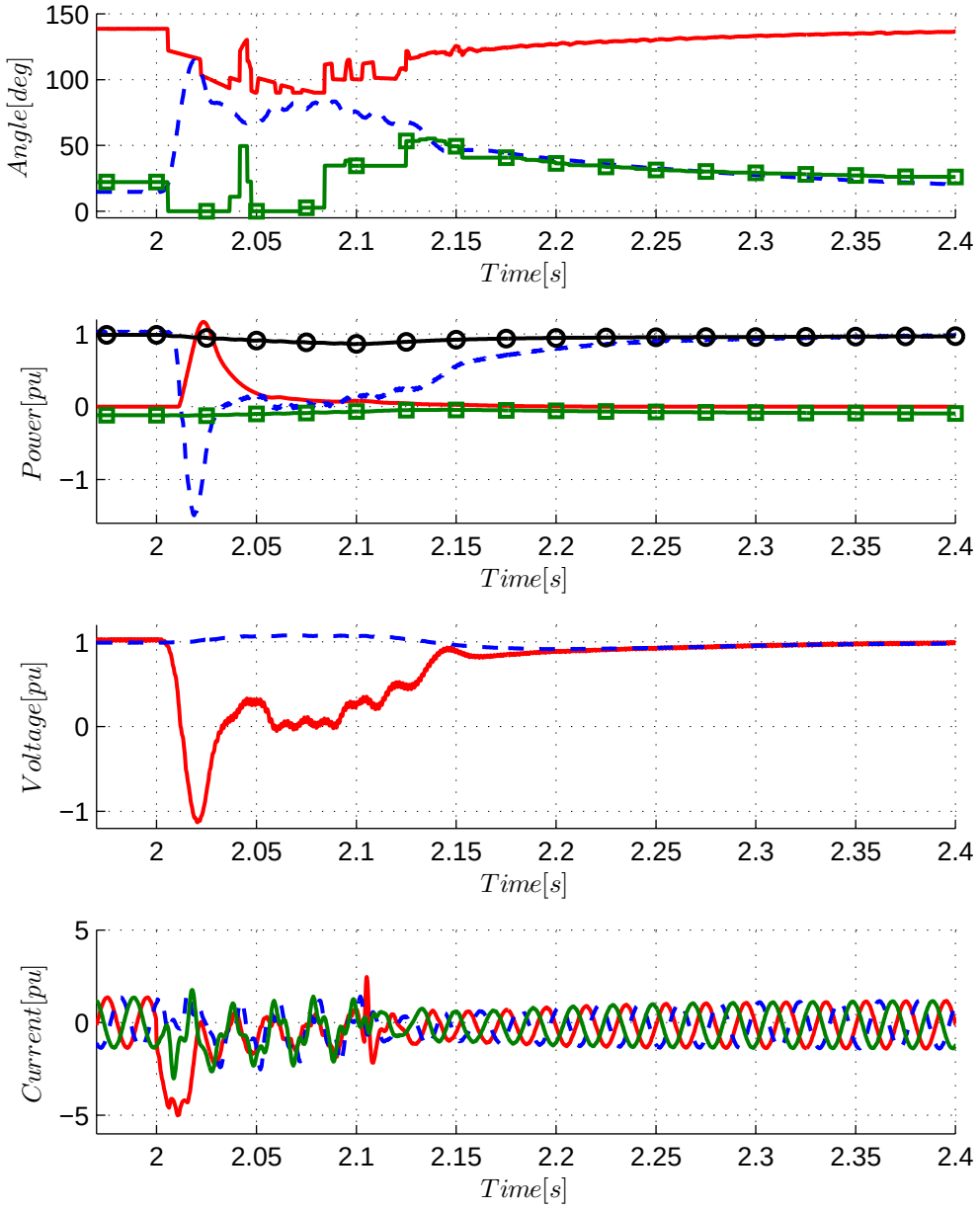

FIGURE 4.10: Scenario 2: Single Phase to Ground (Fault A): a) α_i (—), α_r (- - -) and γ (—□—). b) Q_{LCC} (—), P_{LCC} (- - -), Q_{MMC} (—□—), P_{MMC} (—○—). c) $V_{dc,LCC}$ (—) and $V_{dc,MMC}$ (- - -). d) Currents in phase a (—), phase b (- - -) and phase c (—).

Table 4.1: Fault A: Comparison Angles.

Scenario 1	**Recovery Time [s]**	**Amplitude Change [deg]**
Alpha (I)	0,3	48,6
Alpha (R)	0,4	135.5
Extinction Angle	0,4	43
Scenario 2	**Recovery Time [s]**	**Amplitude Change [deg]**
Alpha (I)	0,2	48,6
Alpha (R)	0,2	100.5
Extinction Angle	0,3	32

Table 4.2: Fault A: Comparison Voltages and Powers.

Scenario 1	**Recovery Time [s]**	**Amplitude Change [pu]**
Reactive Power (LCC)	0,14	1.2
Power (LCC))	0,17	2,6
DC Voltage (LCC)	0,15	2,2
Scenario 2	**Recovery Time [s]**	**Amplitude Change [pu]**
Reactive Power (LCC)	0	1,2
Power (LCC))	0,14	2,4
DC Voltage (LCC)	0,12	2,1
Reactive Power (MMC)	0	0.1
Power (MMC))	0,08	0,2
DC Voltage (MMC)	0,13	0,1

is experiencing commutation failures. The recovery times for the voltages and powers have been summarized in Tab. 4.2. In terms of angles, DC voltage, active and reactive power the recovery times are shorter for scenario 2 than for scenario 1. Fig. 4.9 and Fig. 4.10 shows that the amplitude changes for powers and voltages in the two converters, irrespective of scenario, are substantially higher for LCC than for the MMC. These results indicate that the MMC is not much affected by a single phase to ground fault, as the amplitude changes are quite small. These results therefore indicate that the single phase to ground fault at location A is more severe for the LCC than for the MMC, and that scenario 2 recovers faster.

4.2.2 Single Phase To Ground Fault: Fault B

A single phase to ground fault was implemented at location B (Fig. 4.2), with a fault duration of 0.1 seconds. The fault is now located much closer to the LCC inverter. Simulations of two cases have been performed, one for the LCC stand

alone system (scenario 1) and for the multi-infeed system consisting of a MMC-link and LCC-link (scenario 2). A comparison of these two cases will be made throughout this section.

Fig. 4.11 presents the angles (a), powers (b), DC voltage (c) and three phase currents (d) of scenario 1. Similarly, Fig. 4.12 presents the angles (a), powers (b), DC voltages (c) and three phase currents (d) of scenario 2. Starting with the angles Fig. 4.11(a) and Fig. 4.12(a) shows that the α_r increases quickly to its maximum 150° for the same reason as before: the rectifier station tries to limit the DC over-current. α_r remains above 90° at start of the fault duration for both scenarios, resulting in a negative DC voltage (c) in the LCC during this time interval. The γ (a) is zero for 0.09 seconds and 0.05 seconds for scenario 1 and 2 respectively. In other words, the γ is zero for almost twice the duration for scenario 1. The LCC-link tries to recover the γ, and responds by decreasing the α_i. It drops to its minimum value 90° for both scenarios for almost the entire fault duration, shown in (a). Eventually the LCC-link is able to stabilize in both scenarios. The recovery time and amplitude change for the angles have been summarized and can be seen in Tab. 4.3. The recovery time for the α_i, α_r and γ are greatly reduced for scenario 2 compared to 1.

Table 4.3: Fault B: Comparison Angles.

Scenario 1	**Recovery Time [s]**	**Amplitude Change [deg]**
Alpha (I)	0,5	48,6
Alpha (R)	0,8	137,2
Extinction Angle	0,6	46
Scenario 2	**Recovery Time [s]**	**Amplitude Change [deg]**
Alpha (I)	0,3	48,6
Alpha (R)	0,4	137,2
Extinction Angle	0,4	33

As for the DC power (b) in the LCC-link, it drops significantly for both scenarios. The zero power can be explained in the same way as before: the fault results in a commutation failure indicated by the γ which drops to 0°, and the converter is thus short circuited resulting in zero DC voltage, hence also a zero DC power. The LCC DC power amplitude changes for both scenarios are nearly the same, 2.6 pu and 2.5 pu for scenario 1 and 2 respectively. The LCC DC power recovery times are 0.36 seconds and 0.15 seconds for scenario 1 and 2 respectively. As shown by Tab. 4.4, the recovery times for LCC power and voltage are greatly reduced in scenario 2. The results indicate that the location of the fault is an important parameter, as the recovery times and the amplitude changes for the LCC are significantly higher for location B than location A. The MMC-link is able to ride through both faults without any noticeable problems, as it recovers fast with low amplitude changes.

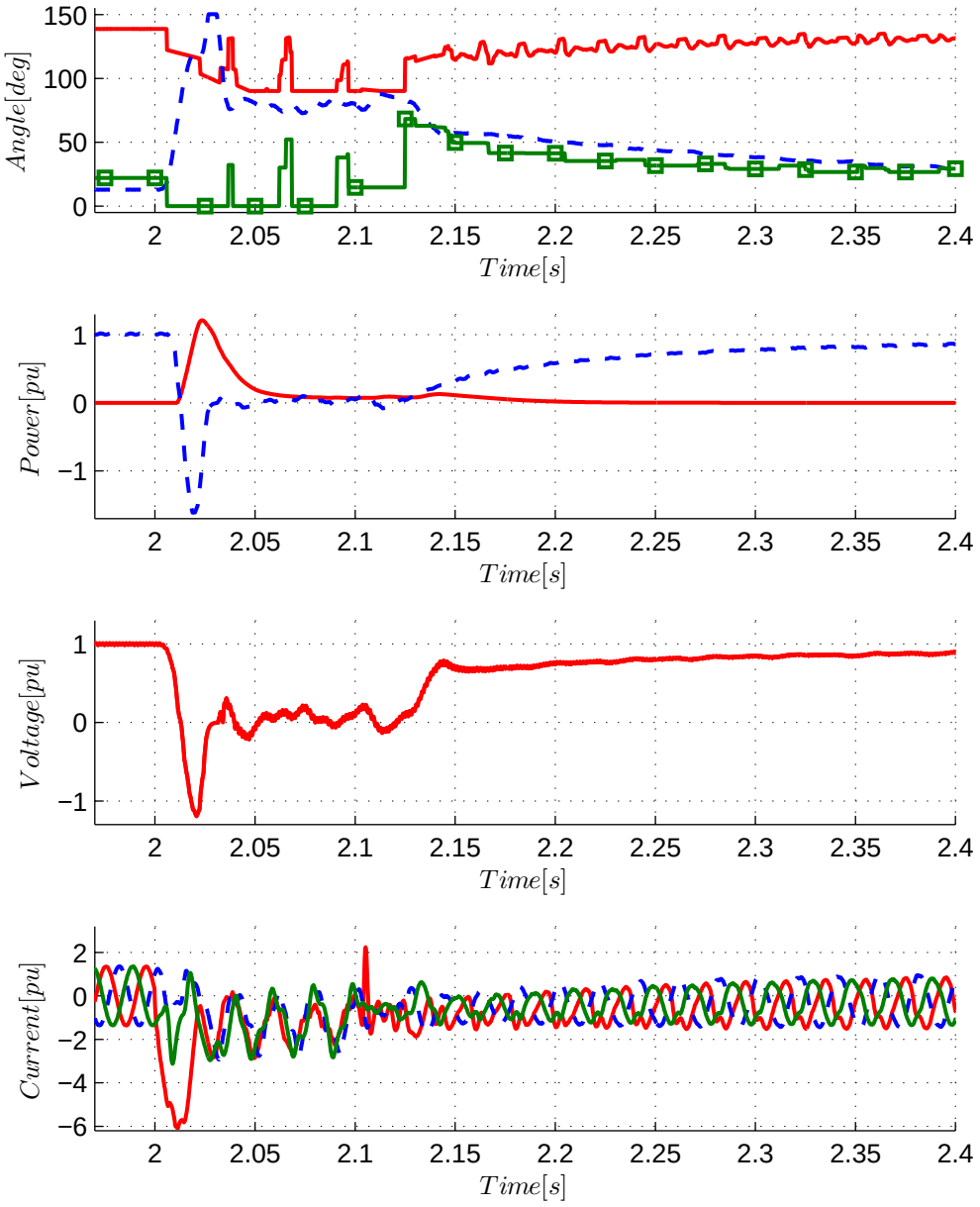

FIGURE 4.11: Scenario 1: Single Phase to Ground (Fault B): a) α_i (—), α_r (- - -) and γ (—□—). b) Q (—) and P (- - -). c) V_{dc} (—). d) Currents in phase a (—), phase b (- - -) and phase c (—).

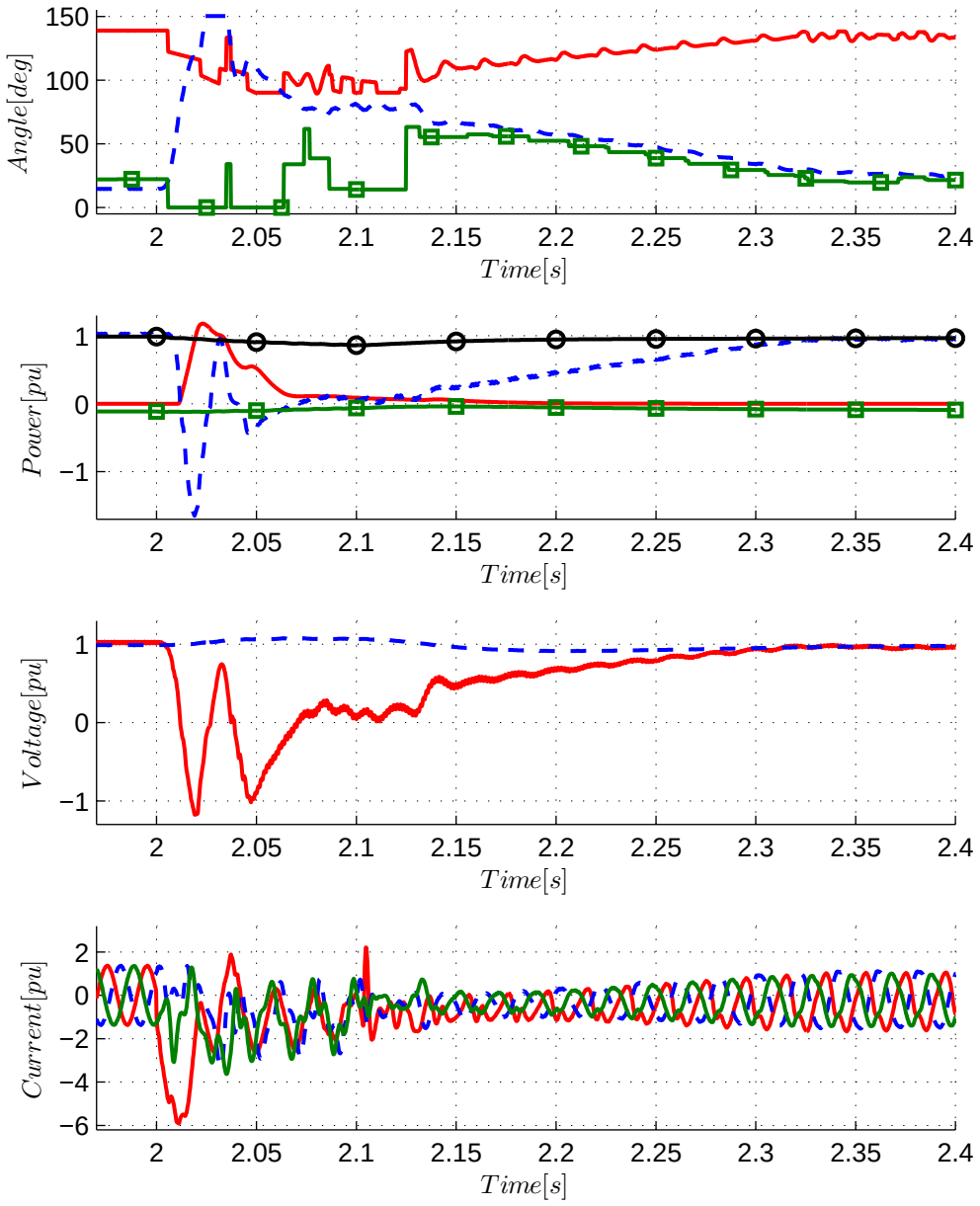

FIGURE 4.12: Scenario 2: Single Phase to Ground (Fault B): a) α_i (—), α_r (- - -) and γ (—□—). b) Q_{LCC} (—), P_{LCC} (- - -), Q_{MMC} (—□—), P_{MMC} (—○—). c) $V_{dc,LCC}$ (—) and $V_{dc,MMC}$ (- - -). d) Currents in phase a (—), phase b (- - -) and phase c (—).

Table 4.4: Fault B: Comparison Voltages and Powers.

Scenario 1	**Recovery Time [s]**	**Amplitude Change [pu]**
Reactive Power (LCC)	0,05	1,2
Power (LCC))	0,4	2,6
DC Voltage (LCC)	0,36	2,2
Scenario 2	**Recovery Time [s]**	**Amplitude Change [pu]**
Reactive Power (LCC)	0	1,2
Power (LCC))	0,25	2,5
DC Voltage (LCC)	0,15	2,1
Reactive Power (MMC)	0	0,1
Power (MMC))	0,03	0,15
DC Voltage (MMC)	0	0,07

4.2.3 Three Phase To Ground Fault

A three phase to ground fault was implemented. As the importance of fault location has been emphasised in the previous section, the three phase to ground fault will only be implemented at one location, namely location A (Tonstad, Fig. 4.2). The fault duration was set to 0.1 seconds. Simulations of two cases have been performed, one for the LCC stand alone system (scenario 1) and for the multi-infeed system consisting of a MMC-link and LCC-link (scenario 2). A comparison of these two cases will be made throughout this section.

Fig. 4.13 presents the angles (a), powers (b), DC voltage (c) and three phase currents (d) of scenario 1. Similarly, Fig. 4.14 presents the angles (a), powers (b), DC voltages (c) and three phase currents (d) of scenario 2. First, the angles (a) in both scenarios behave in the same manner as described for a single phase to ground fault, explained in Section 4.2.1 and Section 4.2.2. The remarkable in a three phase fault is the duration at which the γ is zero, 0.126 seconds and 0.072 seconds for scenario 1 and scenario 2 respectively. This can be explained by the AC phase currents (d), where the three phases fail to commutate properly during the fault duration, especially for scenario 1. The thyristors in the LCC need a negative valve voltage to be able to remove the stored energy. Otherwise it cannot efficiently block the current, and the thyristor looses its controllability. During the fault duration γ is zero hence means the commutation margin is zero, and the thyristors have not regained its blocking capability. Fig. 4.15 shows the current and voltage of one valve in the LCC inverter during the three phase fault. Notice that the valve current in Fig. 4.15(a) for scenario 1 is positive for almost the entire fault duration. For scenario 2 the valve current is normalized after 0.06 seconds. The thyristors in scenario 2 is hence able to remove the stored energy, shown by

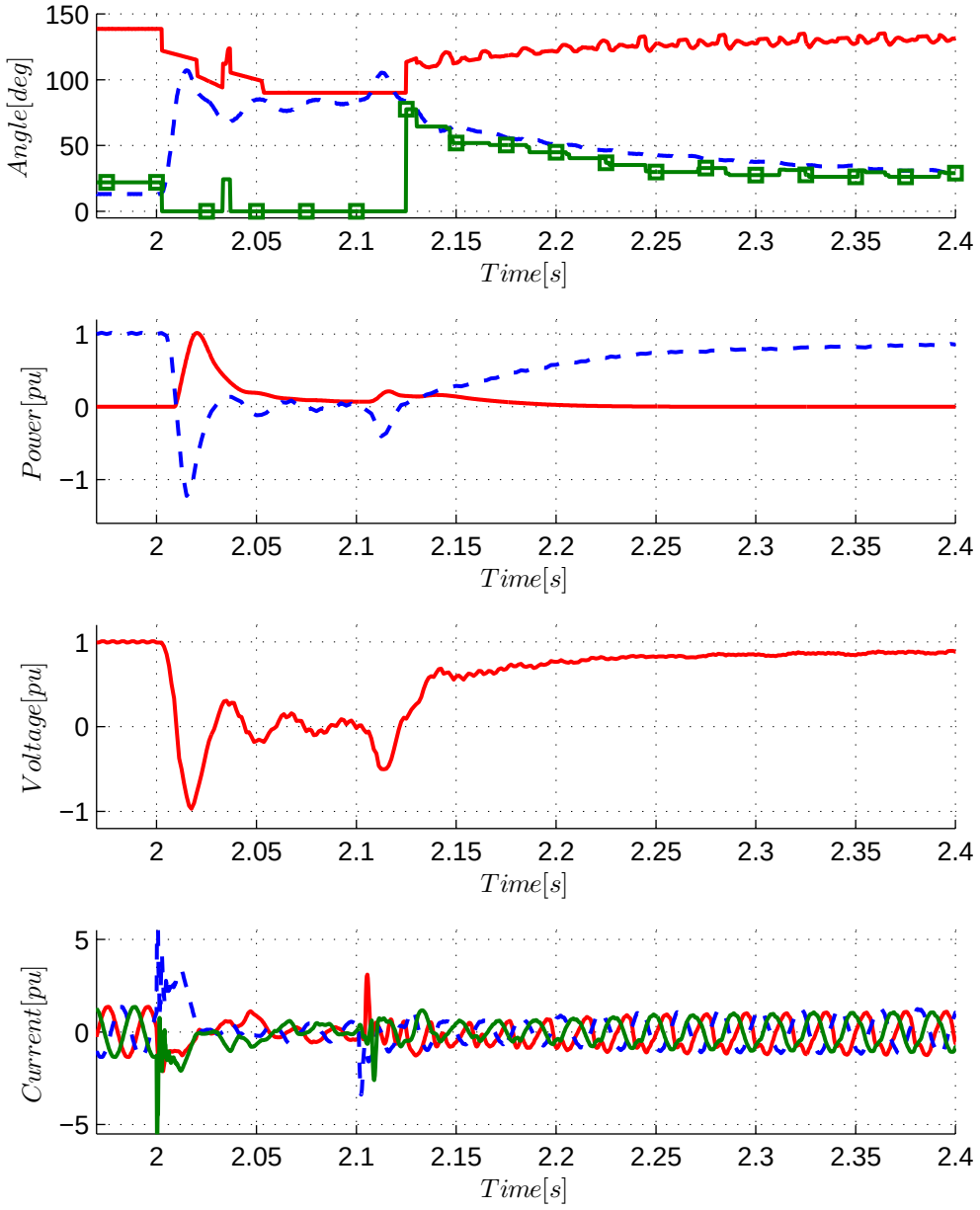

FIGURE 4.13: Scenario 1: Three Phase to Ground: a) α_i (—), α_r (- - -) and γ (—□—). b) Q (—) and P (- - -). c) V_{dc} (—). d) Currents in phase a (—), phase b (- - -) and phase c (—).

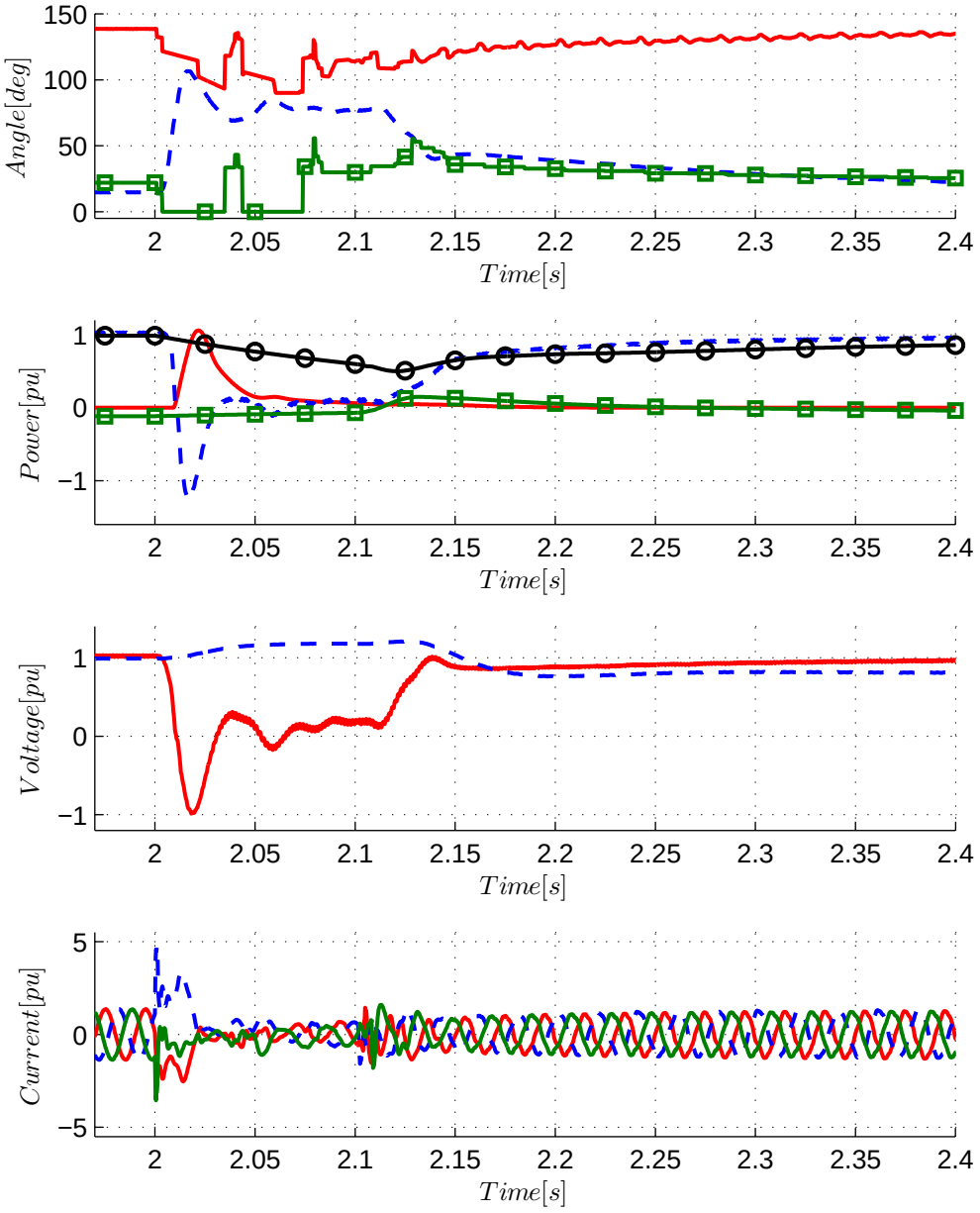

FIGURE 4.14: Scenario 2: Three Phase to Ground: a) α_i (—), α_r (- - -) and γ (—□—). b) Q_{LCC} (—), P_{LCC} (- - -), Q_{MMC} (—□—), P_{MMC} (—○—). c) $V_{dc,LCC}$ (—) and $V_{dc,MMC}$ (- - -). d) Currents in phase a (—), phase b (- - -) and phase c (—).

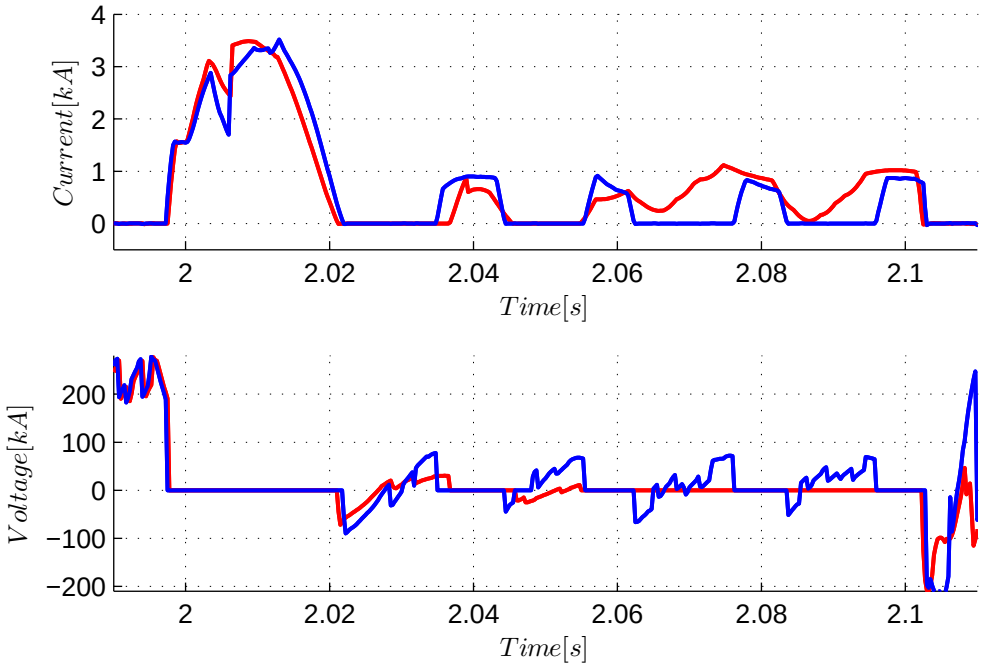

FIGURE 4.15: Thyristor Valve in the LCC inverter During a Three Phase to Ground: a) Valve Current b) Valve Voltage, Scenario 1 (—), Scenario 2 (—).

the negative valve voltage spikes in Fig. 4.15(b), and by the γ which is able to recover during the fault period on Fig. 4.14.

TABLE 4.5: Three Phase to Ground Fault: Comparison Angles.

Scenario 1	**Recovery Time [s]**	**Amplitude Change [deg]**
Alpha (I)	0,38	48,6
Alpha (R)	0,7	94.5
Extinction Angle	0,48	55
Scenario 2	**Recovery Time [s]**	**Amplitude Change [deg]**
Alpha (I)	0.3	48,6
Alpha (R)	0.45	89
Extinction Angle	0.4	36

Looking at the powers, Fig. 4.14(b) shows that the MMC reactive power increases substantially during the fault (0.25 pu). As the three phase fault occurs in the AC grid just outside the MMC inverter, the AC voltage drops to zero. The MMC inverter immediately tries to restore the AC voltage, by supplying reactive power into the grid. This was also seen for the single phase to ground fault, but the response is much clearer for a three phase to ground fault. As the voltage drop is more severe, the response from the MMC is larger. The amplitude of the reactive power is now doubled compared to the single phase fault at location A. Shown in

Table 4.6: Three Phase to Ground Fault: Comparison Voltages and Powers.

Scenario 1	**Recovery Time [s]**	**Amplitude Change [pu]]**
Reactive Power (LCC)	0,06	1,1
Power (LCC))	0,35	2,3
DC Voltage (LCC)	0,34	2
Scenario 2	**Recovery Time [s]**	**Amplitude Change [pu]**
Reactive Power (LCC)	0	1,1
Power (LCC))	0,2	2,25
DC Voltage (LCC)	0,12	2
Reactive Power (MMC)	0.25	0,25
Power (MMC))	0,2	0,4
DC Voltage (MMC)	0,4	0,2

Fig. 4.14(c) the DC voltage of the MMC-link has problems stabilizing after the fault is cleared, but is able to recover after 0.4 seconds. Despite the critical AC voltage drop, the MMC is able to ride through the fault without having any other noticeable problems. In general all the parameters have longer recovery times for scenario 1 than for scenario 2, summarized in Tab. 4.6. This was as expected, and is accordance with the single phase to ground fault.

4.2.4 Closing Remarks

To sum up the transient aspect section, the results indicate that:

- LCC is most affected by faults located at B
- MMC is most affected by faults located at A
- Scenario 2 recovers faster than scenario 1, with smaller amplitude changes (angles, powers, voltages, currents)
- Three phase to ground faults are more severe than single phase to ground faults
- LCC inverter stations in weak AC systems may suffer from commutation failure
- MMC inverter stations are able to ride through relatively severe AC faults (negligible recovery times and amplitudes)
- The control systems respond according to the implemented control design

Fault location is an important parameter when fault situations are discussed. The fact that fault B is electrically closer to the LCC inverter station, seems to affect the angles substantially. Fault B results in a higher drop in AC voltage at the LCC terminals, compared to fault A for the same fault type. Fault B is therefore more severe for the LCC inverter. For a single phase to ground fault, neither fault A nor B cause any noticeable problems for the MMC-link, and minor changes in voltage and powers are quickly stabilized after the fault is cleared. The LCC-link responds to the faults according to the control theory presented in Section 3.2, and tries to stabilize the fault by changing its firing angles. The MMC-link is able to help the LCC inverter for scenario 2 during the AC faults. It can be seen that scenario 2 has lower recovery times for angles, voltages and powers compared to scenario 1, irrespective of the fault type. This is because the MMC-link is able to respond quickly to the AC drop during single and three phase to ground faults. The MMC-link has AC voltage controllers installed. By supplying reactive power to the grid the AC drop is countered, which leads to a reduced impact. For instance during the single phase to ground fault on location A, the reactive power in the MMC changes from -0.1 to 0 pu (increase of 0.1 pu·1400 MVA = 140 MVar). For the three phase to ground fault, the MMC reactive power changes from -0.1 to 0.15 pu (increase of 0.25 pu·1400 MVA = 350 MVar). The results therefore indicate problems with LCC inverter operating in weak AC systems, and the advantages of installing a MMC-link in close proximity to a LCC inverter.

Chapter 5

Commutation Failure Immunity Index for a Multi-Infeed HVDC System

The increasing use of more than one HVDC converter station in close proximity in an AC system (i.e. multi-infeed HVDC system) raises the question on how these converters will impact each other. For LCC systems it is of great interest to see how a multi-infeed systems affects the likelihood of commutation failures. How susceptible a converter is to commutation failures depends mostly on the grid layout as well as the control systems [56]. According to literature it is probable that multi-infeed HVDC interactions will affect the susceptibility of commutation failure due to the changing power system layout and because of interaction between the control systems of the converters [27]. It is therefore of great interest to see how this specific configuration will affect the LCC converter's resilience.

The purpose of this section is to investigate how susceptible the LCC stand alone system (scenario 1) is to commutation failure, and to compare it with the multi-infeed system (scenario 2). It will then be possible to see if the future upgraded system is less vulnerable than today's installed system. First, a brief discussion about commutation failure will be made (Section 5.1). Second, a proposed method for detecting commutation failure will be explained (Section 5.2). Third, the susceptibility to commutation failure for each scenario will be presented and the results will be discussed (Section 5.3).

5.1 Commutation Failure in a LCC

When a thyristor is conducting it will store energy, and this energy must be removed before the thyristor can regain its forward voltage blocking capability. The

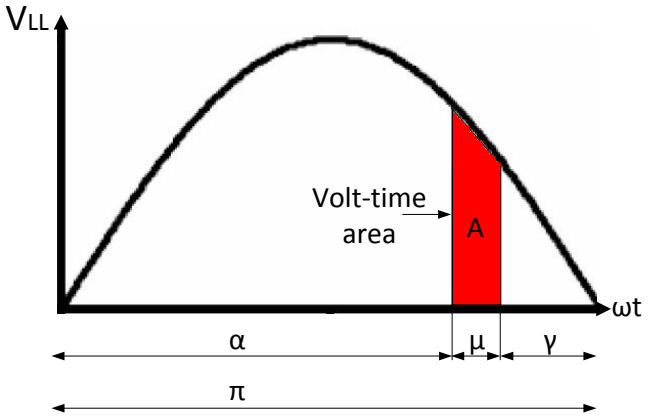

FIGURE 5.1: Volt-Time Area in an Inverter.

valve current across the thyristor must therefore remain zero for some time interval, denoted by the volt-time area in Fig. 5.1. The time duration of this interval is denoted by μ and is typically in the range of 20° to 50° in steady state [50]. During μ the voltage over the thyristor drops to negative value as to remove its stored energy. The time from the valve current goes to zero until the line-line voltage goes to zero can be measured and is denoted by the extinction angle γ in Fig. 5.1. γ is also called the commutation margin, and this time interval should be kept above zero to be sure that the valve has regained its blocking capability.

Commutation failure is a transient event that can occur in a thyristor based converter such as a LCC. It happens when a thyristor fails to remove all its stored energy before the next valve begins to conduct. The thyristor is lacking its forward voltage blocking capability, and thus continues to conduct current instead of turning off. Two valves are now conducting at the same time. This event can be seen as a short circuit of the DC voltage. Possible triggers of commutation failure are reduction in AC line-line voltage magnitude, sudden change in phase angle of the AC line-line voltage or increased DC current. All these changes increase the time needed for commutation (i.e. increases μ), thereby decreasing the commutation margin (i.e. decreases γ). Commutation failure happens mostly on the inverter side. At rectifier side commutation failures are rare. Since the commutation process on rectifier side occur before the line-line voltage has reached 90° the commutation margin is much longer as compared to the inverter station.

Commutation failure is a serious malfunction of the converter, which can cause high over-currents in the valves which again can cause severe and permanent damage to the converter equipment [27]. It can also delay the start-up of a converter station after a fault has been cleared [50]. In general one single commutation failure may not harm the converter, however multiple commutation failures may force the converter to trip [45].

In order to reduce the risk of commutation failure during these transient events it is vital to change the reactive consumption as soon as possible. A LCC normally uses a control system called a voltage dependent current order limiter (VDCOL) which can temporarily decrease the DC current, and thereby also the reactive power consumption during fault situations. A static VAR or other fast acting reactive controllers in the system may also decrease the risk of commutation failures. These controllers can mitigate adverse impacts substantially and help the converter regain stability faster. Other mitigation techniques are to temporary increase extinction angle or firing angles [56].

Currents and voltages of one valve during normal and fault situations is shown in Fig. 5.2(a). When the fault occur after 1 second the thyristor does not remove its stored energy. This can be seen on the voltage, where its value does not go to negative value. The thyristor therefore fails regain its forward blocking capability, and continues to conduct. A commutation failure in one valve has happened, and it results in a relatively high valve current (4 kA).

5.2 Commuation Failure Detection Method

In order to determine if a commutation failure has occurred or not a commutation failure detection method has been developed in PSCAD. A logic circuit was made for each valve in the 12-pulse bridge, shown in Fig. 5.2(b). The idea behind this circuit is to determine if a commutation failure has occurred in one valve.

The upper logic circuit of Fig. 5.2(b) measures the valve current (I_{valve}) and detects when the valve current is larger than a predefined value (Value #1). If $I_{valve} \geq$ Value #1 is true, the circuit outputs 1. The *Sample and Hold* function holds the time value when a logic 1 input is detected. The *Sampler* samples the input signal at discrete intervals, and then holds the output at the sampled level until the next sample is taken. The sampling is triggered by a specified sampling rate, here 50 Hz. The bottom logic circuit does the same as the upper, but the logic is true when $I_{valve} \leq$ Value #1. The time difference between the upper and bottom circuit is then compared to a value equal to a normal commutation period (Value #2). If the input signal exceeds Value #2, a commutation failure has occurred in this specific valve.

Fig. 5.3(a) shows the error logic that has been used for the LCC inverter station. In order to have a commutation failure in the inverter (CF_ total in Fig. 5.3(a)) both six-pulse bridges (CF1 and CF2 in Fig. 5.3(a)) must have at least one of their phases short circuited at the same time. In a six-pulse bridge, one phase is said to be short circuited if two of the valves in the same phase are short circuited at the same time. This means that valve 1 and 4 OR 2 and 5 OR 3 and 6 must

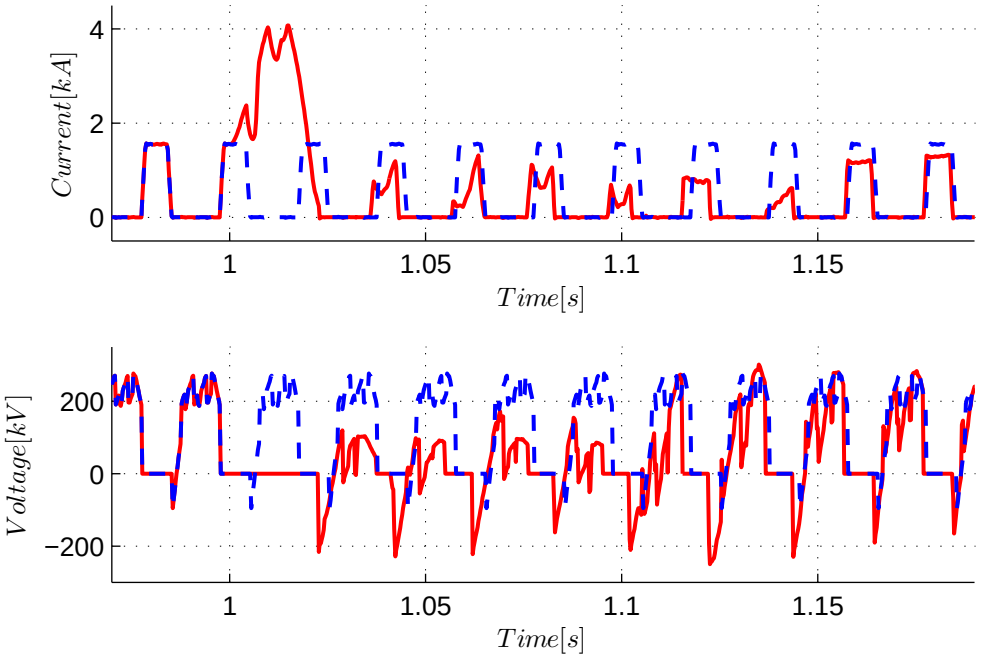

(a) Faulty (—) and Healthy (- - -) Valve Current (Top) and Voltage (Bottom)

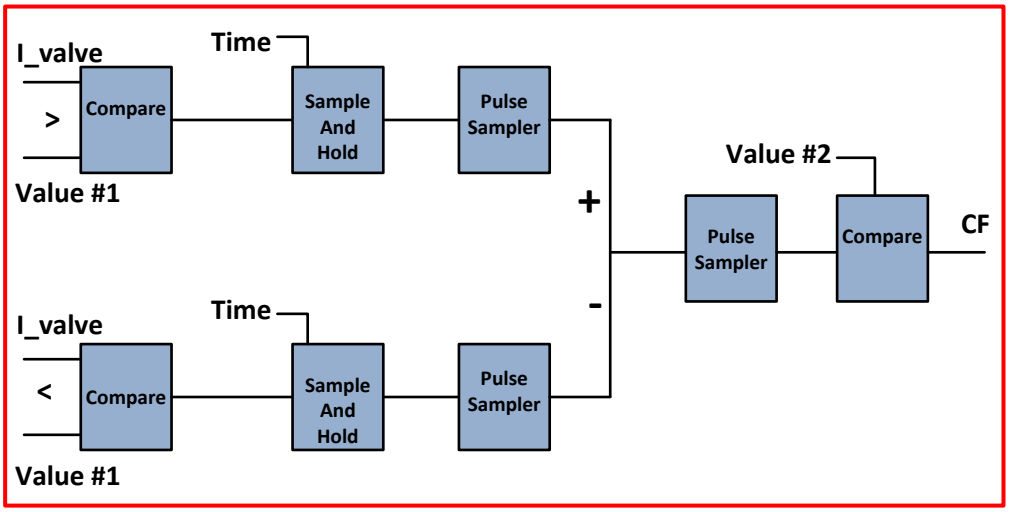

(b) Valve Logic Circuit

FIGURE 5.2: Commutation Failure Detection Method: Error Logic One Valve.

fail to commutate for a six-pulse bridge to short circuit. Fig. 5.3(b) shows the error logic signal when two six-pulse bridges are short circuited at the same time. The resulting commutation failure of the entire 12-pulse bridge is shown on top of Fig. 5.3(b). If the two six-pulse bridges fail to commutate at the same time, a commutation failure in the 12-pulse bridge (i.e. inverter) has occurred. The DC voltage is now short circuited.

5.3 Commutation Failure Immunity Index for a Multi-Infeed HVDC System

To present how susceptible a converter is to commutation failure a Commutation Failure Immunity Index (CFII) has been proposed [27]. The index is defined as follows,

$$\begin{aligned} \text{CFII} &= \frac{\text{Critical Fault MVA}}{\text{Rated DC Power}} \cdot 100\% \\ \text{CFII} &= \frac{(\text{V}_{ac})^2}{\text{R}_f \cdot \text{P}_d} \cdot 100\% \\ \text{CFII} &= \frac{(420\ \text{kV})^2}{\text{R}_f \cdot 700\ \text{MW}} \cdot 100\% \end{aligned} \tag{5.1}$$

where Critical Fault MVA is the worst fault that can happen without experiencing commutation failure in the converter, V_{ac} is the AC grid voltage, P_{dc} is the DC power of the LCC and R_f is the fault resistance to ground. If the critical fault resistance (R_f) is low the converter is more immune. Shown by Eqn. 5.1 this gives a higher CFII.

A CFII study was performed in the following way: a phase to ground fault was applied close to the LCC converter station (location B, Fig. 4.2 on page 57), starting with a relatively high fault resistance. This gives a neglectable fault. The fault resistance was then gradually reduced until a commutation failure was detected by the commutation failure detection method.

The CFII study was performed for two cases, namely LCC stand alone HVDC system (scenario 1) and multi-infeed system consisting of a MMC and LCC (scenario 2). The critical fault resistance without experiencing commutation failure was found to be 9 Ω and 7 Ω for scenario 1 and 2 respectively. Inserting the fault resistance into Eqn. 5.1 leads to a CFII of 28% and 36% for the scenario 1 and 2 respectively. The results are presented in Tab. 5.1.

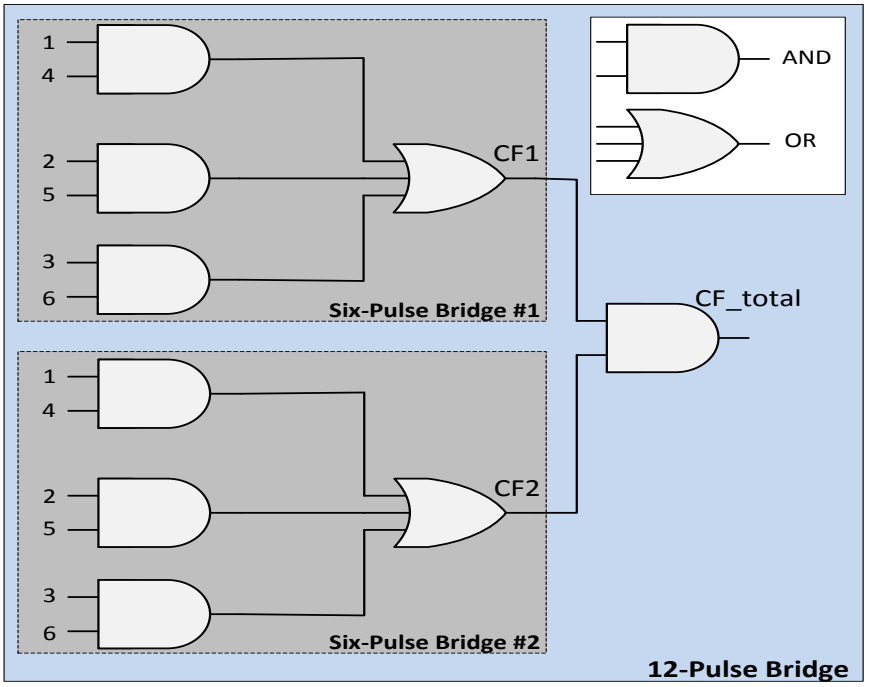

(a) Error Logic for the Entire 12-Pulse Bridge

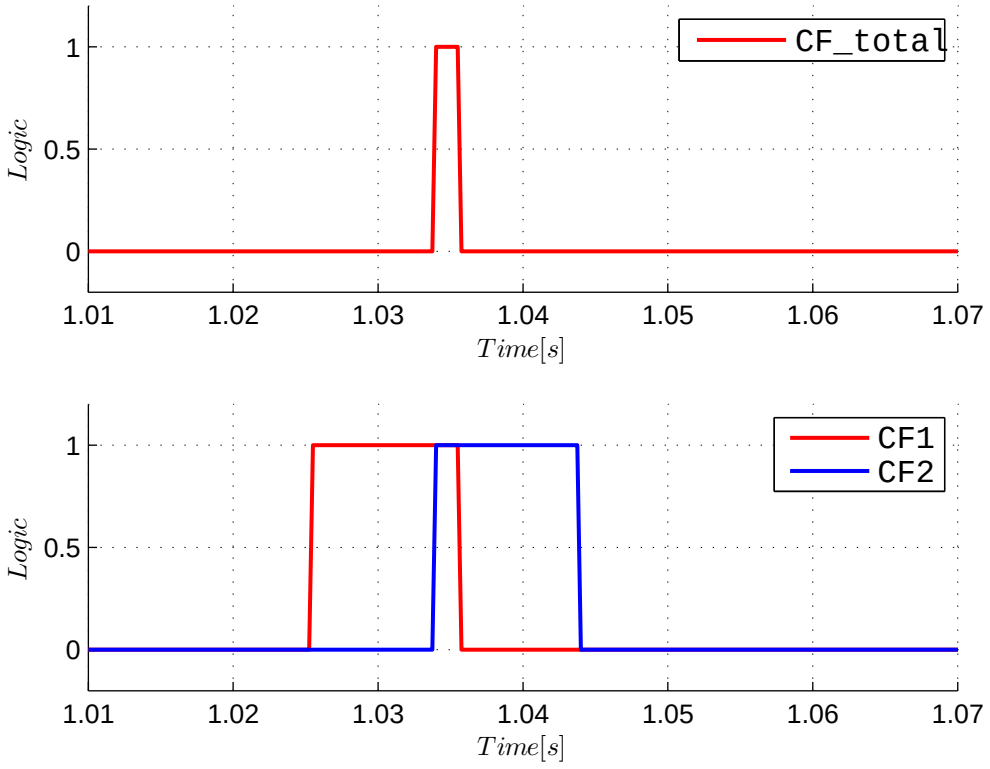

(b) Error Logic Signals. Top: 12-Pulse Bridge. Bottom: Two Six-Pulse Bridges

FIGURE 5.3: Commutation Failure Detection Method: Error Logic.

Table 5.1: Commutation Failure Immunity Index.

Scenario	**CFII** [%]
1: LCC Stand Alone	28
2:Multi-Infeed	36

Shown in Tab. 5.1 scenario 2 is less susceptible to commutation failure than scenario 1. The results therefore indicate that the MMC-link makes the LCC-inverter less prone to commutation failure. The MMC-link is able to stabilize the AC voltage during a phase to ground fault. As a LCC inverter in weak AC systems may suffer from commutation failures, the installation of a MMC station in close proximity thus lead to fewer occurrences of commutation failures. A MMC-link therefore seem like a viable option for a multi-infeed HVDC as it enhances the system strength.

Chapter 6

Coupling Effect Between AC and DC Overhead Lines in Southern Norway

Expansions of the transmission network done by the utility companies often results in overhead lines being built in close proximity to each other. It is common practice for overhead lines to share the same rights-of-way (RoW) due to savings in both investment and maintenance cost, but also to reduce the environmental impact [57]. Statnett is planning to utilize the already existing RoW between Tonstad and Feda in southern Norway. A schematic representation of the RoW is shown in Fig. 6.1. The DC overhead lines for the NordLink interconnector will be a ±500 kV triplex tower, shown in Fig. 6.1(a). The DC overhead lines will go in parallel with the existing AC overhead line between Feda and Tonstad. The existing AC overhead line is a 420 kV duplex tower, shown in Fig. 6.1(b). In addition, there will be an AC voltage upgrade with a new triplex tower of 420 kV, shown in Fig. 6.1(c).

When HVDC and HVAC transmission lines share the same RoW there may be induced currents and voltages from either AC to DC or vice versa. A DC line will be exposed to a coupling effect due to the fundamental frequency in the AC line, and an AC line will be exposed to a coupling effect due to a DC offset induced from the DC line. Two lines are affected by one another due to their mutual inductance and capacitance. A wide range of studies have suggested that coupling effects may cause severe damage to the converter equipment. These effects include the following [57–60],

- Converter transformer core saturation due to unsymmetrical magnetization
- Heating of the converter transformer due to flux leakage

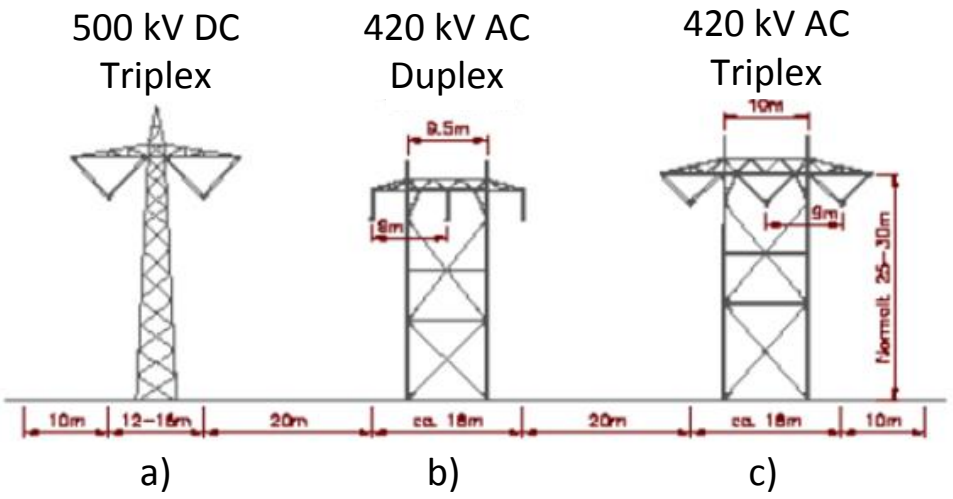

FIGURE 6.1: Rights-of-Way: Tower Distances.

- Loss of lifetime of converter transformer
- Increased noise from the current transformer due to core saturation
- Increased harmonic generation

The coupling effect will modify the currents and voltages and cause problems for the protection relays. Many protection relays, such as distance relays, are impedance based. These relays often measure the current between two or three phases. Therefore an imbalance between the phases caused by coupling effects may cause severe problems for these protection relays. It can in some cases result in immature tripping of lines during steady state or inability to quickly break current during faulty situations. In either case it is highly unwanted, and it is therefore important to minimize these effects [60]. In general, fault currents leads to thermal overheating and mechanical stress which may damage the electrical equipment along a transmission path. The study of fault situations are important for selecting and adjusting relays properly to avoid severe damage when a fault occur. How severe a fault is depends mostly on what kind of fault and where the fault is located in a power system. When a fault occur a new path for the current is created, this path can be described with new impedance to ground. Therefore, a fault represents a change in the equivalent network impedance at the fault location. The fault impedance is relatively small compared to the rest of the power system, which means that most of the current will follow this new path. If the fault impedance is zero the fault is called a bolted fault [54].

The coupling effect between HVAC and HVDC lines have been widely studied in the literature. However, most of the research have been done with respect

to HVDC systems consisting of LCC. New topologies have different operational principles which make significant differences from LCC. As the new MMC topology emerges, more MMC-HVDC overhead lines will be built. It is therefore important to revisit the mutual coupling effect once again.

The coupling effect between transmission lines can be represented by a mutual inductance and mutual capacitance. As for this case the mutual capacitance can be neglected due to the short transmission path. The mutual inductance between two lines can be expressed as [57],

$$Z_{ij} = R_d + j\frac{\omega\mu_0}{2\pi} \cdot ln\frac{D_e}{D_m} \tag{6.1}$$

where R_d is resistance due to earth return, $\omega = 2\pi f$, f is the frequency, D_e is diameter to earth potential and D_m is the mutual distance between the lines. As can be seen the mutual inductance decreases when the distance between the lines increases. Also, the mutual inductance is almost zero for DC frequency.

6.1 Methodology to Investigate the Coupling Effect

First, this chapter aims to detect any coupling effects between the AC and DC overhead lines, and to see how these effects behave in steady state as well as in transient state when different faults are applied. A base case will therefore be presented to set the benchmark for the rest of the analysis (Section 6.1.1). Second, a sensitivity analysis will be made where a number of parameters will be varied, one at a time, while the other parameters remain the same as in the base case (Section 6.1.2). This will make it possible to observe the changes in the coupling effect with respect to the modified variable. It will then be possible to identify which parameters that are most critical. Finally, mitigation methods will be discussed based on the findings in the sensitivity analysis, as to how the coupling effect can be reduced (Section 6.1.3). The coupling effect will be represented by a neutral current (I_n) in the following way [57],

$$I_n = I_a + I_b + I_c \tag{6.2}$$

where I_a, I_b and I_c are phase currents in a three phase system. In balanced systems this neutral current is zero.

TABLE 6.1: Base Case Parameters.

Parameter	Value
Fault duration	$t_d = 0.1$ s
Fault time	$t = 2.0$ s
Coupled line length	38 km
Distance between towers	0 m $\rightsquigarrow$ 31 m $\rightsquigarrow$ 69 m
Fault resistance	0.01 Ω
Ground resistivity	1.5 Ω·m
Mutual coupling	Enabled
Ideal transposition	Disabled

6.1.1 Base Case

The base case will be used as a benchmark for the simulations in this chapter. The parameters used for the base case can be found in Tab. 6.1. These parameters will be applied for the rest of this chapter if not stated otherwise. Technical data for the grounding wires of the overhead lines can be found in Tab. 3.3 on page 51.

In PSCAD it is possible to *enable* and *disable* coupling effects of line segments. This gives the possibility to illustrate the actual effect the coupling has, by comparing the coupled and uncoupled options.

In the base case ***Coupling Disabled*** (- - -) means two AC towers in parallel sharing the same RoW, while one DC tower in a separate RoW. ***Coupling Enabled*** (—) means two AC towers and one DC tower in parallel sharing the same RoW. This is done to illustrate the effect of the AC and DC towers sharing the same RoW. Four cases will be studied, namely:

Case 1.) AC fault, coupling effect in AC lines

Case 2.) AC fault, coupling effect in DC lines

Case 3.) DC fault, coupling effect in AC lines

Case 4.) DC fault, coupling effect in DC lines

In case 1 an AC fault is applied in location B, and the neutral rms current ($I_{n,rms}$) is measured in the AC transmission line in middle AC tower of the RoW (shown in Fig. 4.2). Shown in Appendix C.2 on page 127 the coupling effect (zero sequence current) is largest when single phase and two phase to ground faults are applied. Case 1 has been plotted in Fig. 6.2 with the coupling effect enabled and disabled, in both steady state (a) and in transient state when a single phase to ground fault

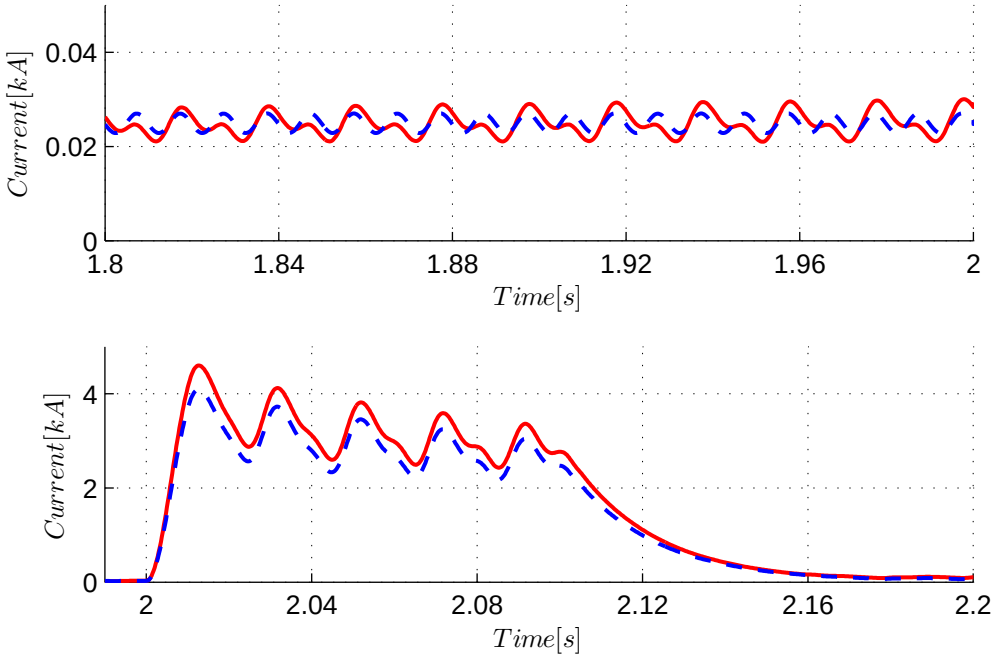

FIGURE 6.2: Base Case: Case 1: $I_{n,rms}$ in AC Transmission Lines. a) Steady State b) Single Phase to Ground Fault. Coupling Enabled (——), Coupling Disabled (- - -).

is implemented (b). First, the steady state $I_{n,rms}$ are quite similar in the uncoupled and coupled scenarios, and only a small, though neglectable, difference between the two curves can be detected. The result therefore indicate that the effect is neglectable in steady state. Second, in transient state the $I_{n,rms}$ is noticeably higher when the coupling is enabled than when the coupling is disabled. The primary part of the $I_{n,rms}$ occurs due to the fault itself. However the increase that can be seen between the two curves in Fig. 6.2(b) is because there is an induced DC current into the AC lines. This result indicate that there is a perceptible coupling effect in the AC lines when an AC fault is applied.

In case 2 a single phase to ground fault is applied in location B, and the DC current and voltage is measured in the DC transmission line (shown in Fig. 4.2). Case 2 is shown in Fig. 6.3. As can be viewed there is a marginal, though still detectable, difference when the coupling effect is toggled ON and OFF. This effect is due to induced AC fundamental frequency current and voltage into the DC overhead lines, when an AC fault is applied. From a power system point of view the DC lines will be much more affected by the relatively large AC voltage drop in the system, than the coupling effect between the AC and DC overhead lines. This result thus indicate that the coupling effect can be neglected in the DC lines, when there is an AC fault.

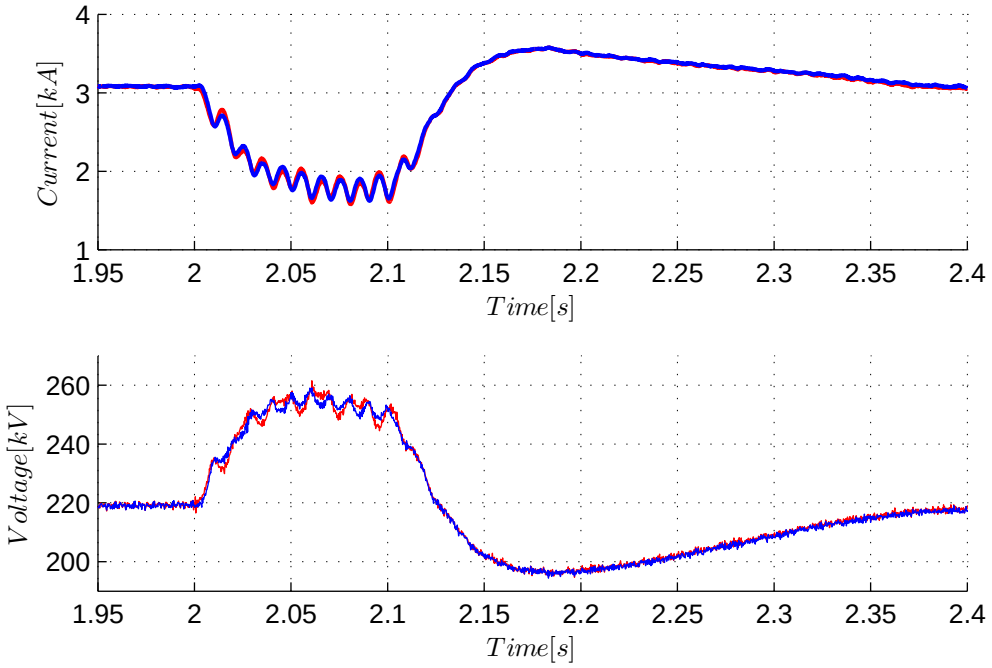

FIGURE 6.3: Base Case: Case 2: a) DC Current Positive Pole b) DC Voltage Positive Pole. Coupling Enabled (—), Coupling Disabled (- - -).

In case 3 DC faults are applied in location D, and the neutral rms current ($I_{n,rms}$) is measured in the AC transmission line (shown in Fig. 4.2). Three different DC faults will be applied namely,

- Positive pole to ground
- Negative pole to ground
- Positive pole to negative pole

Fig. 6.4 shows that the coupling effect is identical for a positive and negative pole to ground fault. This seems reasonable, as these fault are similar. Fig. 6.4 also shows that a pole to pole fault produces a higher peak of $I_{n,rms}$ than a single pole to ground fault. When the DC and AC towers are decoupled the $I_{n,rms}$ in the AC lines does not increase when the DC fault occur. This result indicate that the coupling effects from a DC fault is noticeable in the AC lines when the towers share the same RoW.

Lastly, in case 4 a DC single pole to ground fault is applied at location D, and the DC current and voltage is measured in the DC transmission line (shown in Fig. 4.2). Fig. 6.5 shows that there is hardly any visible difference when the mutual coupling is disabled and enabled. This result is quite similar to case 2. The power

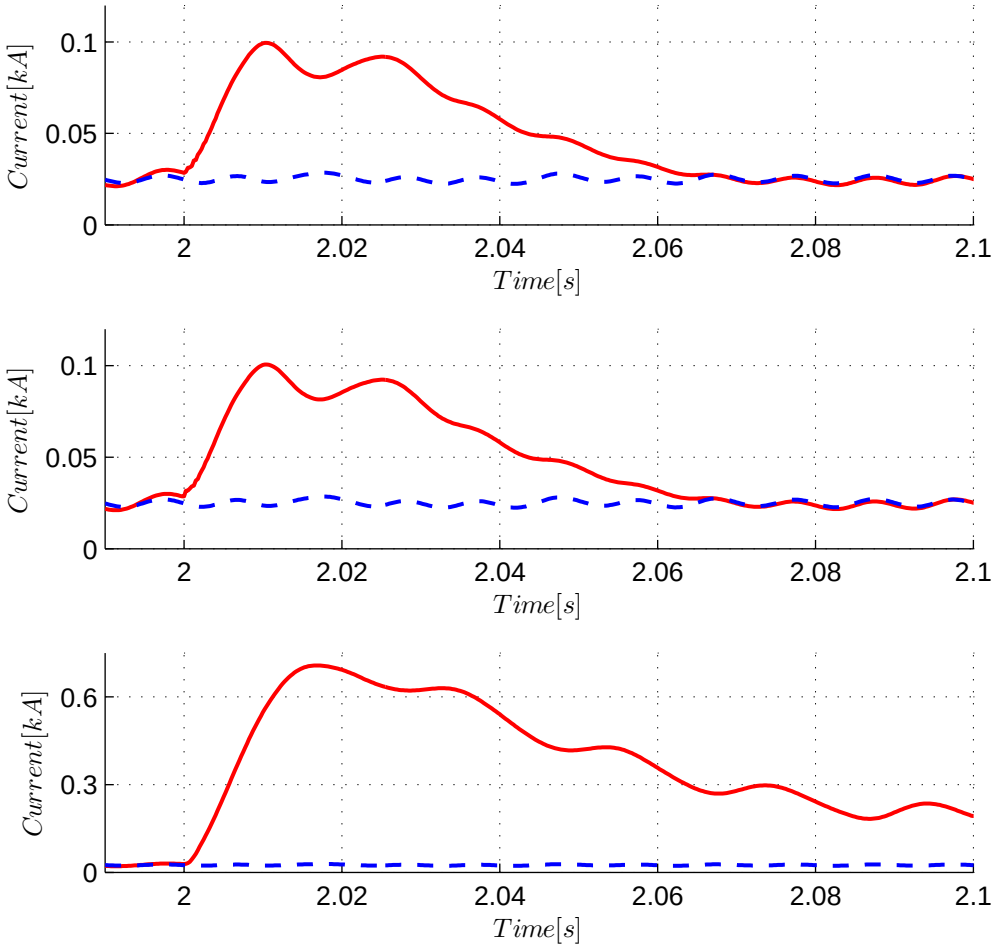

FIGURE 6.4: Base Case: Case 3: $I_{n,rms}$ in AC Transmission Lines. a) Positive Pole to Ground b) Negative Pole to Ground c) Positive Pole to Negative Pole. Coupling Enabled (—), Coupling Disabled (- - -).

system disturbances are too large to see the coupling effects, which are quite small in comparison.

To sum up the base case, the mutual coupling effect between the AC and DC overhead lines sharing the same RoW has been analysed. The results indicate that,

- The mutual coupling effect is detectable
- Effect is visible in transient state, not in steady state
- Noticeable effects in AC overhead lines (both AC and DC faults)
- Negligible effects in DC overhead lines (both AC and DC faults)

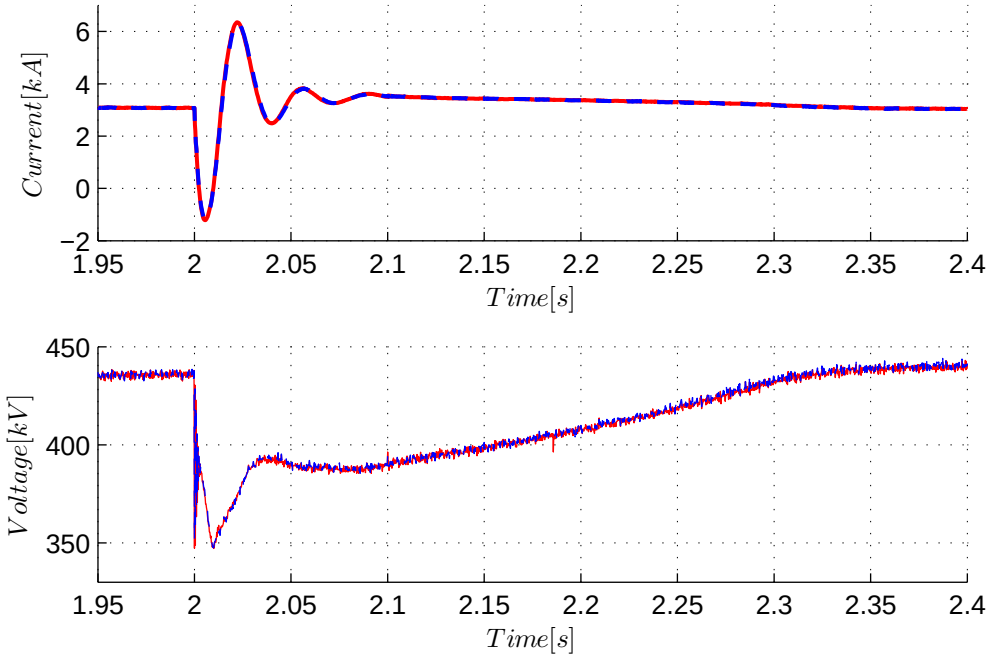

FIGURE 6.5: Base Case: Case 4: a) DC Current Positive Pole b) DC Voltage Line-Line. Coupling Enabled (——), Coupling Disabled (- - -).

Coupling effects measured in DC overhead lines will not be analysed further, as the coupling effects are negligible (case 2 and 4). The power system disturbances dominate these effects, which makes DC measurements unsuitable for investigations of the coupling effect. However, coupling effects measured in AC overhead lines are clearly visible, as the difference between the uncoupled and coupled cases are detectable (case 1 and 3). In case 3 the difference between $I_{n,rms}$ for the uncoupled and coupled cases was larger than for case 1. In case 1 the $I_{n,rms}$ was mainly due to the AC fault itself. The coupling effect is therefore clearer for case 3. Further investigations will be done in order to determine which parameters have the largest impact on the coupling effect, with respect to case 3.

6.1.2 Sensitivity Analysis

This section will further explore the properties of the coupling effect during transient state. The seriousness of the fault with respect to certain parameters will be discussed, as to find out which parameters have the largest impact on the coupling effect. From lessons learnt in Section 6.1.1, the coupling effect was visible and largest when there was induced DC current into the AC lines during DC faults. Also the neutral rms current was negligible when the coupling was disabled for DC faults, and the coupling effect is therefore displayed clearer. For this reason all coupling effects will be measured in the AC overhead line section (location C,

Fig. 4.2). According to literature almost all DC faults are single pole to ground faults [56]. During these faults the faulty pole is unable to transfer power.

In the sensitivity analysis there will be applied a positive pole to ground fault. The sensitivity analysis therefore represents induced DC current into the AC overhead lines due to adjacent DC overhead lines. The fault duration is set to 0.05 seconds. In the sensitivity analysis a duration of 0.1 seconds was found to be too severe, as the system was unable to stabilize after the fault when certain parameters changed. For this reason the base case was adjusted to 0.05 seconds to be comparable with the sensitivity analysis. The following study cases will be analysed,

- Parallel overhead line length
- Transmission tower distance
- Modulation index
- DC fault location
- Fault resistance

The change in the neutral rms current ($I_{n,rms}$), i.e. the coupling effect will be displayed for each study case. For each study case the parameter in question will be altered, while the rest are identical to the base case. To make the following section easier to follow, the base case will in each study be presented by a red solid line (—).

6.1.2.1 Parallel Overhead Line Length

The line length of the coupled section of the AC and DC overhead lines has been varied. The overhead lines were varied in four different ways, shown in Fig. 6.6. Case 3 represents the base case. The length of the two transmission paths were held constant (AC line = 50 km, DC line = 53 km). Changing the total length of the transmission lines above or below its original values would result in a change in the overall system current flow. Therefore, in order to make the results comparable to the other cases, the total length of the transmission lines were held constant.

Fig. 6.7 displays the four study cases when a single pole to ground fault is applied to location D (shown in Fig. 4.2). Case 4 is the longest parallel section and results in the highest peak ($I_{n,rms} = 0.13$ kA). In the shortest parallel section, case 1, the peak was found to be the smallest ($I_{n,rms} = 0.05$ kA). The peak increased with 33% from base case to the worst case. The effect was found to be linear with the length of the coupled section. This result indicate that the longer the two

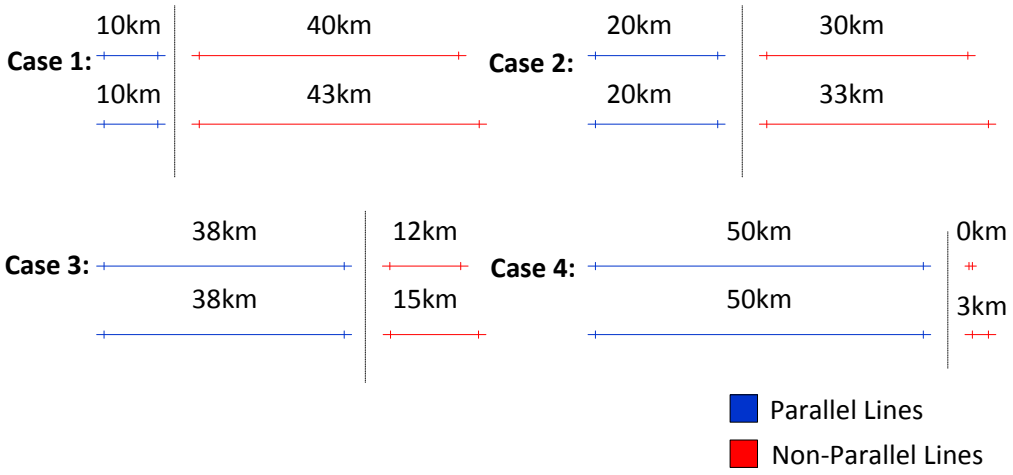

FIGURE 6.6: Overhead Line Length: Four Cases.

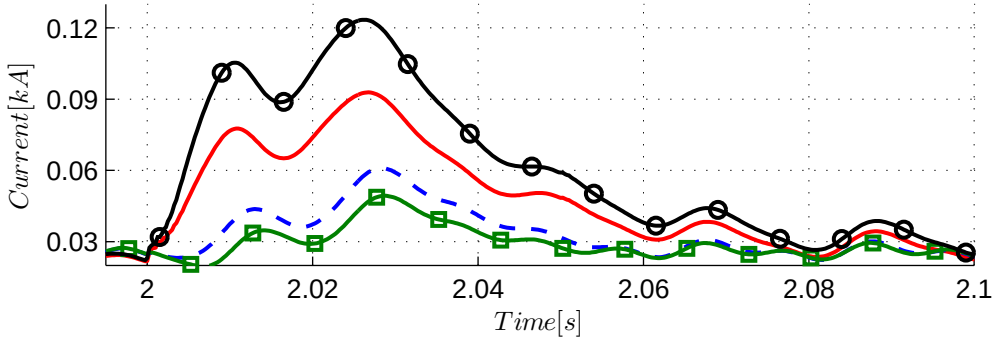

FIGURE 6.7: Sensitivity Analysis: Overhead Line Length: $I_{n,rms}$ in AC Transmission Lines. Case 1 (—□—), Case 2 (- - -), Case 3 (——) and Case 4 (—○—).

transmission paths share the same RoW, the higher the coupling effect between the lines. This sounds reasonable, as the distance where the overhead lines can interact increases. According to literature the fault that results in the highest flux linkage would result in the highest coupling effect [57]. It is therefore evident that the highest coupling should occur where the lines are in parallel the longest, since the distance of interaction increases.

6.1.2.2 Transmission Tower Distance

The transmission tower distance has been altered in simulations. This was done by changing the distance between the three towers sharing the same RoW. All tower distances refer to the tower center, relative to the center of DC tower. A single pole to ground fault was implemented at location D (shown in Fig. 4.2), and $I_{n,rms}$ has been presented for different tower distances. Shown in Fig. 6.8 the

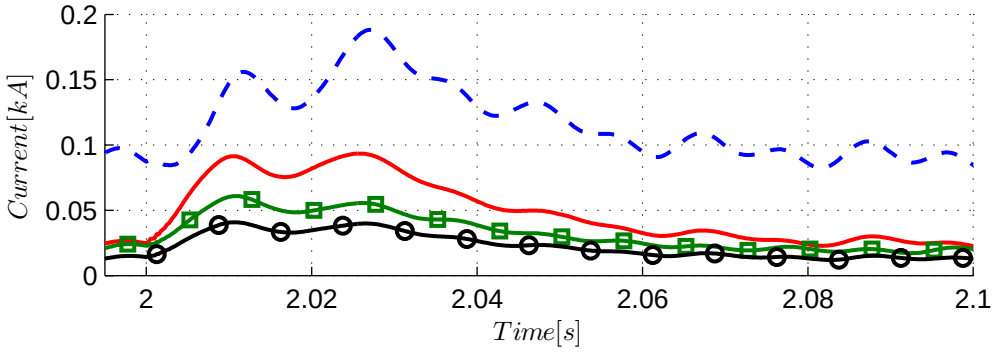

FIGURE 6.8: Sensitivity: Transmission Tower Distance: $I_{n,rms}$ in AC Transmission Lines. $0 \rightsquigarrow 20 \rightsquigarrow 40$ (- - -), $0 \rightsquigarrow 31 \rightsquigarrow 69$ (—), $0 \rightsquigarrow 45 \rightsquigarrow 90$ (—□—) and $0 \rightsquigarrow 60 \rightsquigarrow 120$ (—○—).

highest peak of $I_{n,rms}$ occurred when the towers were 20 meters apart from each other ($I_{n,rms} = 0.19$ kA). As the towers are 19 meters wide, this case is the absolute minimum tower distance. It is also highly unlikely that the tower distance would be 20 meters, as it would cause clashes between the lines in windy weather. When the towers were moved further apart the neutral rms current decreased, and the peak was found to be $I_{n,rms} = 0.04$ kA when the tower distance was 60 meters apart from each other. Moving the towers further apart would likely decrease the neutral rms current even more, however, they may not be categorized as towers sharing the same RoW. The result indicate that the spacing between the towers is an important parameter, as the peak of $I_{n,rms}$ more than doubled (111%) from the base case to the worst case.

6.1.2.3 Modulation Index

As explained in Section 3.1.6 the implemented control system uses a phase-shifted sinusoidal PWM. A triangular reference signal is compared to the carrier wave to determine how many SMs that should be switched ON at each sampling instant. The amplitude ratio between these two signals are defined as the modulation index (m_a) [5],

$$m_a = \frac{\hat{V}_{cr}}{\hat{V}_{tri}} \tag{6.3}$$

where $\hat{V}_{cr}$ is the voltage peak of the carrier signal and $\hat{V}_{tri}$ is the voltage peak of the triangular reference signals. The triangular reference signal is normally kept at constant amplitude, shown by Fig. 6.9(a). The modulation index can be modified with the following formula [5],

$$\begin{aligned} \hat{V}_{ao} &= m_a \cdot \frac{V_d}{2} \qquad m_a \leq 1 \\ \hat{V}_{ao} &= \frac{\hat{V}_{cr}}{\hat{V}_{tri}} \cdot \frac{V_d}{2} \qquad V_{cr} \leq V_{tri} \end{aligned} \tag{6.4}$$

where $\hat{V}_{ao}$ is peak of phase-neutral AC voltage ($\hat{V}_{ao} = \frac{\sqrt{2}}{\sqrt{3}} \cdot V_{LL}$), V_{LL} is the line-line voltage on secondary side of transformer and V_d is the DC voltage. Eqn. 6.4 shows that there is a linear relationship between the voltage and modulation index when $m_a \leq 1$ [5, 38].

The maximal peak phase to neutral voltage ($\hat{V}_{ao,max}$) occurs when all the SM in the upper arm is bypassed, and all the SM in the lower arm is inserted in the MMC. The $\hat{V}_{ao,max}$ is then equal to half the DC voltage (i.e. ma=1 in Eqn. 6.4). The maximum line-line voltage on the secondary side of the transformer ($V_{LL,max}$) can therefore be found in the following way [38],

$$\begin{aligned} V_{LL,max} &= \frac{\sqrt{3}}{\sqrt{2}} \cdot \hat{V}_{ao,max} \\ V_{LL,max} &= \frac{\sqrt{3}}{\sqrt{2}} \cdot 0.5 \cdot V_{dc} \\ V_{LL,max} &= 0.612 \cdot V_{dc} \\ V_{LL,max} &= 306.2 \text{ kV} \end{aligned} \tag{6.5}$$

by inserting rated DC voltage from Tab. 3.1 on page 18. If $V_{LL} \geq 306.2$ kV the peak of the carrier signal is higher than the triangular reference signal ($\hat{V}_{cr} \geq \hat{V}_{tri}$). The converter is no longer in the linear range and is said to be in over-modulation mode [5]. According to [61] in a phase-shifted sinusoidal PWM the harmonic content increases substantially in over-modulation. This is because the modulator cannot compare the two signals properly in the region where the carrier signal exceeds the triangular signal. This region results in a dead-time interval because the modulator cannot insert more (fewer) SMs as they are all inserted (bypassed). Therefore, it is important to keep $m_a \leq 1$. As for this study, for low modulation indices ($m_a \leq 0.5$) the system failed to reach its respective reference values for DC voltage and power. This is because when a low modulation index is utilized, several levels in the MMC are unused. Multi-level converters therefore loose some of the advantages of having several levels, as compared to the two-level converters [62].

A study was performed where the modulation index was altered. Shown by Eqn. 6.4 this was done by changing the line-line voltage on the secondary side of the transformer (V_{LL}). A positive pole to ground fault was implemented at location D

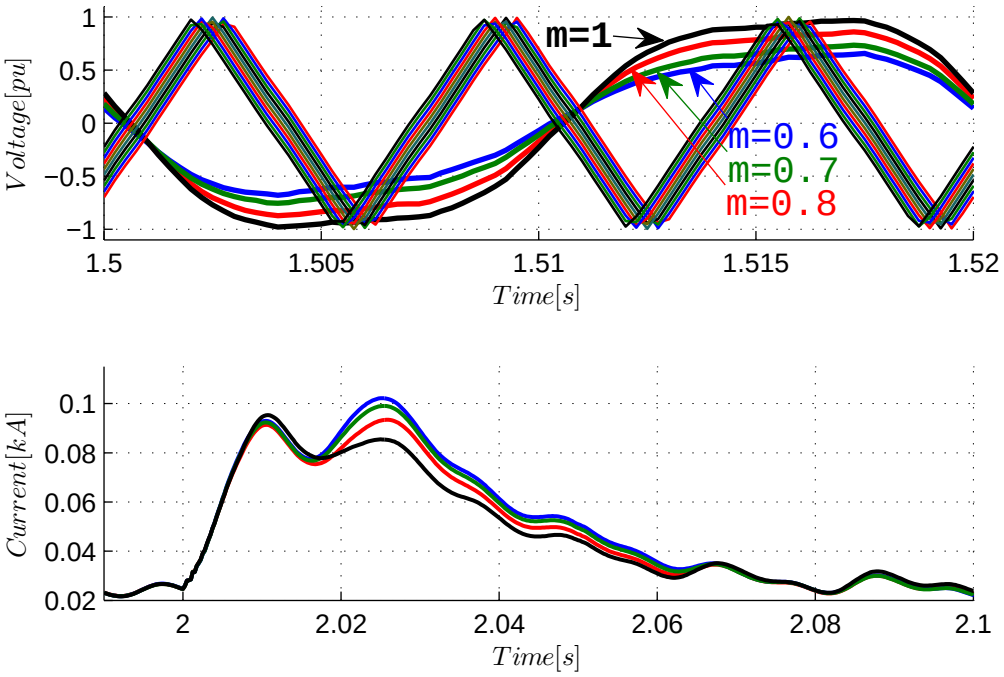

FIGURE 6.9: Sensitivity: Modulation Index. a) Carrier and Voltage Reference Signals b) $I_{n,rms}$ in AC Transmission Lines. $m_a = 0.6$ (—), $m_a = 0.7$ (—), $m_a = 0.8$ (—) and $m_a = 1$ (—).

(shown in Fig. 4.2), and $I_{n,rms}$ has been presented for different modulation indices. Fig. 6.9(b) shows that the modulation index influences the $I_{n,rms}$. The worst case was the lowest modulation index $m_a = 0.6$ which gave a peak of $I_{n,rms} = 0.12$ kA. The worst case corresponds to an increase of the peak of about 11% compared to the base case. The lowest peak ($I_{n,rms} = 0.085$ kA) was found when $m_a = 1$. Fig. 6.10 shows the DC current in the positive pole during fault for base case ($m_a = 0.8$) and worst case ($m_a = 0.6$). The lowest modulation index results in the highest fault current through the parallel section, and it therefore increases the coupling effect. The result indicate that the modulation index has a small, but detectable influence on the coupling effect.

6.1.2.4 DC Fault Location

In general the main disadvantage of the half bridge MMC is the DC fault handling, elaborated in Section 2.4. In a MMC the fault current can flow through the anti-parallel diode in the SM, and the fault current cannot be blocked by control action. This results in large transients during the first cycles after the fault occurs [25]. The DC fault handling remains a problem for the half-bridge MMC, and has spurred the development of new hybrid HVDC breakers [23, 25]. It is worth to

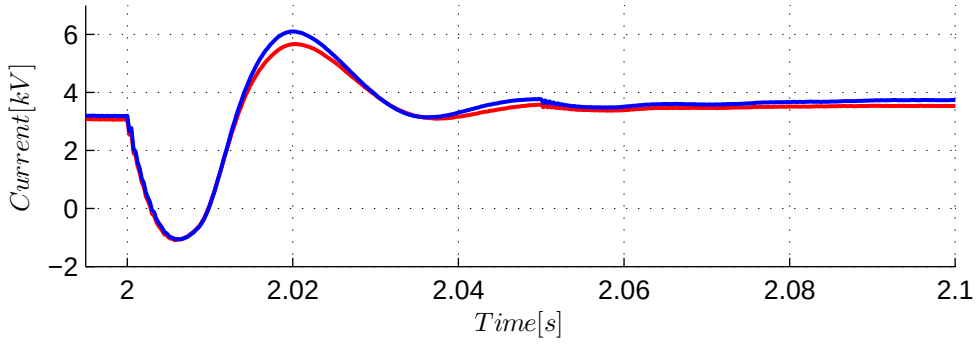

FIGURE 6.10: Sensitivity: Modulation Index: DC Current Positive Pole. Base Case $m_a = 0.8$ (—) and $m_a = 0.6$ (—).

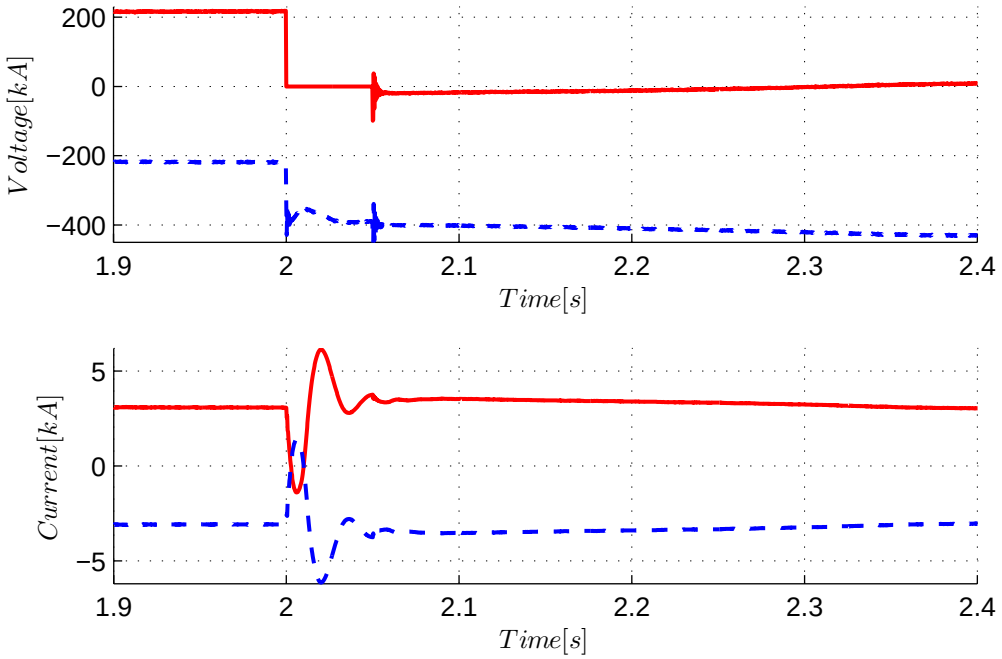

FIGURE 6.11: Sensitivity: DC Fault Location: a) DC Voltage Positive (—) and Negative Pole (- - -), b) DC Current Positive (—) and Negative Pole (- - -).

mention that there are no DC breakers or DC choppers installed in the analysed system.

A positive pole to ground fault was implemented. Fig. 6.11 shows the DC voltage positive and negative pole (a) and DC current positive and negative pole (b) at base case (location D). When the fault occurs, the DC voltage on the faulty pole drops to zero, and as a result the healthy pole immediately raises to double its rated value. In other words, the potential reference point changes position [63]. The currents in both poles returns to their respective prefault values after the fault

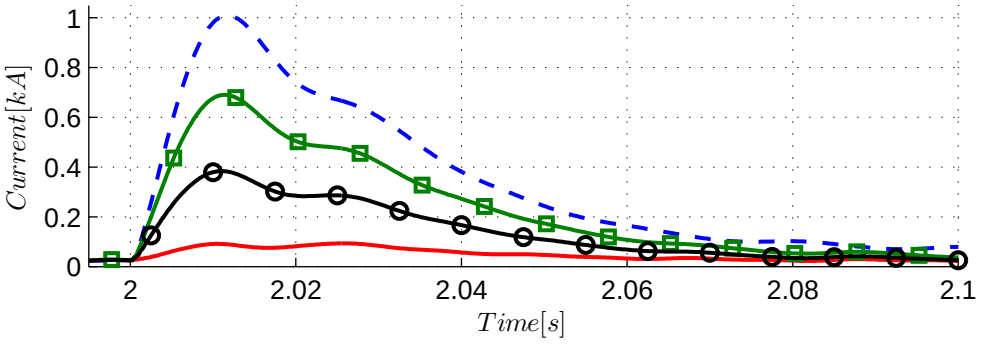

FIGURE 6.12: Sensitivity: DC Fault Location: $I_{n,rms}$ in AC Transmission Lines. Base Case (—), MMC Inverter (- - -), MMC Rectifier (—□—) and Vollesfjord (—○—).

has ended. The transmission system still transmit the same power as the prefault system [63].

As for the case of coupled currents, it would be interesting to see how different DC fault locations affect the neutral rms current in the AC overhead lines. Various DC fault locations (shown in Fig. 4.2) have been studied and includes the following:

- Base case (Location D)
- MMC inverter station (Norwegian side)
- 15 km from MMC inverter
- 30 km from MMC inverter

The fault positions hence represents a DC fault at either side of the coupled line section (base case, MMC inverter) and two locations along the parallel section (15 km and 30 km with respect to the MMC inverter). A positive pole to ground fault was implemented, and Fig. 6.12 presents the $I_{n,rms}$ for the four different fault positions. The fault close to the MMC inverter causes a high peak of $I_{n,rms} = 1$ kA. It is the most severe fault, with a peak more than 10 times as compared to the base case of $I_{n,rms} = 0.09$ kA. The fault at 15 km and 30 km from MMC inverter resulted in a peak of $I_{n,rms} = 0.7$ kA and $I_{n,rms} = 0.4$ kA respectively.

An investigation as to why faults closer to the MMC inverter resulted in such a high peak was done. A hypothesis was suggested: the higher $I_{n,rms}$ for faults closer to MMC inverter is due to other power system disturbances, as the fault is closer to the AC system, and not because of the coupling effect. The hypothesis was then tested. As explained in the base case, $I_{n,rms}$ is calculated using the middle AC tower in the RoW. Fig. 6.13 shows the phase currents of the two AC towers in the six conductors, for fault positions MMC inverter and base case.

The conductors are placed so that I_a in AC tower #1 is the closest to the DC tower and I_c in AC tower #2 is farthest away. Fig. 6.13 shows that the closest conductor is most affected by the fault. In Fig. 6.13(a)(b)(c) phase currents I_a, I_b and I_c are substantially higher for the MMC inverter fault than for the base case fault. In Fig. 6.13(d)(e)(f) phase currents I_a, I_b and I_c of the second AC tower is shown, indicating that the second tower is quite unaffected by the DC single pole to ground fault. It therefore seems reasonable to assume that the unbalanced currents are mainly due to the increased coupling effect, and not because of any other power system disturbances.

According to literature the highest fault current through the parallel section results in the highest coupling effect [57]. Fig. 6.14 shows the DC current in positive pole for fault located at MMC inverter and base case. The fault current is larger for the MMC-fault. The fault current through the parallel section is thus higher, which results in the highest flux linkage between the lines. The coupling effect is therefore higher for faults located closer to the MMC inverter.

6.1.2.5 Fault Resistance

A positive pole to ground fault has been implemented on location D (shown in Fig. 4.2). The fault resistance to ground has been varied. Fig. 6.15 displays the $I_{n,rms}$ for different fault resistances. The result shows that the highest $I_{n,rms}$ occurred with the lowest fault resistance ($R_f = 0.01$, base case) with a peak $I_{n,rms} = 0.09$ kA. When the fault resistance was increased, the $I_{n,rms}$ declined. The lowest peak of $I_{n,rms}$ was found to be 0.06 kA for $R_f = 10$. The result indicate that the $I_{n,rms}$ is affected by the severity of the fault. As the severity of the fault increases, i.e. lower fault resistance, the fault current through the parallel section increased. The mutual inductance between the lines are still the same, but the coupling effect increases because of the increased fault current. The fault current is inversely proportional to the ground resistance ($I_f = \frac{V}{R_f}$). As the fault resistance decreases, the fault current through the parallel section increases, and the $I_{n,rms}$ thus also increases. This is according to what was expected, and the result seem reasonable. It should be noted that the base case has a very low fault resistance, almost zero, and can therefore be seen as a worst case fault. This result hence indicate that if a real life fault occurred it would be likely to have higher resistance than 0.01 Ω, and the coupled currents would therefore be less than what the base case result indicated.

6.1.3 Summary and Mitigation Methods

From the base case the result indicated that the coupling effect was visible in transient and not in steady state. The coupling effect was noticeable for measurements

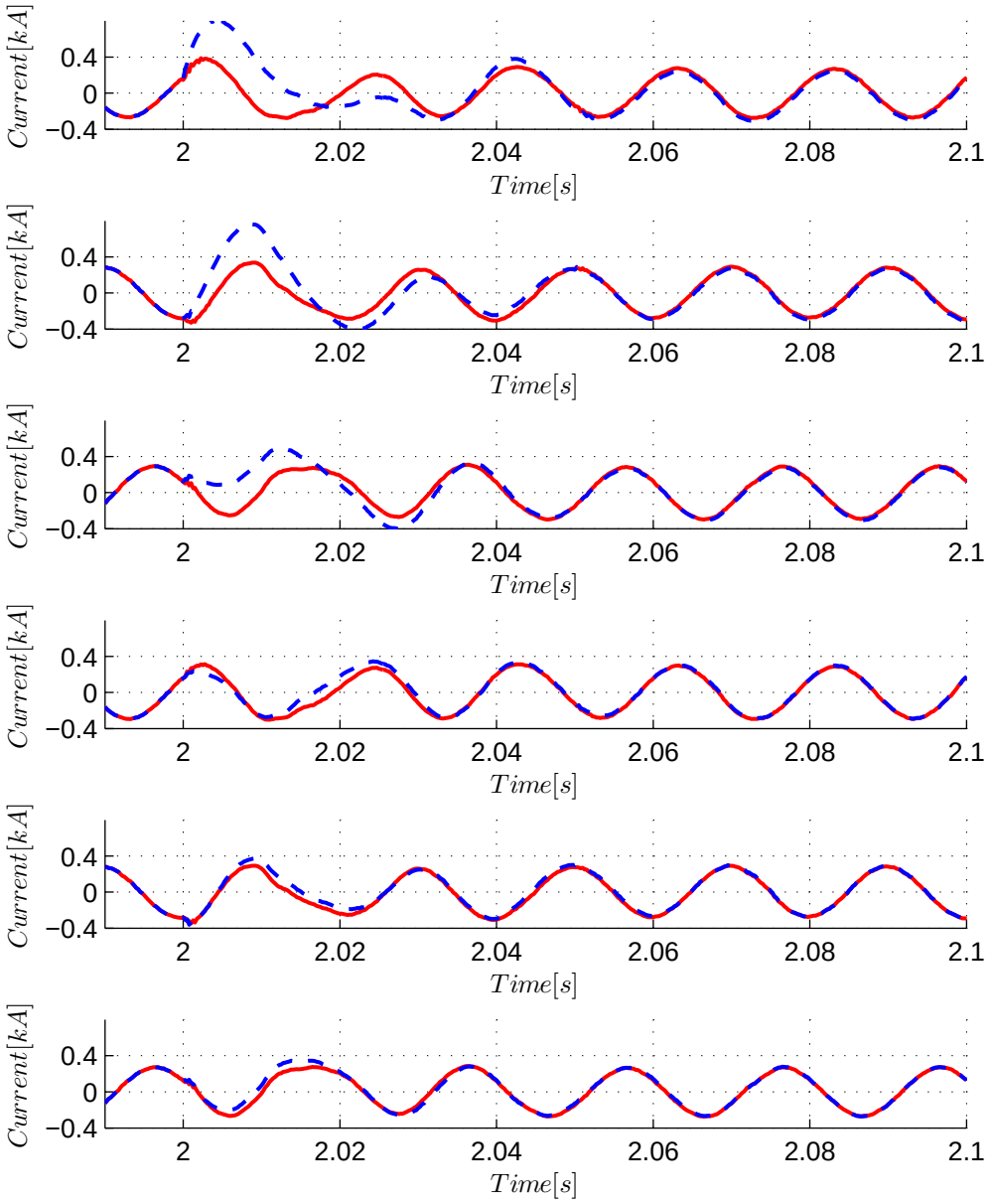

FIGURE 6.13: Sensitivity: DC Fault Location: Phase Currents in AC Tower Conductors a) I_a AC Tower #1, b) I_b AC Tower #1, c) I_c AC Tower #1, d) I_a AC Tower #2, e) I_b AC Tower #2, f) I_c AC Tower #2. Fault at Base Case (——) and Fault at MMC Inverter (- - -).

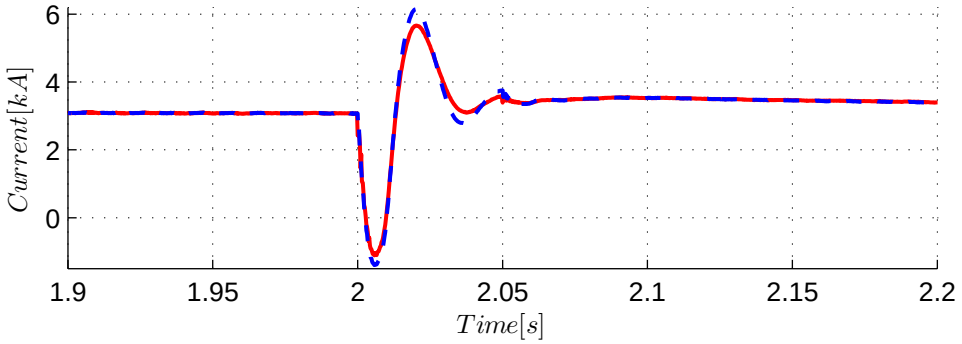

FIGURE 6.14: Sensitivity: DC Fault Location: DC Current Positive Pole. Fault at Base Case (—) and Fault at MMC Inverter (- - -).

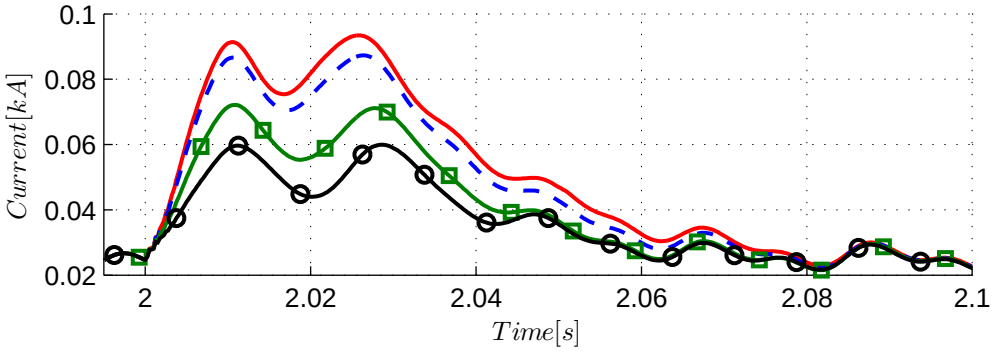

FIGURE 6.15: Sensitivity: Fault Resistance: $I_{n,rms}$ in AC Transmission Lines. $R_f = 0.01$ (—), $R_f = 0.1$ (- - -), $R_f = 5$ (—□—) and $R_f = 10$ (—○—).

in the AC overhead lines for (i) DC faults due to induced DC current into the AC overhead lines and (ii) AC faults due to induced fundamental frequency into the DC overhead lines. The effects was more visible for the latter alternative. The findings obtained in the base case was further developed with a parametric sensitivity analysis to determine the critical parameters with respect to the coupling effect.

A positive pole to ground fault was implemented, and the neutral rms current ($I_{n,rms}$) was measured in the AC lines. The results in the parametric sensitivity analysis have up until now been compared with respect to the peak of $I_{n,rms}$. The peak of the current is not the only thing that determines the severity of the fault. Also the duration of the fault current and how fast the fault current diminishes are equally important. However, looking at the results obtained in the parametric sensitivity analysis (Fig. 6.7, Fig. 6.9, Fig. 6.8, Fig. 6.12 and Fig. 6.15) it is evident that the peak of $I_{n,rms}$ is representative for both the duration and the rate of which the current disappears. In other words: if the peak of $I_{n,rms}$ for one variable is higher than another, the duration of the $I_{n,rms}$ is longer for the same variables. The results from the sensitivity analysis can be summed up as follows, the coupling effect ***increases*** with:

- Increased parallel line length
- Reduced tower distance
- Reduced modulation index
- Fault close to MMC inverter station
- Higher fault current in the coupled section (reduced fault resistance)

Higher fault current through the parallel section resulted in higher coupling effects. The parallel line length was found to be linearly proportional with the coupling effect. As the distance of interaction increased, the coupling thus also increased. However, the total length of the overhead lines were relatively short, only 50 km, and even in the worst case the coupling effect did not increase much (33%). The tower distance had a much larger impact than the line length, as the effect more than doubled (111%) from the worst case to the base case. An increase in tower distance also reduced the impact significantly, and can be a key measure to reduce the coupling effect. The modulation index also made an impact on the coupling effect, where lower values increased the coupling effect. However, the effect for $m_a \in \{0.6\text{-}1\}$ was not significant as the coupling effect only increased with 11% from worst case to best case. Fault position was found to be a key parameter, as the coupling effect increased 10 times for the fault at MMC inverter station ($I_{n,rms} = 1$ kA). Fault resistance also had a large impact, and the fault current was reduced 33% from base case (highest coupling) to the best case. The two preceding parameters (fault location and resistance) are both uncontrollable by nature. However, the simulations indicates that the base case scenario is also a worst case scenario when it comes to fault resistance. As the base case has a $R_f = 0.01$ the resulting fault current is very high, as compared to other fault resistances. It can therefore be expected that the fault currents, hence also coupling effect, in a real fault situation are equal to or less than the base case (since $R_{f,min} = 0$). Measures should be taken to limit both the risk and impact of DC faults close to the MMC inverter as it can have severe effects on both the coupling effect, but more importantly, on the system stability in general. For instance, when a DC fault occur the faulty pole drops to zero voltage while the other immediately raises to double its rated value. This can cause problems to the insulation of the overhead lines, and should be accounted for in the manufacturing process. According to literature maximum insulation voltage level of the insulation should be at least 3 pu of the rated value in order to avoid damage during a single pole to ground fault [63].

Mitigation Methods

Based on these results there are proposed two mitigation methods to reduce the coupling effect, (i) tower separation distance and (ii) transposition of the conductors in the transmission corridor. The first mitigation method was found to be

an effective measure in the parametric sensitivity analysis. However, it would be ineffective to move the towers too far apart, as it would create two separate RoW. This would hence remove the advantage of having the parallel section in the same RoW. As mentioned in the introduction of Chapter 6, utilization of existing RoW corridors have the benefit of savings in both investment and maintenance cost. When building a new RoW, there are also many restrictions such as ecological aspects, geographical aspects, distance to existing structures as well as minimizing the environmental impact. In order to avoid these restrictions, and to make the results more credible, the total width of the RoW was kept constant during the mitigation method. The second proposed mitigation method is to transposition the conductors in the transmission corridor, to reduce the imbalance between the three phase currents and voltages. The two mitigation methods have been tested to clarify their actual effects, and will now be discussed.

First, to mitigate the coupling effect during DC faults, a study was carried out with respect to the tower distance in the RoW. This study was done with respect to DC fault at MMC inverter station, since this was found to be the most critical

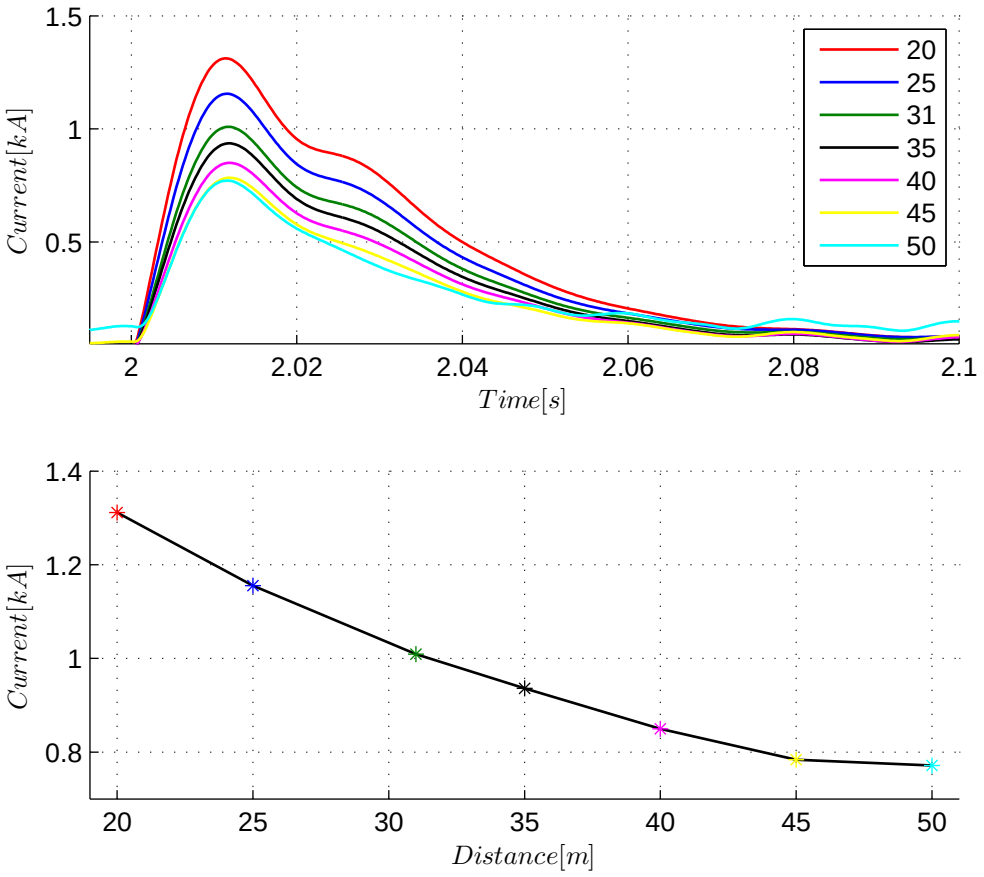

FIGURE 6.16: Mitigation Methods: Changing Tower Distance: a) $I_{n,rms}$ in AC Transmission Lines. b) Peak $I_{n,rms}$ Values.

situation in the sensitivity analysis. The total width of the RoW was kept constant (69 meters). This was done by keeping the DC tower at 0 meters, while one AC tower was held at 69 meters. Then, by alternating the middle AC tower within the RoW, the optimal point with respect to the $I_{n,rms}$ was found. All distances refer to the center of the tower, and the DC tower center is used as reference. Fig. 6.16(a) shows $I_{n,rms}$ for different distances of the middle AC tower, and Fig. 6.16(b) shows the peak $I_{n,rms}$ versus distance of the middle AC tower. Fig. 6.16 indicates that the $I_{n,rms}$ decreases for increased distance to the DC tower. Shown by Fig. 6.16 the neutral rms current, i.e. the coupling effect, can thus be greatly reduced from the base case (31 meters) to the longest distance (50 meters). However, when the towers were 50 meters apart the neutral rms current in steady state increased substantially, indicating that the distance between the two AC towers were too small. In order to limit the neutral rms current in both steady state as well as in transient state during DC faults, the middle AC tower should hence be placed at a safe distance from the other AC tower, indicating that 45 meters would be the preferred choice. 45 meters equals a reduction of the peak $I_{n,rms}$ of 22.3% from the base case ($I_{n,rms} = 777$ A). Fig. 6.16(b) shows that the relationship between the coupling effect and the separation distance is approximately linear for values lower than 45 meters. The effect of increasing separation distance reduces for values higher than 45 meters.

Second, a study was implemented with respect to the transposition of the overhead lines. According to literature transposition of overhead lines can be an effective measure against coupling effects [64]. Transposition means to periodically change the positions of the conductors in a transmission line. Fig. 6.17 shows an ideal transposition of a line segment.Fig. 6.17 presents a forward successive phase transposition scheme, which means the phase positions change in a sequence of ABC-CAB-BCA. Ideal transposition of a line makes the average self and mutual impedances between the lines equal, hence reducing the unbalance between the three phase currents and voltages, i.e. the neutral current and voltage [65].

The study was based on a single pole to ground fault at location D (shown in Fig. 4.2). Two simulations were performed, one without ideal transposition (base case), and one with an ideal transposition of the AC towers in the RoW. Fig. 6.18 shows the two transposition schemes with respect to their neutral rms current. The ideal transposition results in negligible $I_{n,rms}$ in steady state, and a small peak during the fault in transient state as compared to the base case. The result indicate that in steady state, the induction between the two AC lines are efficiently removed with transposition of the line segments. In transient state the ideal transposition results in a suppression of the $I_{n,rms}$. The results therefore indicate that transposition of conductors is a powerful measure, and an efficient way to reduce coupling effect between AC and DC overhead lines. The transposition averages the unbalance between the three phases, hence reducing the coupling effect.

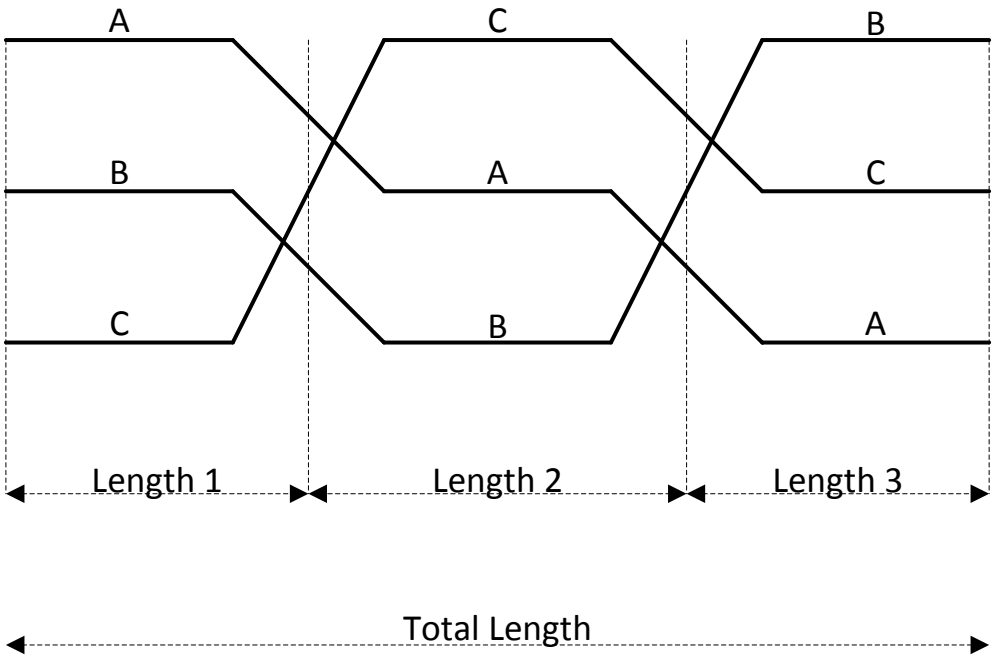

FIGURE 6.17: Mitigation Methods: Forward Successive Phase Transpositon.

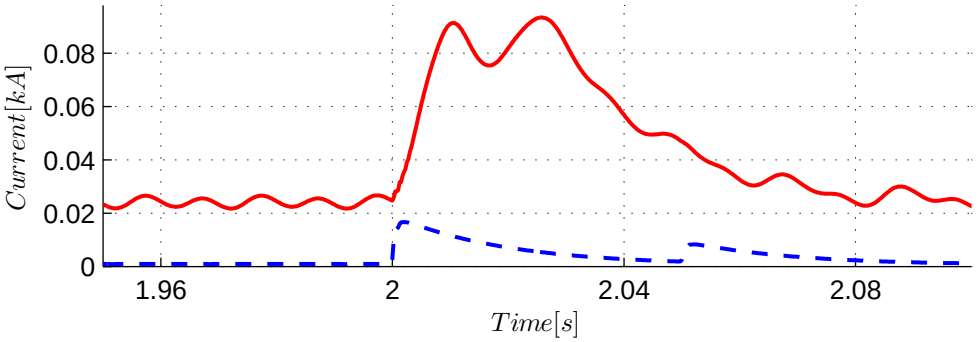

FIGURE 6.18: Mitigation Methods: $I_{n,rms}$ in AC Transmission Lines. No Transposition (—), Ideal Transposition of the two AC Transmission Lines (- - -).

Chapter 7

Accuracy of the Results

Up until now all the results have been assumed to be correct. However, there are a numerous sources of error that may influence the results obtained in this report. This chapter will briefly discuss the accuracy of the results.

- The parameters in a specific case may be tuned to the wrong value. As the values of many variables have been changed back and fourth there may be a glitch due to human error. Especially in the parametric sensitivity analysis, where many variables have been altered frequently. Even though most of the results have been verified twice or thrice, there may still be an error in one of the simulation set-ups.

- Fundamental structural error in the model. The simulation model used in PSCAD might have errors due to mistakes in the building process. The probability of big errors are small due to the fact that the model was tested several times and worked as intended.

- Error in the "Build-model" process during simulations in PSCAD. During simulations there were discovered an error as the simulation program sometimes did not registered that a parameter was changed. This happened when a change was made inside the transmission overhead lines (line length, resistivity, coupling effect, transposition). The problem was solved by using the build-function in PSCAD before running the simulation, as to make sure that the model was built correct.

- As all the plots have been made in MATLAB, there might be an error in the plotting process. The data was gathered from the simulation program, stored in a text-file and the loaded into MATLAB. During this process there might be an error of saving the data incorrectly, which may have lead to plotting of another variable than intended. As many variable values were tested, with a numerous amount of scripts, this seem like one of the most

likely sources of error. However, the author of this report has done his best to limit the possibility.

- Time step was set to 150 μs. A computer program solves the system iteratively. All variables are calculated for each time step and these values are given as input parameters for the next iteration. The time step combines both accuracy and speed. A lower time step is likely to give more accurate results, however it comes with the cost of increasing the simulation time. The model was running quite slow (up to 30 minutes each simulation). As for the time frame for this project, there were no time to rerun all the simulations at a smaller time step. This would be preferable, to check if the obtained results in this report are valid for a smaller time step.

- The references used in this report may not be correct. Throughout the process the author of this report has strived to use the best available references for the given topic. For this reason all the literature search are based upon published scientific material. However, there are no guarantee that these are correct. The probability of this source of error is assumed to be very low.

Conclusion

The consequences of a new Modular-Multi-Level Converter (MMC) interconnector between Norway and Germany (NordLink) has been analysed. It will be connected near the already existing Line Commutated Converter (LCC) interconnector to the Netherlands (NorNed). The impact of the new connection has been studied by developing and comparing two scenarios in PSCAD, namely a LCC stand alone system representing today's configuration (scenario 1) and a multi-infeed system consisting of a MMC-link and a LCC-link inverting into a weak AC grid representing the future system of NordLink and NorNed (scenario 2).

The two scenarios have been tested in both steady state and transient state. In steady state the start-up of the two converter technologies were emphasised. Results from the steady state showed that the MMC is able to control active and reactive power, and thereby enhances AC voltage regulation. The results highlights the importance of AC voltage stability, and how this can be achieved with the use of MMC AC voltage controllers. The existing voltage supporting equipment in the system can thus be utilized for a more continuous voltage regulation when the new MMC-link is connected, and to minimize losses.

Single phase and three phase to ground faults were applied at various locations. These AC faults had a larger impact on the LCC-link, and the MMC-link was found to be almost unaffected. A LCC inverter in weak AC systems may suffer from commutation failure, while the MMC inverter was able to ride through relatively severe AC faults. For all AC faults scenario 2 was able to recover much faster than scenario 1. The results indicate that the multi-infeed system improved the performance during transient state when AC faults were applied. The MMC-link was able to mitigate the impact of AC faults, thus helping the LCC-link recover faster.

The susceptibility to commutation failure for scenario 1 and 2 was investigated. A method for detecting commutation failure was proposed. The commutation failure immunity index was calculated and found to be 28% and 36% for scenario 1 and 2 respectively. The multi-infeed system is therefore less susceptible to commutation failure as compared to the LCC stand alone system. The result indicate that the

MMC-link hence mitigates the weakness of the LCC-link, and makes the LCC inverter less prone to commutation failure.

The coupling between AC and DC lines sharing the same Rights-of-Way (RoW) was investigated. A base case was developed as a benchmark for the rest of the analysis. Induced DC currents into the AC overhead lines were detected in transient state, due to adjacent DC overhead lines. The result of the base case was continued into a parametric sensitivity analysis to observe the changes in coupling effects when certain parameters were varied, as to determine which parameters were the most critical.

In the parametric sensitivity analysis a DC single pole to ground fault was implemented. The simulations showed an increased coupling effect when the parallel line length was extended, because the area of interaction increased. The coupling effect increased when the distance between the towers in the RoW were reduced, as the mutual inductance between the AC and DC lines became higher. The highest coupling effect was found for fault position closest to the MMC inverter with a rms neutral current of 1000 A. This was because it resulted in the highest fault current through the entire parallel section, which lead to a higher flux linkage between the lines. A greater fault current was detected for lower modulation indices and when the severity of the fault increased as a consequence of lower fault resistance.

Based on the findings in the sensitivity analysis, two mitigation methods were proposed. First, the tower distance was altered, as it was found to be a dominant factor. By keeping the RoW width constant, an optimal displacement of the middle AC tower was found to be 45 meters apart from the DC tower. This lead to a reduction of the peak rms neutral current of 22.3% (777 A), as compared to the base case tower displacement. Second, transposition of the conductors proved to be powerful measure, and an efficient way to reduce coupling effect between AC and DC overhead lines. The transposition averages the unbalance between the three phases, hence suppressing the coupling effect.

In this report the advantages of a multi-infeed system consisting of a MMC-link and a LCC-link have been compared against a LCC stand alone system. It has been proven to be an excellent combination for weak AC grid connections, as the MMC-link is able to stabilise the AC voltage and thereby make the LCC inverter less susceptible to commutation failures. A MMC-link can therefore be chosen for multi-infeed systems in an already weak AC grid, as it enhances system performance in steady state and transient state. The coupling effects due to parallel AC and DC overhead lines were studied, and two mitigation methods reduced the coupling effect, with (i) an optimal tower placement in the RoW and with (ii) transposition of the AC overhead lines. The results indicate that if the RoW is properly designed the minor coupling effects are unlikely to cause any problems to the power system stability.

Further Work

The further work can roughly be divided in two main parts namely (i) improvements to the model and (ii) new simulation cases. Starting with the model (i):

- It is desired that the simulation model is representative for the actual system, hence a number of improvements must be made to make the analysis more valid. For starters the work in this master thesis have been based on a Cigre Benchmark monopolar LCC-HVDC. The LCC-link is a standard benchmark for simulations used by scientists all over the world. The model could be adopted to fit the NorNed interconnector. For instance a bipolar configuration can be made, and also a DC sea cable between the inverter and rectifier station.
- The AC voltage system can be improved. The simulation system does not have any AC voltage supporting equipment installed. This makes the results obtained in the steady state AC voltage investigations in Section 4.1.3 invalid for the real system. However, the results reflects the importance of AC voltage stability, and how this can be achieved with the use of MMC AC voltage controllers. If FACTS or capacitor banks were installed, the simulations can be rerun to make the results more accurate and credible.
- The MMC can be optimized and tuned so that the controllers work better. The model is obtained from PSCAD support-team and is actually very well optimized already. However, the model can probably be made even better.

As for new simulation cases (ii):

- Different power cases can be implemented. During this master thesis the power direction has always been from Netherlands to Norway, and from Germany to Norway. This means the Norwegian system consists of two inverters (MMC and LCC). The power flow can be reversed.
- Other combinations for scenarios can be tested. This master thesis compared a LCC stand alone system and a multi-infeed HVDC system consisting of

MMC and LCC. Another multi-infeed system consisting of two LCC-links or two MMC-links can also be made, as for comparison purposes. Different power ratings can also be tested for the scenarios.

- Multi-infeed of three converters can also be tested. Statnett is building a new MMC interconnection to England, and it is planned to be connected at a completely different place (Kvilldal). However, for simulation purposes it would be interesting to see how three converters interact with each other. A number of different combinations exists.

- Different control systems for the MMC-link can be tested. The MMC-link is able to control the active power and DC voltage with d-axis current, and reactive power and AC voltage with q-axis current. Different set-ups can therefore be achieved and tested to see its effects.

- As for the parallel AC and DC overhead lines it would be possible to do project specific measures, and to investigate the restraints in the specific RoW in southern Norway.

Bibliography

[1] A. T. Gullberg. Will Norway Become Europe's Green Battery. http://www.cicero.uio.no/fulltext/index.aspx?id=8939, July 2011. [Online; accessed 15-November-2013].

[2] A. Holthe. The Consequences of a New HVDC Interconnector Between Norway and Germany. *Specialization Project, Norwegian University of Science and Technology, Department of Electrical Engineering*, December 2013.

[3] V. G. Agelidis, G. D. Demetriades, and N. Flourentzou. Recent Advances in High-Voltage Direct-Current Power Transmission Systems. *IEEE International Conference on Industrial Technology*, 2006.

[4] J. Paulinder. Operationd and Control of HVDC Links Embedded in AC Systems. *Chalmers University of Technology, Gothenburg*, 2003.

[5] N. Mohan, T. Undeland, and W.P. Robbins. *Power Electrincs - Converters, Applications and Design*. John Wiley & Sons, 3rd edition, 2003.

[6] K. R. Padiyar. *HVDC Power Transmission Systems - Technology and System Interactions*. John Wiley & Sons, 1990.

[7] N. Mohan. *Electric Power Systems - A First Course*. John Wiley & Sons, 1st edition, 2012.

[8] G. Asplund, K Eriksson, K Svensson, H. Jiang, and J. Lindberg. HVDC Light - DC Transmission Based on Voltage Source Converters. *ABB Power System AB*, 1998.

[9] P. F. Toledo. Modeling and Control of a Line-Commutated HVDC Transmission System. *Royal Institute of Technology, Stockholm*, 2007.

[10] K. Friedrich. Modern HVDC PLUS Application of VSC in Modular Multilevel Converter Topology. *IEEE International Symposium on Industrial Electronics*, July 2010.

[11] M. Davies, M Dommaschk, J. Dorn, J. Lang, D. Retzmann, and D. Soerangr. HVDC PLUS - Basics and Principle of Operation. *Siemens Energy Sector, Technical Paper*, August 2008.

[12] A. Lesnicar and R. Marquardt. An Innovative Modular Multi-Level Converter Topology Suitable for a Wide Power Range. *IEEE PowerTech Conference, Vol.3*, June 2003.

[13] T. Westerweller, K. Friedrich, U. Armonies, A. Orini, D. Parquet, and S. Wehn. Trans Bay Cable - World's First HVDC System Using Multilevel Voltage-Source Converter. *CIGRE, Technical Paper*, January 2010.

[14] G. S. Konstantinou, M. Ciobotaru, and V. G. Agelidis. Effect of Redundant Sub-module Utilization on Modular Multi-Level Converters. *IEEE International Conference on Industrial Technology*, March 2012.

[15] R.L. Sellick and M. Åkeberg. Comparison of HVDC Light and HVDC Classic. *ABB Sweeden, Technical Paper*, December 2012.

[16] M. Ragheb. High Voltage Direct Current Power Transmission. *University of Illinois, USA*, May 2012.

[17] C. C. Davidson and D. R. Trainer. Innovative Concepts For Hybrid Multi-Level Converters For HVDC Power Transmission. *IET 9th International Conference*, October 2010.

[18] H. Saad. Modeling of HVDC-MMC Transmission System for Electromagnetic Transients, June 2013.

[19] IEC. In *Determination of Power Losses in High-Voltage Direct Current (HVDC) Converter Stations with Line Commutated Converters*, volume IEC61803, 2010.

[20] IEC. In *Draft Document - Determination of Power Losses in Voltage Sourced Converter (VSC) for HVDC Systems*, volume IEC62751, 2012.

[21] P. S. Jones and C. C. Davidson. Calculation of Power Losses for MMC-based VSC HVDC Stations. *IEEE Power Electronics and Applications European Conference*, September 2013.

[22] N. M. MacLeod, A.C. Lancaster, and C.D.M. Oates. The Development of a Power Electronic Building Block for use in VSC for HVDC. *Areva T&D*, 2009.

[23] M. Callavik, A. Blomberg, J. Hafner, and B. Jacobson. The Hybrid HVDC Breaker. *ABB Grid Systems, Technical Paper*, November 2012.

[24] C. Y. Zhao, X. JianZhong, and L. Tan. DC Faults Ride-Through Capability Analysis of full-bridge MMC-MTDC Sytem. *China Technical Science, Vol.56 No.1*, January 2013.

[25] Y. Wang and R. Marquardt. Future HVDC-Grids Employing Modular Multilevel Converters and Hybridg DC-Breakers. *IEEE Power Electronics and Applications European Conference*, September 2013.

[26] G.P. Adam, K.H. Ahmed, S.J.Finney, K. Bell, and B.W. Williams. New Breed of Network Fault-Tolerant VSC HVDC Transmission System. *IEEE Transactions Vol.28 No.1*, February 2013.

[27] E. Rahimi, A. M. Gole, J.B. Davies, I.T. Fernando, and K.L. Kent. Commutation Failure in Single- and Multi-Infeed HVDC Systems. *IET International Conference AC and DC Power Transmission*, March 2006.

[28] G. Andersson, P.F. Toledo, and G. Liss. HVDC Multi-Infeed Performance. *ABB Power Systems, Sweeden*, 1996.

[29] P. F. Toledo, J. Pan, K. Srivastava, W. Wang, and C. Hong. Case Study of a Multi-Infeed HVDC System. *IEEE Power System Technology POWERCON*, 2007.

[30] Statnett. Skagerrak 4. http://www.statnett.no/Nettutvikling/Skagerrak-4/, 2013. [Online; accessed 5-October-2013].

[31] Statnett. Nordlink. http://www.statnett.no/Nettutvikling/NORDLINK/, 2014. [Online; accessed 5-May-2014].

[32] ABB. North-East Agra. http://www.abb.com/industries/ap/db0003db004333/9716a8ac9879236bc125785200694f18.aspx, 2013. [Online; accessed 5-December-2013].

[33] IEEE Spectrum. Germany Takes the Lead in HVDC. http://spectrum.ieee.org/energy/renewables/germany-takes-the-lead-in-hvdc, 2013. [Online; accessed 5-December-2013].

[34] Statnett. Funksjonskrav i Kraftsystemet. June 2012.

[35] ABB. HVDC Projects By Type And Power. http://www.abb.com/industries/ap/db0003db004333/718bfd4f5d7fa84bc12574ad00302100.aspx, 2013. [Online; accessed 15-November-2013].

[36] W. Lu and B.T. Ooi. Optimal Acquisition and Aggregation of Offshore Wind Power by Multiterminal Voltage-Soruce HVDC. *IEEE Transactions on Power Delivery, Vol.18 No.1*, January 2003.

[37] L. Tan, Z. Chengyong, X. Jie, C. Xinhong, P. Hui, and L. Chang. Start-up Scheme for HVDC System Based on Modular Multilevel Converter. *IET Renewable Power Generation Conference*, September 2013.

[38] E. N. Abildgaard. Exploring the Properties of a Moldular Multilevel Converter Based HVDC Link. *Norwegian University of Science and Technology, Trondheim*, June 2012.

[39] W. Li, L.A. Gregoire, and J. Belanger. Control and Performance of a Modular Multilevel Converter System. *OPAL-RT Technologies, Cigre Conference on Power Systems*, September 2011.

[40] S. Rohner, S. Bernet, M. Hiller, and R. Sommer. Modelling, Simulation and Analysis of a Modular Multilevel Converter for Medium Voltage Applications. *IEEE International Conference Industrial Technology*, March 2010.

[41] Q. Tu, Z. Xu, and L. Xu. Reduced Switching-Frequency Modulation and Circulating Current Suppression for Modular Multilevel Converters. *IEEE Transactions on Power Delivery, Vol.26 No.3*, February 2011.

[42] J. L. Dominguez-Garcia, F.Bianchi, O. Gomis-Bellmunt, and A. Sudria-Andreu. Power Control of Voltage Source Converter for Distributed Generation. *Physcon*, September 2011.

[43] C. Bajracharya. Control of VSC-HVDC for Wind Power. *Norwegian University of Science and Technology, Trondheim*, June 2008.

[44] C. Du and M. Bollen. Analysis of the Control Algoroithms of Voltage Source Converter HVDC. *IEEE Power Tech Conference*, June 2005.

[45] L. Zhang. Modelling and Control of VSC-HVDC Links Connected to Weak AC Systems. *IEEE Transactions on Power Systems, Vol.26 No.2*, May 2011.

[46] M. Saeedifard and R. Iravani. Dynamic Performance of a Modular Multilevel Back-to-Back HVDC System. *IEEE Transactions on Power Delivery, Vol.25 No.4*, October 2010.

[47] M. Szechtman, T. Wess, and C.V. Thio. A Benchmark Model for HVDC System Studies. *IEEE International Conference, Electra No. 135*, April 1991.

[48] A. Mazumder. Capacitor Commutated Converters for HVDC Transmission System. *Concordia University, Canada*, February 2002.

[49] V. Sookha. Modeling and Investigation of the NorNed HVDC link with RTDS. *Delft University of Technology*, May 2011.

[50] L. Zhang and L. Dofnas. A Novel Method to Mitigate Commutation Failures in HVDC Systems. *IEEE International Conference on Power System Tecnology, Vol.1 No.1*, October 2002.

[51] C. K Kim, V. K. Sood, G.S. Jang, S.J. Lim, and S.J. Lee. *HVDC Transmission Power Conversion Applications in Power Systems*. John IEEE Press, 2009.

[52] A. Muthusamy. Dynamic Performance Control Parameters for Classic HVDC in PSS/E. *Chalmers University of Technology, Gothenburg*, 2010.

[53] J. Xu, C. Zhao, and L. Lu. New Precharge and Submodule Capacitor Voltage Balancing Topologies of Modular Multilevel Converter for VSC-HVDC Application. *IEEE Asian-Pacific Power and Energy Engineering Conference*, March 2011.

[54] H. Saadat. *Power System Analysis*. PSA Publishing, 3rd edition, 2010.

[55] N. D. Tleis. *Power Systems Modelling and Fault Analysis - Theory and Practice*. Elseiver, 2008.

[56] C. R. Bayliss and B.J. Hardy. Transmission and Distribution Electrical Engineering. *Elsevier, 4th Ed.*, November 2013.

[57] T. Arro and O. Silavwe. Coupling of Transients in HVDC Lines to Adjacent HVAC Lines and its Impact on the AC Line Protection. *Chalmers University of Technology, Gothenburg*, 2007.

[58] J. Ulleryd, M. Ye, and G. Moreau. Fundamental Frequency Coupling Between HVAC and HVDC Lines in Quebec-New England. *IEEE International Conference POWERCON '98, Vol.1 No.1*, August 1998.

[59] J. Hu and B. Bisewski. Evalution of Coupling Between DC and AC Transmission Lines on the Same RoW. *RBJ Engineering Corp.*, 2010.

[60] N. Chopra, A.M. Gole, and J. Chand. Zero Sequence Currents in AC Lines Caused by Transients in Adjacent DC Lines. *IEEE Transactions on Power Delivery, Vol.3 No.4*, October 1988.

[61] I. Colak, E. Kabalci, R. Bayindir, and G. Bal. Modeling of a Three Phase SPWM Multilevel VSI With LoW THD Using Matlab/Simulink. *IEEE Power Electronics and Applications European Conference*, September 2009.

[62] L.M. Tolbert, F. Zheng, and T.G. Habetler. Multilevel PWM Methods at Low Modulation Indives. *IEEE Transactions on Power Electronics, Vol.15 No.4*, July 2000.

[63] X. Chen, C. Zhao, and C. Cao. Research on the Fault Characteristics of HVDC Based on Modular Multilevel Converter. *IEEE Electrical Power and Energy Conference*, October 2011.

[64] H. Ding, Y.Z Zhang, A. M. Gole, D.A. Woodford, M.X. Han, and X.N. Xiao. Analysis of Coupling Effects on Overhead VSC-HVDC Transmission Lines From AC Lines With Shared Right of Way. *IEEE Transactions on Power Delivery, Vol.25 No.4*, October 2010.

[65] A.V. Elguera and M.C. Tavares. Influence of Transmission Line Transposition in Electromagnetic Transients Phenomena. *IEEE Transmission & Distribution Conference Latin America*, August 2006.

Appendix A

PSCAD Model

A.1 MMC Per Unit Values

In order to be able to compare different quantities in an interconnected power system, it is common practice to construct a pu system to simplify calculations. By doing this transformation one eliminates different voltage and power levels, and the system is reduced to a simpler one. The quantities are defined as:

$$\text{Quantity in pu} = \frac{\text{Actual quantity}}{\text{Base value of quantity}} \tag{A.1}$$

To construct a pu system one must define four base quantities. Usually base apparent power S_b and base voltage V_b, is chosen according to system requirements. After that base current I_b and base impedance Z_b, can be calculated in order to satisfy circuit laws [54]. The general formulas in three phase quantities are defined as:

$$S_b = \sqrt{3} V_b I_b \tag{A.2}$$

$$S_b = \frac{3}{2} S_{dq,b} \tag{A.3}$$

$$V_b = \sqrt{3} Z_b I_b \tag{A.4}$$

$$V_b = \sqrt{\frac{3}{2}} V_{dq,b} \tag{A.5}$$

$$Z_b = \frac{V_b}{\sqrt{3} I_b} = \frac{V_b^2}{S_b} \tag{A.6}$$

Appendix B

DQ-Transformation

The dq-transformation is done in two steps:

- abc $\rightarrow \alpha, \beta$ (Clark Transformation)
- $\alpha, \beta \rightarrow$ dq (Park Transformation)

The Clark Transformation modify the three phase abc system to a stationary α,β system. It can be seen as a projection of three axis into a stationary two axis system. It is possible to contract this matrix by removing the zero-sequence component (named homopolar component). This vector is orthogonal to α and β and is zero in balanced system. It is therefore neglected in further analysis [42]. The following analysis is done with respect to current, but the same equations is also valid for voltage, and flux linkages. Clark Transformation can be done with the following matrix,

$$\begin{bmatrix} i_\alpha \\ i_\beta \end{bmatrix} = \frac{2}{3} \begin{bmatrix} 1 & -\frac{1}{2} & \frac{1}{2} \\ 0 & \frac{\sqrt{3}}{2} & -\frac{\sqrt{3}}{2} \end{bmatrix} \begin{bmatrix} i_a \\ i_b \\ i_c \end{bmatrix} \tag{B.1}$$

where i_a, i_b and i_c are phase currents on AC side of the converter in Fig. 3.5 on page 26.

Park's Transformation is used to modify the stationary α, β system to a rotating dq system. To simplify the analysis the stationary α is in phase with the stationary phase a. The dq system is rotating with speed ω. The position of the d-axis is given by $\theta = \omega * t$. The q-axis is leading d-axis by $\frac{\Pi}{2}$. Fig. B.1 shows a graphical representation of the different axis [43].

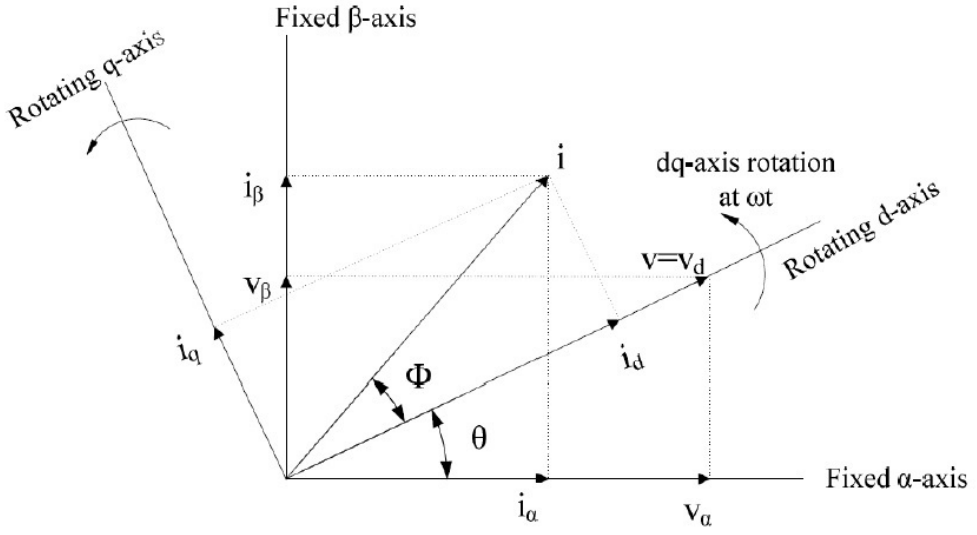

FIGURE B.1: Graphical Representation of Park and Clark Transformation [43].

The Park Transformation from α, β to dq is done with the following matrix [42],

$$\begin{bmatrix} i_d \\ i_q \end{bmatrix} = \begin{bmatrix} -sin(\theta) & cos(\theta) \\ cos(\theta) & sin(\theta) \end{bmatrix} \begin{bmatrix} i_\alpha \\ i_\beta \end{bmatrix} \tag{B.2}$$

It is also possible to transform directly from an abc system to dq system with just one matrix by combining the above equations [54],

$$\begin{bmatrix} x_d \\ x_q \\ x_0 \end{bmatrix} = T(\theta) \begin{bmatrix} x_a \\ x_b \\ x_c \end{bmatrix} = \frac{2}{3} \begin{bmatrix} cos(\theta) & cos(\theta - \frac{2\Pi}{3}) & cos(\theta + \frac{2\Pi}{3}) \\ sin(\theta) & sin(\theta - \frac{2\Pi}{3}) & sin(\theta + \frac{2\Pi}{3}) \\ \frac{1}{2} & \frac{1}{2} & \frac{1}{2} \end{bmatrix} \begin{bmatrix} x_a \\ x_b \\ x_c \end{bmatrix} \tag{B.3}$$

where the variable x is used to represent either voltage, current or flux linkages on AC side of the converter.

Appendix C

Fault Studies Based on Sequence Currents and Voltages

The aim of this section is to see how different AC faults affect the AC power system with respect to sequence currents. It is aimed to study and compare balanced and unbalanced AC faults, as a supplement to the study of transient behaviours in Section 4.2 on page 64. First symmetrical components will be presented and explained (Section C.1). Then, an analysis based on different AC faults will be made (Section C.2). All measurements of the currents and voltages will be done in the AC transmission path at location C, and the faults are located at Feda, location B (see Fig. 4.2 on page 57).

C.1 Symmetrical Components

AC faults can be divided between balanced and unbalanced faults. Balanced faults are faults where all the phases connect to ground simultaneously, i.e. a three phase to ground fault. It is called balanced fault because the all of the phases are affected equally, and the system therefore remains balanced. These types of faults are relatively rare, and according to [54] 5 % of all transmission faults are balanced faults. Nevertheless they are the easiest to analyse, because they can be solved by reducing the system to per-unit and by replacing the grid with a simple Thevenin equivalent, explained in detail in [54]. Balanced faults are also the most severe fault type. Circuit-breakers rated MVA are therefore selected based on a three phase short circuit [55].

Unbalanced faults are faults involving one or two phases. These faults are more difficult to analyse since the system is no longer balanced. The most common type of unbalanced faults are single phase to ground fault followed by line to line fault and double phase to ground fault. These faults account for 95 % of all

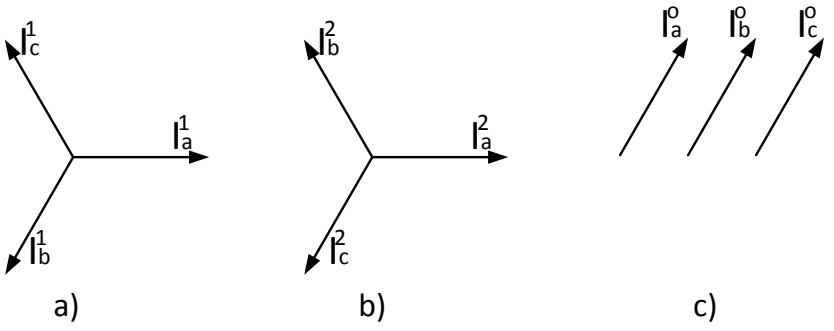

FIGURE C.1: Representation of Symmetrical Components.

faults on a transmission line [54]. Unbalanced faults are solved using symmetrical components, decomposed into three different sequences namely,

- Positive Sequence
- Negative Sequence
- Zero Sequence

Symmetrical components are a powerful tool when it comes to solving unbalanced networks. The use of symmetrical components makes it possible to represent unbalanced quantities, such as voltages and currents, with three balanced symmetrical components. The positive (a), negative (b) and zero sequence (c) is drawn in Fig. C.1. The following analysis is done for currents, although the same conventions also yield for voltages. The three phases abc refers to the conventional phases in a three phase electrical system so that,

$$\mathbf{I}_{abc} = \mathbf{I}^0_{abc} + I^1_{abc} + \mathbf{I}^2_{abc} \tag{C.1}$$

where the superscripts ^{120} refers to positive, negative and zero sequence quantities respectively. The symmetrical components are defined as "the order in which they pass through a positive maximum" [54]. An operator named a is defined as a 120° counter-clockwise rotation of a phase quantity. Using this definition, it is possible to write the positive (Eqn. C.2), negative (Eqn. C.3) and zero sequence (Eqn. C.4) in the following way,

$$\begin{aligned} I_a^1 &= I_a^1 \angle \underline{0^\circ} = I_a^1 \\ I_b^1 &= I_a^1 \angle \underline{240^\circ} = a^2 I_a^1 \\ I_c^1 &= I_a^1 \angle \underline{120^\circ} = a I_a^1 \end{aligned} \tag{C.2}$$

$$\begin{aligned} I_a^2 &= I_a^2 \angle \underline{0^\circ} = I_a^2 \\ I_b^2 &= I_a^2 \angle \underline{120^\circ} = a I_a^2 \\ I_c^2 &= I_a^2 \angle \underline{240^\circ} = a^2 I_a^2 \end{aligned} \tag{C.3}$$

$$I_a^0 = I_b^0 = I_c^0 \tag{C.4}$$

By inserting the equations for symmetrical components into Eqn. C.1 one gets the following equation written in compact matrix form,

$$\begin{bmatrix} I_a \\ I_b \\ I_c \end{bmatrix} = \begin{bmatrix} 1 & 1 & 1 \\ 1 & a^2 & a \\ 1 & a & a^2 \end{bmatrix} \begin{bmatrix} I_a^0 \\ I_a^1 \\ I_a^2 \end{bmatrix} \tag{C.5}$$

C.2 AC Faults

The AC faults that will be investigated can be seen on Fig. C.2:

- Phase ABC to ground
- Phase AB to ground
- Phase A to ground
- Phase A to B

All faults are located at Feda with a fault duration of 0.5 seconds, and the measurements have been done in the AC transmission line location C (Fig. 4.2 on page 57). On Fig. C.3 and on Fig. C.4 the (a) positive, (b) negative and (c) zero sequence currents and voltages respectively can be seen for different AC faults.

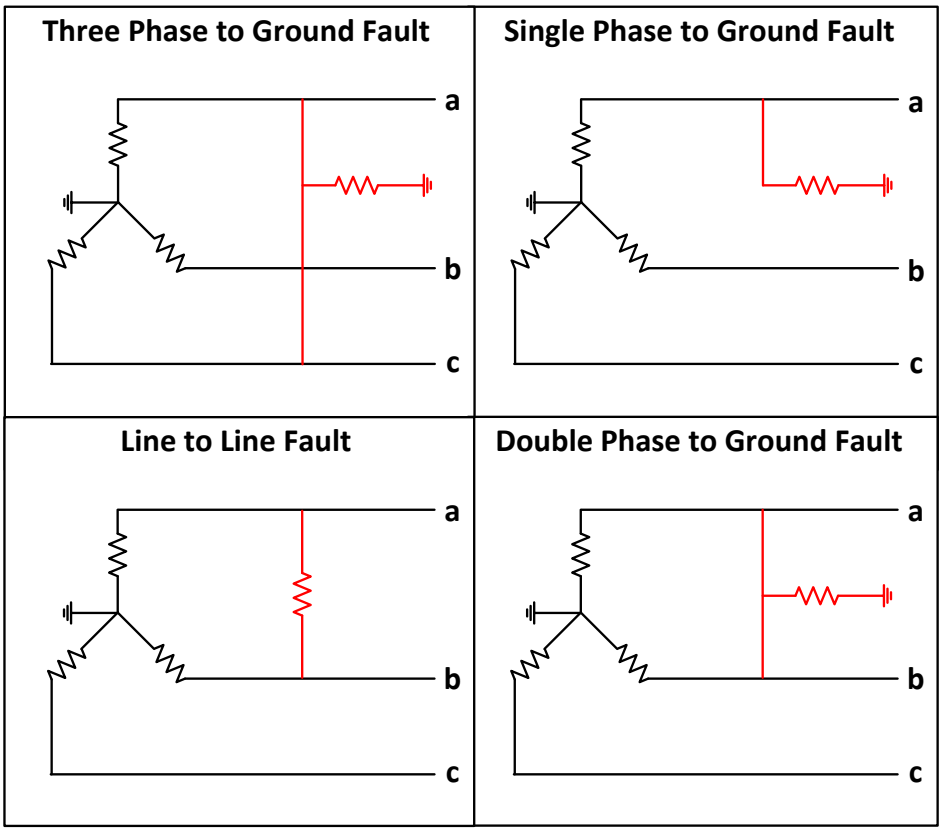

FIGURE C.2: AC Faults Types.

Starting with the balanced three phase to ground fault, one can see that this fault has the highest fault current in positive sequence of 3.3 kA. It also has the largest voltage drop in positive sequence of about 230 kV. This illustrates that a three phase to ground fault is the most severe fault. It is therefore reasonable that the switchgear in the power system is rated to withstand these kind of faults. Further it can be observed that a three phase to ground fault produces neglectable zero sequence currents and voltages during the fault duration. This can be explained by the fact that this is a balanced fault, where all the phases are short circuited and affected equally. The phases are said to be balanced during the fault, their magnitudes and phases are equally reduced, thus results in a small amount of neutral current and voltage. When the fault is cleared the zero sequence currents and voltages increases due to transients related to the removal of the fault resistance.

Continuing with the unbalanced faults, Fig. **??** and Fig. C.4 shows that single phase and double phase to ground faults behave very similar. These two faults trigger a relatively large amount of zero sequence currents and voltages. This seems reasonable, because they produce an imbalance between the phase currents

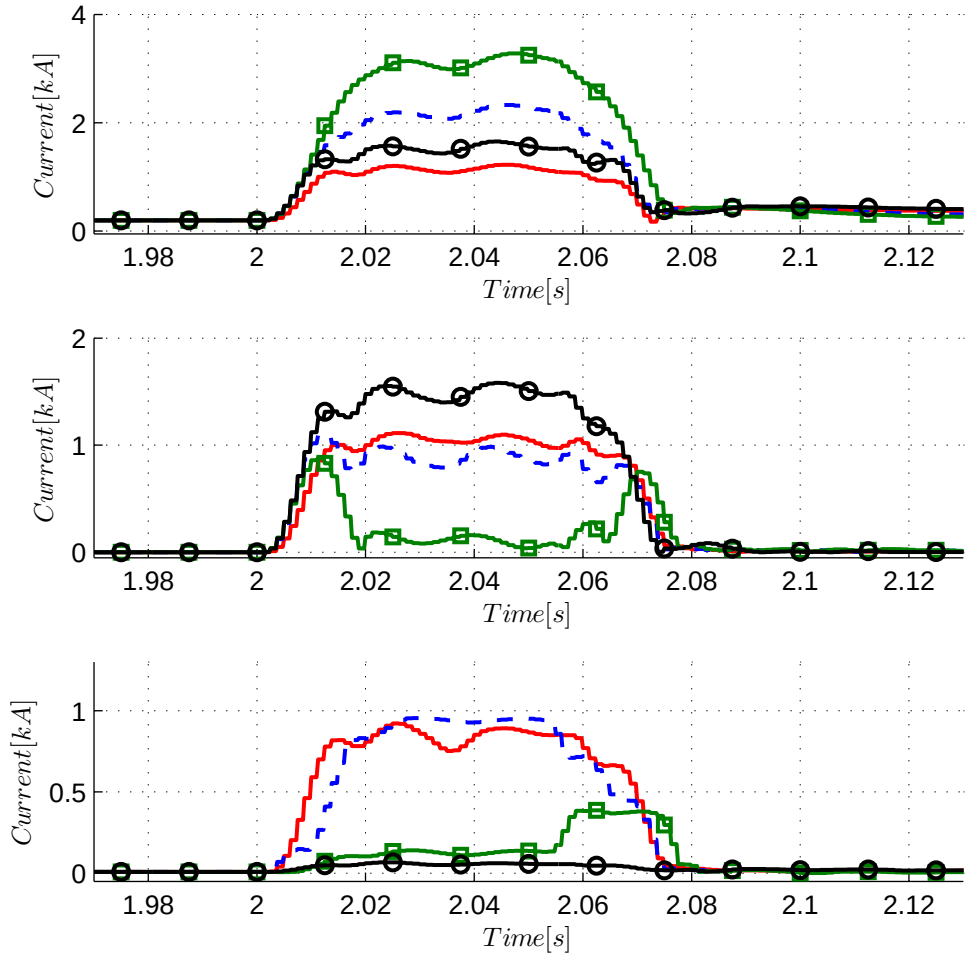

FIGURE C.3: AC Faults: Sequence Currents: A to Ground (—), AB to Ground (- - -), ABC to Ground (—□—) A to B (—o—) a) Positive Sequence b) Negative Sequence c) Zero Sequence.

and voltages. The three phases summed together does therefore not equal zero. A double phase to ground produces more fault current and voltage than the single phase to ground, shown by the positive sequence. The line to line fault does not produce any zero sequence current, but a large negative sequence voltage and current can be detected during fault.

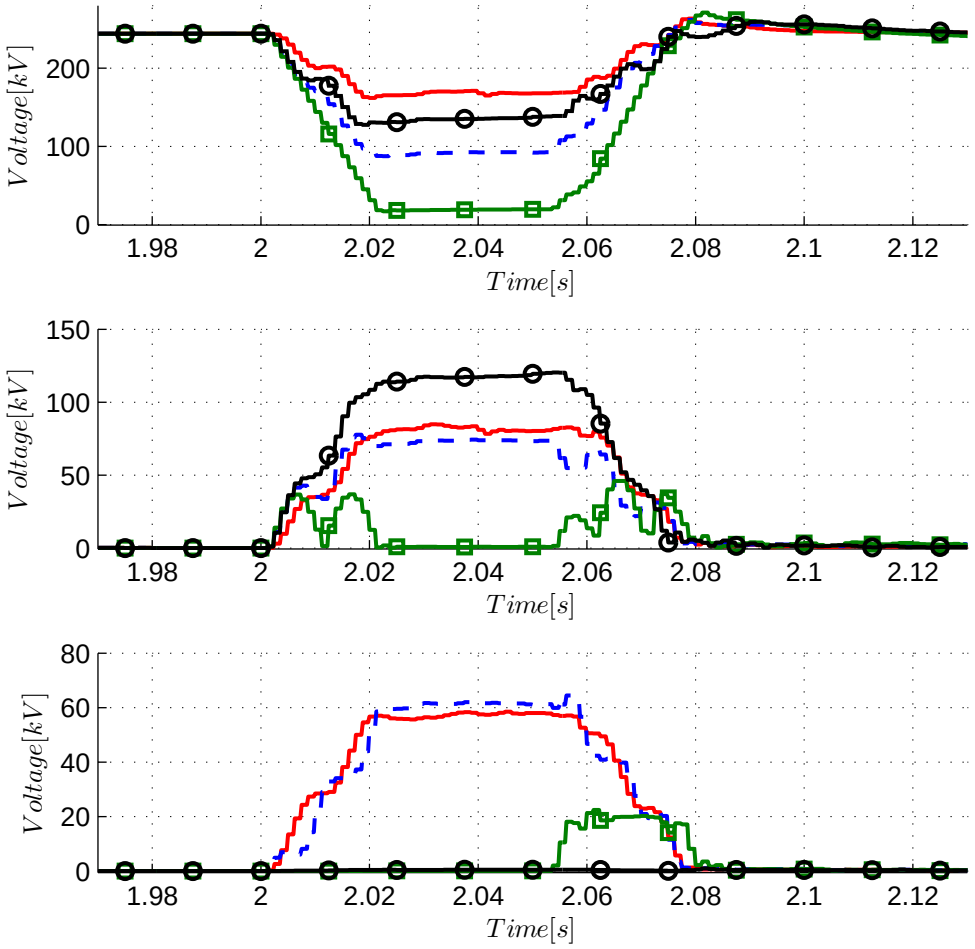

FIGURE C.4: AC Faults: Sequence Voltages: A to Ground (—), AB to Ground (- - -), ABC to Ground (—□—) A to B (—○—) a) Positive Sequence b) Negative Sequence c) Zero Sequence.